

# CITATION REPORT

List of articles citing

## Dielectric relaxation in solids

DOI: 10.1088/0022-3727/32/14/201

Journal Physics D: Applied Physics, 1999, 32, R57-R70.

**Source:** <https://exaly.com/paper-pdf/30494960/citation-report.pdf>

**Version:** 2024-04-28

This report has been generated based on the citations recorded by exaly.com for the above article. For the latest version of this publication list, visit the link given above.

The third column is the impact factor (IF) of the journal, and the fourth column is the number of citations of the article.

#	Paper	IF	Citations
1437	Analytical evaluation of distribution of relaxation time.		0
1436	Phase Transitions in $[N(C_2H_5)_4]_2MeCl_2Br_2$ (Me = Zn, Co, Cu) Solid Solutions. <b>1997</b> , 161, 515-521		5
1435	Variable-range-hopping conduction and dielectric relaxation in disordered $Sr_{0.97}(Ti_{1-x}Fex)O_3$ <b>1998</b> , 57, 11858-11861		55
1434	Universal dielectric response of variously doped $CeO_2$ ionically conducting ceramics. <b>1998</b> , 58, 8398-8406		75
1433	Dielectric relaxation at the glass transition of confined N-methyl-e-caprolactam. <b>1998</b> , 58, 5336-5345		37
1432	Low-frequency divergence of the dielectric constant in metal-insulator nanocomposites with tunneling. <b>1998</b> , 58, R13375-R13378		21
1431	Impedance spectroscopy of brushite composites and a scaling approach to the dispersion behavior of inhomogeneous ionic conductors. <b>1998</b> , 58, 5390-5407		14
1430	Dynamic cluster model of the ac conductivity of crystalline materials and glasses. <b>1998</b> , 58, 8407-8410		5
1429	Low-frequency dielectric dispersion in $NaNbO_3$ single crystals. <b>1998</b> , 215, 65-73		9
1428	Low-temperature dielectric relaxation peaks involving proton tunneling in $Ba_{1-x}NdxCeO_3$ . <b>1999</b> , 60, R3713-R3715		18
1427	Dielectric spectroscopy of confinement effects in polar materials. <b>1999</b> , 59, 9214-9228		88
1426	Ionizing-irradiation-induced thermally stimulated currents in $Al_2O_3:Mg$ . <b>1999</b> , 59, 7480-7485		
1425	Universal Approach for Scaling the ac Conductivity in Ionic Glasses. <b>1999</b> , 82, 3653-3656		242
1424	Alternating current characterization of sputter deposited Ti oxide films. <i>Journal Physics D: Applied Physics</i> , <b>2000</b> , 33, 24-27	3	
1423	Particle dynamics in the random barrier model: Monte Carlo simulations at low temperatures. <b>2000</b> , 61, 5993-5997		17
1422	Dielectric characterization of the water-matrix interaction in porous materials by thermal depolarization spectroscopy. <b>2000</b> , 61, 16514-16521		18
1421	Nonuniversal features of the ac conductivity in ion conducting glasses. <b>2000</b> , 85, 1274-7		56

1420	Estimation of the intrinsic heterogeneity of ionic glass-forming melts. <b>2000</b> , 61, 2121-4	1
1419	Scaling of the conductivity spectra in ionic glasses: dependence on the structure. <b>2000</b> , 84, 2188-90	291
1418	Dielectric spectra and electrical conduction in Fe-doped SrTiO <sub>3</sub> . <b>2000</b> , 61, 3922-3926	96
1417	Defect dominated charge transport in amorphous Ta <sub>2</sub> O <sub>5</sub> thin films. <b>2000</b> , 88, 850-862	185
1416	Scaling of the ac permittivity in ion-conducting glasses. <b>2000</b> , 62, 5503-5507	38
1415	Charge carrier transport via defect states in Cu(In,Ga)Se <sub>2</sub> thin films and Cu(In,Ga)Se <sub>2</sub> /CdS/ZnO heterojunctions. <b>2000</b> , 61, 16052-16059	15
1414	Scaling behavior of the alpha relaxation in fragile glass-forming liquids under conditions of high compression. <b>2000</b> , 61, 526-31	31
1413	Influence of the wettability on the electrical response of microporous systems. <i>Journal Physics D: Applied Physics</i> , <b>2000</b> , 33, 1036-1047	3 22
1412	A mathematical comparison of two models of the electrical properties of biological tissues. <b>2001</b> , 46, 867-77	4
1411	Ionic conduction in glass: new information on the interrelation between the "Jonscher behavior" and the "nearly constant-loss behavior" from broadband conductivity spectra. <b>2001</b> , 87, 085901	84
1410	Non-Arrhenius stretched exponential dielectric relaxation in antiferromagnetic TiBO <sub>3</sub> single crystals. <b>2001</b> , 64,	10
1409	Origin of constant loss in ionic conductors. <b>2001</b> , 86, 1279-82	172
1408	Analysis of Alternating Current Conduction and Impedance Spectroscopy Study of BaBi <sub>2</sub> Nb <sub>2</sub> O <sub>9</sub> Thin Films. <b>2001</b> , 688, 1	
1407	Electroactive properties of flexible piezoelectric composites. <b>2001</b> , 4, 201-204	27
1406	Identification of a new function model for the AC-impedance of thermally evaporated undoped selenium films using the Eigen-coordinates method. <b>2001</b> , 396, 282-296	26
1405	Measurement of the low temperature electrical properties of solid tantalum capacitors. <b>2001</b> , 41, 285-288	3
1404	Microwave characterization of filled polymers. <b>2001</b> , 89, 4532-4540	183
1403	Coulomb glass origin of defect-induced dielectric loss in thin-film oxides. <b>2001</b> , 78, 4016-4018	2

1402	Glassy dynamics and enzymatic activity of lysozyme. <b>2001</b> , 64, 052905	19
1401	Test of universal scaling of ac conductivity in ionic conductors. <b>2001</b> , 64,	27
1400	Electrical relaxations: Simple versus complex ionic systems. <b>2001</b> , 63,	74
1399	Temporal fractal model for the anomalous dielectric relaxation of inhomogeneous media with chaotic structure. <b>2001</b> , 64, 031504	44
1398	Dielectric relaxation in flux grown $\text{KTiOPO}_4$ and isomorphous crystals. <b>2001</b> , 89, 1850	25
1397	Characterization of the stretched-exponential trap-time distributions in one-dimensional coupled map lattices. <b>2002</b> , 66, 066205	8
1396	Cation mass dependence of the nearly constant dielectric loss in alkali triborate glasses. <b>2002</b> , 88, 125902	41
1395	Domain wall relaxation, creep, sliding, and switching in superferromagnetic discontinuous $\text{Co(80)Fe(20)/Al(2)O}_3$ multilayers. <b>2002</b> , 89, 137203	75
1394	Distinguishing two contributions to the nearly constant loss in ion-conducting glasses. <b>2002</b> , 89, 195901	32
1393	Restricted dynamics of a supercooled liquid in a polymer matrix. <b>2002</b> , 66,	20
1392	New general susceptibility response function: Comparison with dielectric relaxation data of a glass former in confinement. <b>2002</b> , 82, 517-522	1
1391	Effects of confinement on the phase separation in emeraldine base polyaniline cast from 1-methyl-2-pyrrolidinone studied via dielectric spectroscopy. <b>2002</b> , 14, 11769-11778	29
1390	Relaxation properties of glass and graphite loaded PTFE composites. <b>2002</b> , 305, 379-385	2
1389	Recognition of a new permittivity function for glycerol by the use of the eigen-coordinates method. <b>2002</b> , 305, 96-111	32
1388	Dielectric and pyroelectric properties of a composite of ferroelectric ceramic and polyurethane. <b>2002</b> , 5, 257-260	16
1387	Advances in understanding the relationship between rock wettability and high-frequency dielectric response. <b>2002</b> , 33, 87-99	13
1386	Characterization of ethylene-vinylalcohol copolymer doped with chlorophyll. <b>2002</b> , 21, 571-576	4
1385	Generalized effective medium theory and dielectric relaxation in particle-filled polymeric resins. <b>2002</b> , 91, 3197-3204	84

1384	Competing tunneling and capacitive paths in Co <sub>2</sub> FeO <sub>2</sub> granular thin films. <b>2003</b> , 67,		20
1383	Dielectric relaxation assessment of a heat treated metal oxide varistor. <b>2003</b> , 150, 141-147		4
1382	Complex permittivities and dielectric relaxation of granular activated carbons at microwave frequencies between 0.2 and 26 GHz. <b>2003</b> , 41, 1801-1807		65
1381	Computational electromagnetics and the rational design of new dielectric heterostructures. <b>2003</b> , 48, 373-456		134
1380	Signal processing and recognition of true kinetic equations containing non-integer derivatives from raw dielectric data. <b>2003</b> , 83, 2433-2453		19
1379	Influence of synthesis process on the AC response of PLZT (8/65/35) ferroelectric ceramics. <b>2003</b> , 23, 1337-1343		6
1378	New approach in the description of dielectric relaxation phenomenon: correct deduction and interpretation of the Vogel-Fulcher-Tamman equation. <b>2003</b> , 15, 3481-3503		23
1377	Stress testing and characterization of high-k dielectric thin films.		2
1376	Phase transformations in calcite from electrical impedance measurements. <b>2003</b> , 76, 1015-1028		20
1375	Dielectric properties of residual water in amorphous lyophilized mixtures of sugar and drug. <i>Journal Physics D: Applied Physics</i> , <b>2003</b> , 36, 330-335	3	38
1374	Influence of stoichiometry on the dielectric properties of sputtered strontium titanate thin films. <b>2003</b> , 94, 3390-3396		34
1373	Frequency dependence of the dielectric properties of La-doped Pb(Zr <sub>0.35</sub> Ti <sub>0.65</sub> )O <sub>3</sub> thin films. <b>2003</b> , 83, 2892-2894		19
1372	Temperature dependence of the dielectric response of anodized Al <sub>2</sub> O <sub>3</sub> /metal capacitors. <b>2003</b> , 93, 3461-3469		12
1371	The justified data-curve fitting approach: recognition of the new type of kinetic equations in fractional derivatives from analysis of raw dielectric data. <i>Journal Physics D: Applied Physics</i> , <b>2003</b> , 36, 2281-2294	3	23
1370	Dielectric spectroscopy and thermally stimulated discharge current in PEEK film. <b>2003</b> , 28, 49-53		9
1369	Dielectric characterization of materials at microwave frequency range. <b>2003</b> , 6, 97-101		27
1368	High frequency dielectric relaxation in lanthanum modified PbTiO <sub>3</sub> ferroelectric ceramics. <b>2004</b> , 7, 325-328		6
1367	A time-domain analysis of dipolar effects in copper phthalocyanine thin films on indium oxide substrates. <b>2004</b> , 19, 1075-1080		4

1366	Lithium dynamics in the fast ionic conductor $\text{Li}_{0.18}\text{La}_{0.61}\text{TiO}_3$ probed by $\text{Li}^7$ NMR spectroscopy. <b>2004</b> , 70,	16
1365	Generalized regular singular-point description of low-frequency dielectric responses. <b>2004</b> , 70,	
1364	Conductivity spectra in fast ion conducting glasses: Mobile ions contributing to transport process. <b>2004</b> , 70,	51
1363	Dielectric response due to stochastic motion of pinned domain walls. <b>2004</b> , 70,	26
1362	AC Loss Modeling in $\text{Ba}_{0.5}\text{Sr}_{0.5}\text{TiO}_3$ Using Dielectric Relaxation. <b>2004</b> , 833, 20	1
1361	Ionic diffusion and space charge polarization in structural characterization of biological tissues. <b>2004</b> , 14, 137-42	9
1360	Microwave permittivity and dielectric relaxation of a high surface area activated carbon. <b>2004</b> , 79, 125-129	79
1359	Dielectric study of the phase diagram of the poly(Ebenzyl-L-glutamate)/dimethylformamide system. <b>2004</b> , 42, 3943-3952	1
1358	Influence of charge-ordering on the dielectric response of $\text{La}_{1-x}\text{Sr}_x\text{MnO}_3$ . <b>2004</b> , 323, 473-476	16
1357	Distinctive contributions from organic filler and relaxorlike polymer matrix to dielectric response of $\text{CuPc-P(VDF-TrFE-CFE)}$ composite. <b>2004</b> , 92, 047604	48
1356	Large dielectric constant and Maxwell-Wagner relaxation in $\text{Bi}_2\text{Cu}_3\text{Ti}_4\text{O}_{12}$ . <b>2004</b> , 70,	411
1355	Evidence for power-law frequency dependence of intrinsic dielectric response in the $\text{CaCu}_3\text{Ti}_4\text{O}_{12}$ . <b>2004</b> , 70,	103
1354	Synthesis, structure and electrical behaviour of lanthanum-doped barium stannate. <i>Journal Physics D: Applied Physics</i> , <b>2004</b> , 37, 1483-1491	3 56
1353	. <b>2004</b> , 4, 488-494	32
1352	Nonintrinsic origin of the colossal dielectric constants in $\text{CaCu}_3\text{Ti}_4\text{O}_{12}$ . <b>2004</b> , 70,	551
1351	Dielectric properties of epoxy nanocomposites containing $\text{TiO}_2$ , $\text{Al}_2\text{O}_3$ and $\text{ZnO}$ fillers.	8
1350	Ferroelectric Properties of $\text{Na}_{0.5}\text{K}_{0.5}\text{NbO}_3$ Films at Low Temperatures. <b>2004</b> , 67, 59-68	6
1349	An assessment of ageing of oxide varistors exposed to pulse hazards using dielectric spectroscopy.	3

1348	Electrical properties in granular Co-ZrO <sub>2</sub> thin films. <b>2005</b> , 2, 43	7
1347	Molecular dynamics simulation of the hollandite Na <sub>x</sub> (Ti <sub>8-x</sub> Cr <sub>x</sub> )O <sub>16</sub> : ion transport and high frequency dielectric absorption. <b>2005</b> ,	
1346	Hydrophobic ionic liquids based on the 1-butyl-3-methylimidazolium cation for lithium/seawater batteries. <b>2005</b> , 144, 191-196	27
1345	High pressure behaviour of KHSO <sub>4</sub> studied by electrical impedance spectroscopy. <b>2005</b> , 136, 16-21	9
1344	Dielectric behaviors of relaxor ferroelectric Pb(Mg <sub>1/2</sub> Nb <sub>1/2</sub> )O <sub>3</sub> 5 % PbTiO <sub>3</sub> : temperature and frequency dependences. <b>2005</b> , 117, 265-270	15
1343	HIGH FREQUENCY LOSS MODELING USING DIELECTRIC RELAXATION. <b>2005</b> , 77, 87-92	3
1342	.	2
1341	Dielectric constant dispersion of yttrium-doped (Ba,Sr)TiO <sub>3</sub> films in the high-frequency (10kHz-7GHz) domain. <b>2005</b> , 87, 232903	7
1340	Effect of alkaline-earth ions on the dynamics of alkali ions in bismuthate glasses. <b>2005</b> , 72,	11
1339	Extracting the spectral density function of a binary composite without a priori assumptions. <b>2005</b> , 71,	29
1338	Cooperative oxygen ion dynamics in Gd <sub>2</sub> Ti <sub>2</sub> ZrO <sub>7</sub> . <b>2005</b> , 71,	45
1337	Relaxation dynamics and colossal magnetocapacitive effect in CdCr <sub>2</sub> S <sub>4</sub> . <b>2005</b> , 72,	48
1336	Glassy behavior of a percolative water-protein system. <b>2005</b> , 71, 031506	16
1335	Implications of the detailed fluctuation theorem for the sources of irreversibility in interfacial charge transfer processes. <b>2005</b> , 72, 056115	
1334	Phase separation in La <sub>2</sub> CuO <sub>4+y</sub> ceramics probed by dielectric measurements. <b>2005</b> , 72,	40
1333	Power-law decay in first-order relaxation processes. <b>2005</b> , 72,	5
1332	Nonlinear and scaling properties of the dielectric response of SrTi <sub>18</sub> O <sub>3</sub> in the quantum paraelectric regime. <b>2005</b> , 71,	28
1331	High-permittivity core/shell structured NiO-based ceramics and their dielectric response mechanism. <b>2005</b> , 72,	79

1330	Scaling of conductivity spectra in the acceptor-doped ferroelectric SrBi <sub>2</sub> Ta <sub>2</sub> O <sub>9</sub> . <b>2005</b> , 72,		15
1329	Dielectric characteristics of spin-coated dielectric films using on-wafer parallel-plate capacitors at microwave frequencies. <b>2005</b> , 1151-1161		27
1328	Terahertz conductivity at the Verwey transition in magnetite. <b>2005</b> , 72,		52
1327	Characterization of insulating particles by dielectric spectroscopy: Case study for CaCO <sub>3</sub> powders. <b>2005</b> , 59, 2842-2849		20
1326	Superferromagnetic domain state of a discontinuous metal insulator multilayer. <b>2005</b> , 72,		30
1325	Frequency-temperature response of ferroelectromagnetic Pb(Fe <sub>1-x</sub> Nb <sub>1-x</sub> )O <sub>3</sub> ceramics obtained by different precursors. Part II. Impedance spectroscopy characterization. <b>2005</b> , 97, 084108		101
1324	Dielectric Response. <b>2006</b> , 187-212		7
1323	Dielectric properties of doping-free NaMn <sub>7</sub> O <sub>12</sub> : Origin of the observed colossal dielectric constant. <b>2006</b> , 74,		18
1322	FREQUENCY DEPENDENCE OF THE DIELECTRIC PROPERTIES AND COERCIVE FIELD OF PbZr <sub>0.4</sub> Ti <sub>0.6</sub> O <sub>3</sub> THIN FILMS. <b>2006</b> , 85, 31-38		4
1321	Scaling of terahertz conductivity at the metal-insulator transition in doped manganites. <b>2006</b> , 73,		11
1320	Impedance spectroscopy of TiO <sub>2</sub> thin films showing resistive switching. <b>2006</b> , 89, 082909		94
1319	Temperature Dependent Dielectric Absorption of MIM Capacitors: RF Characterization and Modeling. <b>2006</b> ,		4
1318	Modelling and simulation of dielectric heterostructures: a physical survey from an historical perspective. <i>Journal Physics D: Applied Physics</i> , <b>2006</b> , 39, 1277-1294	3	149
1317	Colossal magnetocapacitance and colossal magnetoresistance in HgCr <sub>2</sub> S <sub>4</sub> . <b>2006</b> , 96, 157202		129
1316	Investigations of the conduction mechanism and relaxation properties of semiconductor Sm doped a-Se films. <i>Journal Physics D: Applied Physics</i> , <b>2006</b> , 39, 2059-2066	3	28
1315	Electrical conduction and dielectric relaxation in semiconductor SeSm <sub>0.005</sub> . <i>Journal Physics D: Applied Physics</i> , <b>2006</b> , 39, 190-195	3	33
1314	Dynamics of alkyl ammonium intercalants within organically modified montmorillonite: Dielectric relaxation and ionic conductivity. <b>2006</b> , 110, 20143-57		52
1313	Polaron conductivity mechanism in oxalic acid dihydrate: ac conductivity experiment. <b>2006</b> , 74,		8



1312	Experimental study of relaxations in unidirectional piezoelectric composites. <b>2006</b> , 37, 1-8	49
1311	Performance of polyolefin composites containing recycled paper fibers. <b>2006</b> , 17, 954-966	13
1310	Thermal impedance plots of micro-scaled devices. <b>2006</b> , 46, 174-177	23
1309	Microwave characterization of dielectric materials in the temperature range of 90-500K. <b>2006</b> , 36, 65-70	4
1308	A new equation for the description of dielectric losses under microwave irradiation. <i>Journal Physics D: Applied Physics</i> , <b>2006</b> , 39, 2255-2258	3 11
1307	Dielectric Permittivity Enhancement in PZT by Light Doping with Gd. <b>2006</b> , 966, 1	
1306	Finite-difference time-domain simulation of heterostructures with inclusion of arbitrarily complex geometry. <b>2006</b> , 99, 063502	26
1305	Oxygen-vacancy-related dielectric anomaly in CaCu <sub>3</sub> Ti <sub>4</sub> O <sub>12</sub> : Post-sintering annealing studies. <b>2006</b> , 74,	72
1304	Relaxation and hysteresis in a two-dimensional dipolar lattice. <b>2006</b> , 73,	1
1303	Electrical modeling of liquid crystal displays-LCDs. <b>2006</b> , 13, 204-210	22
1302	Changes in functional behavior of 93%Pb(Mg <sub>1/3</sub> Nb <sub>2/3</sub> )O <sub>3</sub> /7%PbTiO <sub>3</sub> thin films induced by ac electric fields. <b>2006</b> , 73,	7
1301	Dynamics of Ag <sup>+</sup> ions in Ag <sub>2</sub> S-doped superionic AgPO <sub>3</sub> glasses. <b>2006</b> , 73,	27
1300	Evidence of secondary relaxations in the dielectric spectra of ionic liquids. <b>2006</b> , 73,	94
1299	Absorption Properties of Materials under Microwave Irradiation. <b>2006</b> ,	
1298	Dielectric spectroscopy analysis of the h-BN ceramic. <i>Journal Physics D: Applied Physics</i> , <b>2007</b> , 40, 6034-6038	7
1297	Relaxation dynamics of Ag <sub>4</sub> Te <sub>3</sub> O <sub>8</sub> glass nanocomposites embedded with Ag <sub>2</sub> S nanoparticles. <b>2007</b> , 127, 044708	3
1296	Charge trapping properties of ultra-thin TiO <sub>2</sub> films on strained-Si. <b>2007</b> , 22, 774-783	9
1295	Mechanical and electrical driving field induced high-frequency dielectric anomalies in ferroelectric systems. <b>2007</b> , 19, 386217	11

1294	Dielectric relaxation mechanism of single crystal and polycrystal bismuth germanate. <b>2007</b> , 102, 034105	10
1293	Finite-element modeling method for the study of dielectric relaxation at high frequencies of heterostructures made of multilayered particle. <b>2007</b> , 102, 124107	17
1292	Electromagnetomechanical coupling characteristics of plastroferrites. <b>2007</b> , 102, 024907	21
1291	Frequency dependence of effective permittivity of carbon nanotube composites. <b>2007</b> , 101, 094106	49
1290	ac and dc percolative conductivity of magnetite-cellulose acetate composites. <b>2007</b> , 75,	14
1289	Influence of thermally induced oxygen order on mobile ion dynamics in $Gd_2(Ti_{0.65}Zr_{0.35})_2O_7$ . <b>2007</b> , 75,	36
1288	Impossibility of pressure-induced crossover from ferroelectric to nonergodic relaxor state in a $Pb(Mg_{1-B}Nb_{2B})_{0.7}Ti_{0.3}O_3$ crystal: Dielectric spectroscopic study. <b>2007</b> , 76,	9
1287	Dielectric anomaly at TN in $LaMnO_3$ as a signature of coupling between spin and orbital degrees of freedom. <b>2007</b> , 76,	14
1286	Modes of periodic domain wall motion in ultrathin ferromagnetic layers. <b>2007</b> , 99, 097203	41
1285	Wait-and-switch relaxation model: relationship between nonexponential relaxation patterns and random local properties of a complex system. <b>2007</b> , 75, 021114	7
1284	Nanostructural origin of the ac conductance in dielectric granular metals: The case study of $Co_{20}(ZrO_2)_{80}$ . <b>2007</b> , 91, 052108	6
1283	Extrinsic contributions to the apparent thickness dependence of the dielectric constant in epitaxial $Pb(Zr,Ti)O_3$ thin films. <b>2007</b> , 75,	45
1282	Properties of highly (100) oriented $Pb(Mg_{1-B},Nb_{2B})O_3BbTiO_3$ films on $LaNiO_3$ bottom electrodes. <b>2007</b> , 91, 232912	14
1281	Calculation of the Relaxation Time of h-BN Based on the Dielectric Data. <b>2007</b> ,	
1280	Microwave dielectric properties of carbon black filled polymers under uniaxial tension. <b>2007</b> , 101, 084111	56
1279	Conductivity spectroscopy in aromatic polyimide from 200to400°C. <b>2007</b> , 91, 122913	29
1278	Dielectric spectroscopy and nonequilibrium phase transitions in $TlGaSe_2$ layered crystals. <b>2007</b> , 22, 843-850	18
1277	Determining the mobility of ions by transient current measurements at high voltages. <b>2007</b> , 99, 086104	23

1276	Correlation between transport, dielectric, and optical properties of oxidized and nonoxidized porous silicon. <b>2007</b> , 75,		14
1275	Modeling of nonlinearities in the capacitance-voltage characteristics of high-k metal-insulator-metal capacitors. <b>2007</b> , 90, 142906		72
1274	Dielectric Properties of Polybutylene Succinate and Polybutylene Succinate Adipate. <b>2007</b> ,		7
1273	. <b>2007</b> , 45, 1271-1281		23
1272	Thermal Characterization of Electronic Packages Using the Nyquist Plot of the Thermal Impedance. <b>2007</b> , 30, 660-665		18
1271	Geometry-Dependent Quality Factors in $\text{Ba}_{0.5}\text{Sr}_{0.5}\text{TiO}_3$ Parallel-Plate Capacitors. <b>2007</b> , 55, 410-417		4
1270	Influence of dopant on dielectric properties of polyaniline weakly doped with dichloro and trichloroacetic acids. <i>Journal Physics D: Applied Physics</i> , <b>2007</b> , 40, 4347-4354	3	34
1269	Dielectric relaxation in slightly hydrated bovine tendon collagen. <i>Journal Physics D: Applied Physics</i> , <b>2007</b> , 40, 25-30	3	48
1268	Impedance spectroscopy of epitaxial multiferroic thin films. <b>2007</b> , 75,		110
1267	Experimental study on dielectric relaxation in alfa fiber reinforced epoxy composites. <b>2007</b> , 106, 3631-3640		47
1266	Dielectric and conductivity measurements as proxy method to monitor contamination in sandstone. <b>2007</b> , 142, 520-5		27
1265	Electromagnetic measurements on Martian soil analogs: Implications for MARSIS and SHARAD radars in detecting subsoil water. <b>2007</b> , 55, 193-202		8
1264	Biomonitoring of environmental pollution using dielectric properties of tree leaves. <b>2007</b> , 133, 69-78		27
1263	Complex permittivity characterization of benzocyclobutene for terahertz applications. <b>2008</b> , 85, 2276-2281		75
1262	Characteristic Instabilities in HfAlO Metal/Insulator/Metal Capacitors Under Constant-Voltage Stress. <b>2008</b> , 55, 1359-1365		10
1261	Tuning the Li Diffusivity of Poor Ionic Conductors by Mechanical Treatment: High Li Conductivity of Strongly Defective LiTaO <sub>3</sub> Nanoparticles. <b>2008</b> , 112, 9291-9300		89
1260	Electric Techniques. <b>2008</b> , 5, 209-268		3
1259	ac conductivity in Gd doped Pb(Zr <sub>0.53</sub> Ti <sub>0.47</sub> )O <sub>3</sub> ceramics. <b>2008</b> , 104, 073511		26

1258	Charge transport and mass transport in imidazolium-based ionic liquids. <b>2008</b> , 77, 051202	156
1257	Dielectric relaxation in carbon black-epoxy composite materials. <b>2008</b> , 103, 094103	67
1256	Temperature-dependent dielectric properties of slightly hydrated horn keratin. <b>2008</b> , 42, 292-7	20
1255	Investigation of the electronic structure of the charge-ordered phase in epitaxial and polycrystalline $\text{La}_{1-x}\text{Ca}_x\text{MnO}_3$ ( $x=0.55,0.67$ ) perovskite manganites. <b>2008</b> , 77,	33
1254	Universal electromagnetic waves in dielectric. <b>2008</b> , 20, 175223	28
1253	Electrical conduction processes in polyimide-teflon/spl reg/ FEP films - II. <b>2008</b> , 15, 671-677	2
1252	Study on the dielectric properties of Ag doped ZnO by Universal Power Law <b>2008</b> ,	
1251	Effects of Crystallinity on Thermally Stimulated Current and Complex Permittivity of Poly(L-lactide). <b>2008</b> ,	6
1250	Electric-field-induced submicrosecond resistive switching. <b>2008</b> , 78,	32
1249	Dielectric spectroscopic measurements on transformer oil-paper insulation under controlled laboratory conditions. <b>2008</b> , 15, 1100-1111	95
1248	Reliability of Dielectric Less Electrostatic Actuators in RF-MEMS Ohmic Switches. <b>2008</b> ,	
1247	Integrated (Ba,Sr)TiO <sub>3</sub> Thin-Film Technology for RF and Microwave Applications. <b>2008</b> , 1075, 1	
1246	Fractional equations of Curie von Schweidler and Gauss laws. <b>2008</b> , 20, 145212	18
1245	Hopping conduction and low-frequency dielectric relaxation in 5mol% Mn doped (Pb,Sr)TiO <sub>3</sub> films. <b>2008</b> , 104, 104113	38
1244	Reliability of Dielectric Less Electrostatic Actuators in RF-MEMS Ohmic Switches. <b>2008</b> ,	4
1243	Cation size effects in oxygen ion dynamics of highly disordered pyrochlore-type ionic conductors. <b>2008</b> , 78,	46
1242	Physical aging of plastoferrites under tensile stress and its effect on microwave properties. <b>2008</b> , 104, 064108	13
1241	Magnetocapacitance in nonmagnetic composite media. <b>2008</b> , 101, 166602	52

1240	Modified Lampert triangle in an organic field effect transistor with traps. <b>2008</b> , 78,		7
1239	Temperature effect on dielectric properties of carbon black filled epoxy polymer composites. <b>2008</b> , 41, 215-220		14
1238	Temperature Dependence of Complex Permittivity in Biodegradable Polybutylene Succinate. <b>2008</b> , 128, 647-651		17
1237	Far-infrared response of free charge carriers localized in semiconductor nanoparticles. <b>2009</b> , 79,		90
1236	Spatially resolved spectroscopic mapping of polarization reversal in polycrystalline ferroelectric films: crossing the resolution barrier. <b>2009</b> , 103, 057601		27
1235	Dielectrical properties of metal-insulator-metal aluminum nitride structures: Measurement and modeling. <b>2009</b> , 105, 044111		26
1234	ac conductance in granular insulating Co-ZrO <sub>2</sub> thin films: A universal response. <b>2009</b> , 79,		6
1233	Influence of the electrode material on HfO <sub>2</sub> metal-insulator-metal capacitors. <b>2009</b> , 27, 286		24
1232	Dielectric relaxation in particle-filled polymer: Influence of the filler particles and thermal treatments. <b>2009</b> , 105, 054108		18
1231	Impact of dipole-induced dielectric relaxation on high-frequency performance in La-incorporated HfSiON/metal gate nMOSFET. <b>2009</b> ,		
1230	The robustness of the emergent scaling property of randomRCnetwork models of complex materials. <i>Journal Physics D: Applied Physics</i> , <b>2009</b> , 42, 064001	3	19
1229	Mn-Doped BaTiO <sub>3</sub> Thin Film Sintered Using Nanocrystals and Its Dielectric Properties. <b>2009</b> , 48, 111408		8
1228	Dispersive capacitance and conductance across the phase transition boundary in metal-vanadium oxide-silicon devices. <b>2009</b> , 106, 034101		13
1227	II. Electrical Properties of Ni/Silica Gel and Pt/Alumina Catalysts in Relation to Catalytic Activity. <b>2009</b> , 27, 1572-1591		11
1226	Application of the Maxwell-Wagner-Olson effective medium theory to the analysis of the interfacial polarization relaxations in conducting composite films. <i>Journal Physics D: Applied Physics</i> , <b>2009</b> , 42, 015302	3	10
1225	Electrical properties of Ni/silica gel and Pt/Alumina catalysts in relation to metal content in the frequency domain. <b>2009</b> , 113, 790-796		16
1224	Electrical properties and mineralogical investigation of Egyptian iron ore deposits. <b>2009</b> , 114, 313-318		23
1223	Charging in Dielectricless Capacitive RF-MEMS Switches. <b>2009</b> , 57, 231-236		60

1222	. <b>2009</b> , 56, 399-407	26
1221	Copolymerization of Cyanovinyl acetate with acrylonitrile and methacrylonitrile: Synthesis, characterization, and study of their dielectric behavior. <b>2009</b> , 114, 1094-1104	7
1220	Quasi-static and dynamic piezoelectric d33 coefficients of irradiation cross-linked polypropylene ferroelectrets. <b>2009</b> , 44, 2459-2465	16
1219	Electrical and mechanical properties of alkali barium titanium alumino borosilicate glass-ceramics containing strontium or magnesium. <b>2009</b> , 20, 507-516	21
1218	Effect of electrode contact impedance on A.C. electrical properties of a wet hematite sample. <b>2009</b> , 30, 265-276	32
1217	Fractional integro-differential equations for electromagnetic waves in dielectric media. <b>2009</b> , 158, 355-359	83
1216	Relaxation studies of spray deposited Bi <sub>2</sub> Co <sub>0.1</sub> V <sub>0.9</sub> O <sub>5.35</sub> solid electrolyte thin films on stainless steel substrate. <b>2009</b> , 15, 453-458	2
1215	Thermal effect of magma intrusion on the electrical properties of magnetic rocks from Hammamat sediments, Cairo, Egypt. <b>2009</b> , 57, 141-149	21
1214	Saturation effect on electrical properties of hematitic sandstone in the audio frequency range using non-polarizing electrodes. <b>2009</b> , 57, 1091-1100	29
1213	Studies of dielectric relaxation in natural fiber/polymer composites. <b>2009</b> , 67, 717-722	50
1212	Impedance of solid electrolyte systems. <b>2009</b> , 45, 11-24	14
1211	Relaxation processes in the paraelectric phase of ceramic oxides with a perovskite structure. <b>2009</b> , 51, 1455-1457	1
1210	Differential equations with fractional derivative and universal map with memory. <b>2009</b> , 42, 465102	41
1209	Electrical, thermophysical and micromechanical properties of ethylene-vinyl acetate elastomer composites with surface modified BaTiO <sub>3</sub> nanoparticles. <i>Journal Physics D: Applied Physics</i> , <b>2009</b> , 42, 245407	64
1208	Polaron relaxation and hopping conductivity in LaMn <sub>1-x</sub> FexO <sub>3</sub> . <b>2009</b> , 79,	47
1207	Electrical conductivity and dielectric properties of polypyrrole/Na <sup>+</sup> montmorillonite (PPy/Na <sup>+</sup> MMT) clay nanocomposites. <i>Journal Physics D: Applied Physics</i> , <b>2009</b> , 42, 095415	3 35
1206	Variable-temperature measurements of the dielectric relaxation in carbon black loaded epoxy composites. <b>2009</b> , 105, 124102	26
1205	Investigation of voltage dependent relaxation, charge trapping, and stress induced leakage current effects in HfO <sub>2</sub> /Dy <sub>2</sub> O <sub>3</sub> gate stacks grown on Ge (100) substrates. <b>2009</b> , 27, 439	12

1204	Electrode polarization and charge transport at solid interfaces. <b>2009</b> , 80,	202
1203	Dielectric resonances at optical frequencies using metal nanoshells. <i>Journal Physics D: Applied Physics</i> , <b>2009</b> , 42, 135420	3 8
1202	Kinetics and relaxation of electroresistance in transition metal oxides: Model for resistive switching. <b>2009</b> , 80,	8
1201	High dielectric loss and its monotonic dependence of conducting-dominated multiwalled carbon nanotubes/silica nanocomposite on temperature ranging from 373 to 873 K in X-band. <b>2009</b> , 94, 233110	267
1200	Evolution of electrical parameters of dielectric-less ohmic RF-MEMS switches during continuous actuation stress. <b>2009</b> ,	16
1199	SILC decay in Ge-based MOS devices with La <sub>2</sub> O <sub>3</sub> gate dielectrics subjected to constant voltage stress. <b>2009</b> ,	1
1198	A mechanistic model for the spectral induced polarization of clay materials. <b>2009</b> , 114,	131
1197	Pulsed electric field induced changes in dielectric properties of biological cells. <b>2009</b> ,	1
1196	Colloquium: Understanding ion motion in disordered solids from impedance spectroscopy scaling. <b>2009</b> , 81, 999-1014	154
1195	Effect Of Trapping On Dielectric Conduction Mechanisms Of ULK/Cu Interconnects. <b>2009</b> , 1156, 1	
1194	Complex impedance spectroscopy and ionic transport properties of natural leucite, K <sub>0.90</sub> Na <sub>0.08</sub> [Al <sub>0.98</sub> Si <sub>2.02</sub> ]O <sub>6</sub> , as a function of temperature and pressure. <b>2010</b> , 74, 507-519	8
1193	Nanoscale ordering and multiferroic behavior in Pb(Fe <sub>1/2</sub> Ta <sub>1/2</sub> )O <sub>3</sub> . <b>2010</b> , 82,	37
1192	Terahertz spectroscopy of low-energy excitations in charge-ordered La <sub>0.25</sub> Ca <sub>0.75</sub> MnO <sub>3</sub> . <b>2010</b> , 81,	21
1191	Dielectric properties of carbon black and carbonyl iron filled epoxy-silicone resin coating. <b>2010</b> , 45, 1885-1888	25
1190	Tri-Level Resistive Switching in Metal-Nanocrystal-Based $\text{Al}_2\text{O}_3/\text{SiO}_2$ Gate Stack. <b>2010</b> , 57, 3001-3005	6
1189	Improved dielectric properties of lead lanthanum zirconate titanate thin films on copper substrates. <b>2010</b> , 64, 22-24	17
1188	Wideband frequency and in situ characterization of ultra thin ZrO <sub>2</sub> and HfO <sub>2</sub> films for integrated MIM capacitors. <b>2010</b> , 87, 301-305	16
1187	On a thermodynamical model for dielectric relaxation phenomena. <b>2010</b> , 405, 175-179	16

1186	A.c. conductivity behavior of LiNiVO <sub>4</sub> ceramics. <b>2010</b> , 405, 1706-1708	5
1185	Modified isothermal discharge current theory and its application in the determination of trap level distribution in polyimide films. <b>2010</b> , 68, 243-248	43
1184	BaxSr1-xTi1.02O3 metal-insulator-metal capacitors on planarized alumina substrates. <b>2010</b> , 518, 2854-2859	4
1183	Thermally activated conduction mechanisms in Silicon Nitride MIS structures. <b>2010</b> , 518, 2357-2360	2
1182	SILC decay in La <sub>2</sub> O <sub>3</sub> gate dielectrics grown on Ge substrates subjected to constant voltage stress. <b>2010</b> , 54, 979-984	9
1181	A shortcut to inverse Fourier transforms: Approximate reconstruction of transient heating curves from sparse frequency domain data. <b>2010</b> , 49, 1319-1332	5
1180	Hydrothermal Barium Titanate Thin-Film Characteristics and their Suitability as Decoupling Capacitors. <b>2010</b> , 93, 2764-2770	7
1179	Dielectric measurements in large frequency and temperature ranges of an aromatic polymer. <b>2010</b> , 49, 10401	15
1178	Measurement of dielectric losses in amorphous thin films at gigahertz frequencies using superconducting resonators. <b>2010</b> , 23, 075008	13
1177	Ionic conductivity of nanocrystalline yttria-stabilized zirconia: Grain boundary and size effects. <b>2010</b> , 81,	69
1176	Overshooting and undershooting subordination scenario for fractional two-power-law relaxation responses. <b>2010</b> , 81, 041123	33
1175	Charge disproportionation in TlGaSe <sub>2</sub> crystals detected by dielectric spectroscopy. <b>2010</b> , 108, 074114	8
1174	A comparison between physical properties of carbon black-polymer and carbon nanotubes-polymer composites. <b>2010</b> , 108, 074108	61
1173	Multiphonon-induced charge trapping-detrapping and damage in insulators. <b>2010</b> , 81,	12
1172	Fabrication of fluoropolymer piezoelectrets by using rigid template: Structure and thermal stability. <b>2010</b> , 108, 064113	34
1171	Structural, dielectric, and magnetic properties of La <sub>0.8</sub> Bi <sub>0.2</sub> Fe <sub>1-x</sub> MnxO <sub>3</sub> (0.0 ≤ x ≤ 0.4) multiferroics. <b>2010</b> , 107, 103916	56
1170	Relaxation dynamics in covalently bonded organic monolayers on silicon. <b>2010</b> , 82,	15
1169	Label-free toxin detection by means of time-resolved electrochemical impedance spectroscopy. <b>2010</b> , 10, 655-69	15



1168	Anomalous diffusion with under- and overshooting subordination: a competition between the very large jumps in physical and operational times. <b>2010</b> , 82, 051120	14
1167	Characterization of solid complex multiphase systems based on oscillatory photon correlation spectroscopy. <b>2010</b> , 35, 3754-6	5
1166	Phase coexistence and multiple dielectric relaxations in the single layered manganite Nd <sub>0.22</sub> Sr <sub>1.78</sub> MnO <sub>4</sub> . <b>2010</b> , 107, 014108	8
1165	Fractional dissipative standard map. <b>2010</b> , 20, 023127	33
1164	Electric modulus-based analysis of the dielectric relaxation in carbon black loaded polymer composites. <b>2010</b> , 107, 124111	55
1163	Piezoelectricity and dynamic characteristics of laminated fluorocarbon films. <b>2010</b> , 17, 1001-1007	8
1162	Water-titanate intercalated nanotubes: fabrication, polarization, and giant dielectric property. <b>2010</b> , 12, 12638-46	12
1161	Low-frequency electrical properties of ice-silicate mixtures. <b>2010</b> , 114, 6065-73	48
1160	Charging and discharging characteristics of metal nanocrystals in degraded dielectric stacks. <b>2010</b> ,	3
1159	Frequency Effect on Voltage Linearity of $\text{ZrO}_2$ -Based RF Metal/Insulator/Metal Capacitors. <b>2010</b> , 31, 114-116	27
1158	Mechanisms leading to nonlinear electrical response of a nano p-SiC/silicone rubber composite. <b>2010</b> , 17, 1687-1696	65
1157	Influence of absorbed moisture on the dielectric properties of epoxy resins. <b>2010</b> ,	5
1156	Dielectric response of transformer insulation - comparison of time domain and frequency domain measurements. <b>2010</b> ,	4
1155	Study of the charge leakage of dual layer Pt metal nanocrystal-based high- $\kappa$ SiO <sub>2</sub> flash memory cell - a relaxation current point of view. <b>2011</b> ,	
1154	Observation and Effective Suppression of Dielectric Relaxation in Charge-Trap NAND Flash Memory. <b>2011</b> ,	
1153	Charge Transport Through Thin Amorphous Titanium and Tantalum Oxide Layers. <b>2011</b> , 158, P65	20
1152	Dielectric relaxation behavior of acceptor (Mg)-doped BaTiO <sub>3</sub> . <b>2011</b> , 109, 084117	19
1151	AC conductance measurement and analysis of the conduction processes in HfO <sub>x</sub> based resistive switching memory. <b>2011</b> , 99, 232105	28

1150	Electrical modulus analysis on the Ni/CCTO/PVDF system near the percolation threshold. <i>Journal Physics D: Applied Physics</i> , <b>2011</b> , 44, 475305	3	35
1149	Dielectric relaxation spectroscopy for evaluation of the influence of solvent dynamics on ion transport in succinonitrile-salt plastic crystalline electrolytes. <b>2011</b> , 115, 2148-54		16
1148	Impedance spectroscopy analysis of Ba <sub>0.7</sub> Sr <sub>0.3</sub> TiO <sub>3</sub> /La <sub>0.7</sub> Sr <sub>0.3</sub> MnO <sub>3</sub> heterostructure. <i>Journal Physics D: Applied Physics</i> , <b>2011</b> , 44, 105302	3	73
1147	Transport, electronic, and structural properties of nanocrystalline CuAlO <sub>2</sub> delafossites. <b>2011</b> , 83,		32
1146	A Study on the Dielectric Behaviour of Epoxy/Hafnium Oxide Nanopowder Composites. <b>2011</b> , 20, 096369351102000		
1145	Complex Permittivity of Graphite, Carbon Black and Coal Powders in the Ranges of X-band Frequencies (8.2 to 12.4 GHz) and between 1 and 10 GHz. <b>2011</b> , 51, 1766-1772		94
1144	Ultra wide band frequency characterization of integrated TiTaO-based metal-insulator-metal devices. <b>2011</b> , 110, 044110		7
1143	Electrical properties of perovskite-like compounds in the Bi <sub>2</sub> O <sub>3</sub> -Fe <sub>2</sub> O <sub>3</sub> -TiO <sub>2</sub> system. <b>2011</b> , 47, 420-425		19
1142	Investigation of charge trapping and breakdown characteristics of sputtered-Y <sub>2</sub> O <sub>3</sub> on n-GaAs substrates. <b>2011</b> , 520, 47-52		3
1141	Anomaly diffuse and dielectric relaxation in strontium doped lanthanum molybdate. <b>2011</b> , 46, 2502-2505		7
1140	. <b>2011</b> , 58, 3549-3558		10
1139	. <b>2011</b> , 53, 943-949		27
1138	Piezoelectric coefficients of cross-linked polypropylene films stretched at elevated temperatures. <b>2011</b> , 69, 554-558		17
1137	Studies of dielectric relaxation in natural fibres reinforced unsaturated polyester. <b>2011</b> , 46, 3698-3707		29
1136	Magnetic and Dielectric Properties of R <sub>2</sub> CuTiO <sub>6</sub> Compounds (R=Y, La, Pr and Nd). <b>2011</b> , 24, 1829-1838		13
1135	Studies on grain boundary effects in spray deposited BICOVOX 0.1 films on platinum-coated stainless steel substrate. <b>2011</b> , 17, 69-74		2
1134	Relaxation studies of bulk samarium doped ceria electrolyte. <b>2011</b> , 17, 61-68		3
1133	Effect of tacticity on the dielectric properties of polystyrene. <b>2011</b> , 6, 299-303		13

1132	Effects of crystallinity on dielectric properties of poly(L-lactide). <b>2011</b> , 94, 1-8	14
1131	Phase transitions in CsHSO <sub>4</sub> up to 2.5GPa: Impedance spectroscopy under pressure. <b>2011</b> , 72, 236-244	6
1130	Vanadium-substituted porous manganese oxides with Li-ion intercalation properties. <b>2011</b> , 196, 2149-2154	32
1129	Electrical characterization of aluminium oxide/aluminium thin film composites by impedance spectroscopy. <b>2011</b> , 51, 1225-1229	3
1128	Effect of La substitution on conductivity and dielectric properties of Bi <sub>1-x</sub> La <sub>x</sub> FeO <sub>3</sub> ceramics: An impedance spectroscopy analysis. <b>2011</b> , 406, 2669-2677	88
1127	Effects of ZnO on the dielectric, conductive and piezoelectric properties of low-temperature-sintered PMnN-PZT based hard piezoelectric ceramics. <b>2011</b> , 31, 2013-2022	31
1126	Low-temperature polaronic relaxations with variable range hopping conductivity in FeTiMO <sub>6</sub> (M=Ta,Nb,Sb). <b>2011</b> , 84,	38
1125	Current instabilities in rare-earth oxides-HfO <sub>2</sub> gate stacks grown on germanium based metal-oxide-semiconductor devices due to Maxwell/Wagner instabilities and dielectrics relaxation. <b>2011</b> , 29, 01AB06	3
1124	Origin and stability of the dipolar response in a family of tetragonal tungsten bronze relaxors. <b>2011</b> , 83,	36
1123	Relaxation dynamics of multiferroic domain walls in DyMnO <sub>3</sub> with cycloidal spin order. <b>2011</b> , 83,	16
1122	Localized charge trapping and lateral charge diffusion in metal nanocrystal-embedded High- $\kappa$ /SiO <sub>2</sub> gate stack. <b>2011</b> , 99, 222102	5
1121	Study of automatic recovery on the metal nanocrystal-based Al <sub>2</sub> O <sub>3</sub> /SiO <sub>2</sub> gate stack. <b>2011</b> , 98, 083504	
1120	Experimental evidence of the role of compound counting processes in random walk approaches to fractional dynamics. <b>2011</b> , 83, 051102	4
1119	Zoom-in front-end circuit for high-performance capacitive displacement sensors. <b>2011</b> ,	
1118	Scaling of low-temperature conductivity spectra of BaSn <sub>1-x</sub> Nb <sub>x</sub> O <sub>3</sub> ( $x \leq 0.100$ ): Temperature and compositional-independent conductivity. <b>2011</b> , 84,	28
1117	Interface and Bulk Properties of High-K Gadolinium and Neodymium Oxides on Silicon. <b>2011</b> , 276, 167-178	3
1116	Superiority of syndiotactic polystyrene as an electrical insulating polymer. <b>2011</b> ,	2
1115	EFFECT OF BARIUM ON DIELECTRIC, FERROELECTRIC, IMPEDANCE AND ELECTRICAL MODULUS PROPERTIES OF Bi <sub>0.5</sub> Na <sub>0.5</sub> TiO <sub>3</sub> CERAMICS. <b>2011</b> , 25, 2931-2948	7

1114	Time and frequency domains dc conductivity analysis in thin dielectric films at high temperature. <i>Journal Physics D: Applied Physics</i> , <b>2011</b> , 44, 105402	3	12
1113	Microstructure and electrical properties of LaNiO <sub>3</sub> thin films by RF sputtering for the growth of (Pb,La)(Zr,Ti)O <sub>3</sub> films on silicon and nickel substrates. <b>2012</b> , 30, 061505		1
1112	Temperature control of ion guiding through insulating capillaries. <b>2012</b> , 86,		45
1111	Improved properties of barium strontium titanate thin films grown on copper foils by pulsed laser deposition using a self-buffered layer. <i>Journal Physics D: Applied Physics</i> , <b>2012</b> , 45, 175304	3	10
1110	Effect of plasma deposited thin carbon layer on dielectric characteristics of Au-PI-Au structures. <b>2012</b> , 19, 2137-2144		1
1109	Effect of electrode resistance on dielectric and transport properties of multiferroic superlattice: A Impedance spectroscopy study. <b>2012</b> , 2, 032136		43
1108	Temperature-dependent relaxation current on single and dual layer Pt metal nanocrystal-based Al <sub>2</sub> O <sub>3</sub> /SiO <sub>2</sub> gate stack. <b>2012</b> , 112, 104503		1
1107	Dielectric dispersion analysis of copolymer L-B thin film. <b>2012</b> , 57, 20302		
1106	High pressure effect on the dielectric properties of rock-salt CdS. <b>2012</b> , 111, 113718		
1105	Non-volatile gated variable resistor based on doped La <sub>2</sub> CuO <sub>4</sub> + $\delta$ and SrTiO <sub>3</sub> heterostructures. <b>2012</b> , 111, 056101		2
1104	An alternative dielectric model for low and high frequencies: A non-equilibrium thermodynamic approach. <b>2012</b> , 37,		10
1103	Use of Impedance Spectroscopy for Characterization of Modified Membranes. <b>2012</b> , 21-40		2
1102	Electrical Characterization of Advanced MIM Capacitors With $\{\text{ZrO}_2\}$ Insulator for High-Density Packaging and RF Applications. <b>2012</b> , 2, 502-509		11
1101	Dielectric frequency response of oil-paper composite insulation modified by nanoparticles. <b>2012</b> , 19, 510-520		30
1100	Limit on the electron electric dipole moment using paramagnetic ferroelectric Eu <sub>0.5</sub> Ba <sub>0.5</sub> TiO <sub>3</sub> . <b>2012</b> , 109, 193003		34
1099	Investigation of trap states and mobility in organic semiconductor devices by dielectric spectroscopy: Oxygen-doped P3HT:PCBM solar cells. <b>2012</b> , 86,		10
1098	The Effect of Temperature on Complex Permittivity and Microwave Absorption Properties of an Ilmenite Concentrate at 2450MHz. <b>2012</b> , 741-750		
1097	Dielectric properties of nanopowder dispersions in paraffin oil. <b>2012</b> , 19, 1502-1507		51

1096	High temperature breakdown strength and voltage endurance characterization of nanofilled polyamideimide. <b>2012</b> , 19, 2090-2101	18
1095	Dielectric properties of Ba(Zn <sub>1/3</sub> Ta <sub>2/3</sub> )O <sub>3</sub> thin films on Pt-coated Si substrates. <b>2012</b> , 522, 112-116	7
1094	Study of field driven electroluminescence in colloidal quantum dot solids. <b>2012</b> , 111, 113701	30
1093	Dielectric properties of (Bi <sub>0.9</sub> La <sub>0.1</sub> ) <sub>2</sub> NiMnO <sub>6</sub> thin films: Determining the intrinsic electric and magnetoelectric response. <b>2012</b> , 86,	23
1092	Dielectric response of epitaxially strained CoFe <sub>2</sub> O <sub>4</sub> spinel thin films. <b>2012</b> , 86,	22
1091	Exploring the dielectric behaviour of nano-structured Al <sup>3+</sup> doped BiFeO <sub>3</sub> ceramics synthesized by auto ignition process. <b>2012</b> , 530, 63-70	34
1090	Impedance spectroscopic and dielectric analysis of Ba <sub>0.7</sub> Sr <sub>0.3</sub> TiO <sub>3</sub> thin films. <b>2012</b> , 529, 84-88	31
1089	Magnetite (Fe <sub>3</sub> O <sub>4</sub> ): a new variant of relaxor multiferroic?. <b>2012</b> , 24, 086007	33
1088	Phthalocyanine with a giant dielectric constant. <b>2012</b> , 41, 3773-9	17
1087	Electronic conduction and microstructure in polymer composites filled with carbonaceous particles. <b>2012</b> , 112, 034118	24
1086	Effect of Mn doping on the temperature-dependent anomalous giant dielectric behavior of CaCu <sub>3</sub> Ti <sub>4</sub> O <sub>12</sub> . <b>2012</b> , 85,	50
1085	Fractional power-law spectral response of CaCu <sub>3</sub> Ti <sub>4</sub> O <sub>12</sub> dielectric: Many-body effects. <b>2012</b> , 101, 062908	6
1084	Dynamic piezoresponse force microscopy: Spatially resolved probing of polarization dynamics in time and voltage domains. <b>2012</b> , 112, 052021	28
1083	Understanding S-Shaped Current/Voltage Characteristics in Organic Solar Cells Containing a TiO <sub>x</sub> Interlayer with Impedance Spectroscopy and Equivalent Circuit Analysis. <b>2012</b> , 116, 16333-16337	100
1082	Properties of aluminium oxide thin films deposited in high effective reactive pulsed magnetron sputtering process. <b>2012</b> , 30, 323-328	1
1081	Direct estimation of the distribution of relaxation times from induced-polarization spectra using a Fourier transform analysis. <b>2012</b> , 10, 517-531	25
1080	Dielectric properties of poly(phenylene sulfide) as a function of temperature and frequency. <b>2012</b> , 7, 116-120	4
1079	Domain-wall dynamics coupled to proton motion in a hydrogen-bonded organic ferroelectric. <b>2012</b> , 85,	7

1078	Magnetoimpedance spectroscopy of epitaxial multiferroic thin films. <b>2012</b> , 86,	74
1077	A dielectric model of self-assembled monolayer interfaces by capacitive spectroscopy. <b>2012</b> , 28, 9689-99	68
1076	Structure, spectroscopic and piezoelectric properties of BNBT nanocrystalline ceramics. <b>2012</b> , 86, 625-634	4
1075	Electrical Properties of Pb <sub>0.92</sub> La <sub>0.08</sub> Zr <sub>0.52</sub> Ti <sub>0.48</sub> O <sub>3</sub> Thin Films Grown on SrRuO <sub>3</sub> Buffered Nickel and Silicon Substrates by Chemical Solution Deposition. <b>2012</b> , 9, 45-51	1
1074	On the Analysis of Cd <sub>2</sub> Nb <sub>2</sub> O <sub>7</sub> Dielectric Dispersion. <b>2012</b> , 25, 15-21	1
1073	GPR detectability of rocks in a Martian-like shallow subsoil: A numerical approach. <b>2012</b> , 62, 31-40	16
1072	In situ dielectric spectroscopy for water detection on the lunar surface. <b>2012</b> , 65, 76-82	3
1071	Magnetic and dielectric properties of alkaline earth Ca <sup>2+</sup> and Ba <sup>2+</sup> ions co-doped BiFeO <sub>3</sub> nanoparticles. <b>2012</b> , 324, 1483-1487	38
1070	Power-Efficient High-Speed and High-Resolution Capacitive-Sensor Interface for Subnanometer Displacement Measurements. <b>2012</b> , 61, 1315-1322	22
1069	Dielectric properties of polypyrrole/pillared clay nanocomposites. <b>2012</b> , 54, 401-406	8
1068	A percolating membrane with superior polarization and power retention for rechargeable energy storage. <b>2012</b> , 24, 76-81, 75	7
1067	Effect of humidity on the complex permittivity of epoxy-based nanodielectrics with metal oxide fillers. <b>2013</b> , 23, 846-852	6
1066	Electrical properties and geochemistry of carbonate rocks from the Qasr El-Sagha Formation, El-Faiyum, Egypt. <b>2013</b> , 61, 630-644	15
1065	Characterization of UV-irradiated Lexan polycarbonate films. <b>2013</b> , 22, 341-349	21
1064	Multivariate analysis of the dielectric response of materials modeled using networks of resistors and capacitors. <b>2013</b> , 20, 995-1008	9
1063	The equivalent circuits for polaronic relaxation: Taking the LaNi <sub>3</sub> /4Mo <sub>1</sub> /4O <sub>3</sub> as a model sample. <b>2013</b> , 31, 75-80	
1062	Dielectric properties of polyamide-imide. <i>Journal Physics D: Applied Physics</i> , <b>2013</b> , 46, 185302	3 15
1061	Dielectric properties of MSWI bottom ash for non-invasive monitoring of moisture. <b>2013</b> , 185, 7053-63	2

1060	Solvent-Free Nanocomposite Colloidal Fluids with Highly Integrated and Tailored Functionalities: Rheological, Ionic Conduction, and Magneto-Optical Properties. <b>2013</b> , 25, 3834-3843		21
1059	Growth, structural, thermal, dielectric, mechanical and optical characterization of 2, 3-Dimethoxy-10-oxostrychnidinium hydrogen oxalate dihydrate single crystal. <b>2013</b> , 383, 43-50		14
1058	Effect of temperature on dielectric property and microwave heating behavior of low grade Panzihua ilmenite ore. <b>2013</b> , 23, 3462-3469		25
1057	A study of random resistor-capacitor-diode networks to assess the electromagnetic properties of carbon nanotube filled polymers. <b>2013</b> , 103, 243104		18
1056	Origin of colossal permittivity in BaTiO <sub>3</sub> via broadband dielectric spectroscopy. <b>2013</b> , 113, 024102		70
1055	Out-of-Plane Carrier Transport in Conjugated Polymer Thin Films: Role of Morphology. <b>2013</b> , 117, 9590-9597		14
1054	Effect of Zn doping on structural, magnetic and dielectric properties of LaFeO <sub>3</sub> synthesized through sol-gel auto-combustion process. <b>2013</b> , 48, 4506-4512		87
1053	Specific features of the dielectric spectrum of CaCu <sub>3</sub> Ti <sub>4</sub> O <sub>12</sub> in the low-frequency range. <b>2013</b> , 55, 1651-1654		5
1052	From capacitive to tunnelling conduction through annealing in metal-insulating granular films: the role of ultra-small particles. <i>Journal Physics D: Applied Physics</i> , <b>2013</b> , 46, 495304	3	3
1051	Dielectric frequency response of oil-paper composite insulation with transient moisture distribution. <b>2013</b> , 20, 1380-1387		16
1050	Interpenetrating network formation in isotactic polypropylene/graphene composites. <b>2013</b> , 54, 3680-3690		36
1049	Magnetic, dielectric and magnetoelectric properties of CoFe <sub>2</sub> O <sub>4</sub> Bi <sub>0.85</sub> La <sub>0.15</sub> FeO <sub>3</sub> multiferroic composites. <b>2013</b> , 579, 187-191		23
1048	Lithium Thiophosphate Glasses and Glass-ceramics as Solid Electrolytes: Processing, Microstructure, and Properties. <b>2013</b> , 4, 414-425		34
1047	Power-Law Relaxation and Cumulative Information. <b>2013</b> , 153, 479-485		2
1046	Dielectric and impedance spectroscopy of zirconium modified (Na <sub>0.5</sub> Bi <sub>0.5</sub> )TiO <sub>3</sub> ceramics. <b>2013</b> , 39, 5695-5704		99
1045	A correlation between the flashover voltage and the electrical bulk conductivities AC and DC on silicone rubber insulator during thermal ageing. <b>2013</b> ,		1
1044	Study of dielectric properties of composite insulators for use in medium voltage overhead lines. <b>2013</b> , 71, 892-897		4
1043	A new measurement set-up to investigate the charge trapping phenomena in RF MEMS packaged switches. <b>2013</b> ,		6

1042	Ionic semiconductor: DC and AC conductivity of anilinium tetrathiafulvalene-2-carboxylate. <b>2013</b> , 42, 3821-6	6
1041	Metallopolymeric structures containing highly flexible siloxane sequence. <b>2013</b> , 54, 43-53	17
1040	Wall-Voltage Stability in AC-PDP Dielectric Barrier Discharges. <b>2013</b> , 41, 159-164	5
1039	Effects of carbon nanotubes aspect ratio on the qualitative and quantitative aspects of frequency response of electrical conductivity and dielectric permittivity in the carbon nanotube/polymer composites. <b>2013</b> , 54, 105-112	89
1038	Polaron relaxation and non-ohmic behavior in CaCu <sub>3</sub> Ti <sub>4</sub> O <sub>12</sub> ceramics with different cooling methods. <b>2013</b> , 139, 844-850	58
1037	Electrical conduction behavior and hopping rates estimate of cadmium zinc telluride single crystal. <b>2013</b> , 372, 175-179	6
1036	Sintering behavior and dielectric properties of KCa <sub>2</sub> Nb <sub>3</sub> O <sub>10</sub> ceramics. <b>2013</b> , 33, 907-911	11
1035	Microstructure and dielectric relaxation of dipolar defects in Mn-doped (1-x)Pb(Mg <sub>1/3</sub> Nb <sub>2/3</sub> )O <sub>3</sub> -xPbTiO <sub>3</sub> single crystals. <b>2013</b> , 69, 377-380	31
1034	Electrical behavior of an octahedral layered OL-1-type manganese oxide material. <b>2013</b> , 19, 201-214	8
1033	Structural and dielectric properties of Bi <sub>1-x</sub> Sr <sub>x</sub> MnO <sub>3</sub> (0.40 ≤ x ≤ 0.55). <b>2013</b> , 39, 6165-6174	21
1032	High Temperature Structural, Dielectric, and Ion Conduction Properties of Orthorhombic InVO <sub>4</sub> . <b>2013</b> , 96, 166-173	11
1031	Impedance and electric modulus study of amorphous TiTaO thin films: highlight of the interphase effect. <i>Journal Physics D: Applied Physics</i> , <b>2013</b> , 46, 065308	3 50
1030	Electrical charge conductivity behavior of electrodeposited Cu <sub>2</sub> O/ZnO heterojunction thin films on PET flexible substrates by impedance spectroscopy analysis. <b>2013</b> , 48, 3334-3340	13
1029	Characterizing epoxy composites filled with carbonaceous nanoparticles from dc to microwave. <b>2013</b> , 113, 124103	33
1028	N-(2-hydroxyethyl)-ethylenediamine-based ionic liquids: Synthesis, structural characterization, thermal, dielectric and catalytic properties. <b>2013</b> , 177, 369-375	14
1027	Growth of a three-dimensional anisotropic lattice of Ge quantum dots in an amorphous alumina matrix. <b>2013</b> , 46, 709-715	7
1026	Dielectric Spectrum of CaCu <sub>3</sub> Ti <sub>4</sub> O <sub>12</sub> from the Giant Permittivity to its Negative Values. <b>2013</b> , 705, 52-55	3
1025	Development of Magnetic Nanoparticles as Microwave-Specific Catalysts for the Rapid, Low-Temperature Synthesis of Formalin Solutions. <b>2013</b> , 3, 1318-1323	36



1024	Preparation and electrical properties of NaNbO <sub>3</sub> ceramics synthesized by topochemical microcrystal conversion. <b>2013</b> , 39, S365-S368	5
1023	Universality of Polarization Switching Dynamics in Ferroelectric Capacitors Revealed by 5D Piezoresponse Force Microscopy. <b>2013</b> , 23, 3971-3979	20
1022	Observation of high coercivity in multiferroic lanthanum doped BiFeO <sub>3</sub> . <b>2013</b> , 554, 271-276	54
1021	Dielectric properties investigation of Cu <sub>2</sub> O/ZnO heterojunction thin films by electrodeposition. <b>2013</b> , 178, 496-501	9
1020	Dynamics of amphiphilic surfactants confined in montmorillonite slits with different cation exchange capacities. <b>2013</b> , 117, 13667-78	6
1019	Effect of initiator nature on ionic conduction in radiation cured epoxies. <b>2013</b> ,	0
1018	Green Up-Conversion Photoluminescence and Dielectric Relaxation of Ho <sup>3+</sup> /Yb <sup>3+</sup> -Codoped Bi <sub>2</sub> Ti <sub>2</sub> O <sub>7</sub> Pyrochlore Thin Films. <b>2013</b> , 96, 3768-3774	18
1017	Silica nanofibers based impedance type humidity detector prepared on glass substrate. <b>2013</b> , 87, 1-6	13
1016	On the Feasibility of Using Poles Computed from Frequency Domain Spectroscopy to Assess Oil Impregnated Paper Insulation Conditions. <b>2013</b> , 6, 2204-2220	30
1015	Dielectric spectroscopy of a thin surface layer by differential time-domain reflectometry using a coplanar waveguide circuit line probe. <b>2013</b> , 24, 025501	1
1014	Charge carriers and small-polaron migration as the origin of intrinsic dielectric anomalies in multiferroic TbMnO <sub>3</sub> polycrystals. <b>2013</b> , 25, 475401	8
1013	Forward and inverse modelling of the electrical properties of magnetite intruded by magma, Egypt. <b>2013</b> , 194, 1527-1540	19
1012	Energy landscape in frustrated systems: Cation hopping in pyrochlores. <b>2013</b> , 103, 022901	6
1011	Temperature-dependence of dielectric properties for copper clad laminate used in integrated power module. <b>2013</b> ,	
1010	Evidence for space-charge-limited conduction in organic photovoltaic cells at open-circuit conditions. <b>2013</b> , 87,	17
1009	Study of dielectric loss mechanisms in Bi <sub>1.5</sub> MgNb <sub>1.5</sub> O <sub>7</sub> thin film varactors. <b>2013</b> , 114, 014104	6
1008	Processing and Performance of Polymeric Transparent Conductive Composites. <b>2013</b> , 2013, 1-13	2
1007	Estimation of thermal expansion coefficients of polymeric insulating films from temperature dependence of dielectric permittivity. <b>2014</b> , 53, 071501	31

1006	Nanoscale and macroscopic electrical ac transport along conductive domain walls in lithium niobate single crystals. <b>2014</b> , 1, 035012	29
1005	Ferroelectrics, Piezoelectric, and Impedance Spectroscopy Characterizations of CuO Doped (Na <sub>0.52</sub> K <sub>0.44</sub> )(Nb <sub>0.9</sub> Sb <sub>0.06</sub> )O <sub>3</sub> · 0.04LiTaO <sub>3</sub> Lead Free Ceramics. <b>2014</b> , 473, 171-186	1
1004	Impedance Analysis of Gellan Gum - Poly(vinyl pyrrolidone) Membranes. <b>2014</b> , 604, 84-95	4
1003	Contactless probing of the intrinsic carrier transport in single-walled carbon nanotubes. <b>2014</b> , 7, 1623-1630	16
1002	Effect of solvent polarity on the self-assembly and dielectric dynamics of non-aqueous lyotropic liquid crystalline phases. <b>2014</b> , 41, 701-706	11
1001	Influence of Extending Ratio on Mechanical and Piezoelectric Properties of Irradiation Cross-Linked Polypropylene Films. <b>2014</b> , 1053, 407-413	
1000	Dielectric Behaviour of Zn/Al-NO <sub>3</sub> LDHs Filled with Polyvinyl Chloride Composite at Low Microwave Frequencies. <b>2014</b> , 2014, 1-6	7
999	Trapping-charging ability and electrical properties study of amorphous insulator by dielectric spectroscopy. <b>2014</b> , 116, 104104	5
998	Phase boundary, poling conditions, and piezoelectric activity and their relationships in (K <sub>0.42</sub> Na <sub>0.58</sub> )(Nb <sub>0.96</sub> Sb <sub>0.04</sub> )O <sub>3</sub> (Bi <sub>0.5</sub> K <sub>0.5</sub> ) <sub>0.90</sub> Zn <sub>0.10</sub> ZrO <sub>3</sub> lead-free ceramics. <b>2014</b> , 4, 64835-64842	33
997	Structural and optical characterization of Cr <sub>2</sub> O <sub>3</sub> nanostructures: Evaluation of its dielectric properties. <b>2014</b> , 4, 027121	110
996	Dynamics of nanoscale polarization fluctuations in a uniaxial relaxor. <b>2014</b> , 113, 167601	11
995	Real-time crystallization in fluorinated parylene probed by conductivity spectra. <b>2014</b> , 104, 112902	1
994	Dielectric Characterization of Biopolymer/Poly(ε-Caprolactone) Hydrogels. <b>2014</b> , 19, 234-244	1
993	Investigation of the conduction processes in PZT-based multiferroics: Analysis from Jonscher's formalism. <b>2014</b> , 251, 1020-1027	6
992	Frequency and Temperature-Independent Electrical Transport Properties of 2BaO · 0.5Na <sub>2</sub> O · 0.5Nb <sub>2</sub> O <sub>5</sub> · 0.5B <sub>2</sub> O <sub>3</sub> Glass-Ceramics. <b>2014</b> , 97, 3582-3588	8
991	Cyclic voltammetry on sputter-deposited films of electrochromic Ni oxide: Power-law decay of the charge density exchange. <b>2014</b> , 105, 163502	21
990	Photo-induced change of dielectric response in BaCoSiO <sub>4</sub> stuffed tridymite. <b>2014</b> , 115, 164103	13
989	Characterization and Modeling of the Conduction and Switching Mechanisms of HfO <sub>x</sub> Based RRAM. <b>2014</b> , 1631, 1	5

988	Novel monoclinic zirconolite in $\text{Bi}_2\text{O}_3\text{-CuO-Ta}_2\text{O}_5$ ternary system: Phase equilibria, structural and electrical properties. <b>2014</b> , 592, 140-149	7
987	Effect of maleic anhydride on dielectric properties of natural fiber composite. <b>2014</b> , 72, 156-160	20
986	Solid- and liquid-state studies of a wide range of chemicals by isothermal and scanning dielectric thermal analysis. <b>2014</b> , 115, 2253-2260	3
985	Dielectric properties and electrical conduction of $\text{La}_2\text{O}_3$ -doped $(\text{Bi}_{0.5}\text{Na}_{0.5})_{0.94}\text{Ba}_{0.06}\text{TiO}_3$ ceramics. <b>2014</b> , 114, 551-558	23
984	Dielectric Properties and Defect Chemistry of $\text{WO}_3$ -Doped $\text{K}_{0.5}\text{Na}_{0.5}\text{NbO}_3$ Ceramics. <b>2014</b> , 43, 1055-1061	28
983	Effect of Ca substitution on structural, magnetic and dielectric properties of $\text{BiFeO}_3$ . <b>2014</b> , 87, 527-540	12
982	Correction of the power law of ac conductivity in ion-conducting materials due to the electrode polarization effect. <b>2014</b> , 89, 032303	44
981	Microstructural variation and dielectric properties of $\text{KTiNbO}_5$ and $\text{K}_3\text{Ti}_5\text{NbO}_{14}$ ceramics. <b>2014</b> , 40, 5861-5867	9
980	On the theory of the universal dielectric relaxation. <b>2014</b> , 94, 1788-1815	18
979	Impedance spectroscopic studies, dielectric properties and microstructure of rutile type chromium niobate $\text{CrNbO}_4$ . <b>2014</b> , 40, 12129-12137	7
978	All-nanosheet ultrathin capacitors assembled layer-by-layer via solution-based processes. <b>2014</b> , 8, 2658-66	71
977	Blue and near-infrared up-conversion photoluminescence and dielectric relaxation of $\text{Tm}^{3+}/\text{Yb}^{3+}$ -co-doped $(\text{Bi}, \text{Y})_2\text{Ti}_2\text{O}_7$ pyrochlore thin films. <b>2014</b> , 148, 121-128	9
976	Structural, magnetic and dielectric properties of Pr-modified $\text{BiFeO}_3$ multiferroic. <b>2014</b> , 584, 232-239	69
975	Modelling of dielectric relaxation processes of epoxy-resin filled with carbon black particles. <b>2014</b> , 433, 62-66	16
974	The effect of fast and continuous change of dielectric permittivity on whispering gallery modes in circular microcavity. <b>2014</b> , 46, 1519-1528	
973	Molecular mobility of amorphous S-flurbiprofen: a dielectric relaxation spectroscopy approach. <b>2014</b> , 11, 112-30	30
972	Studies on structural, dielectric, and transport properties of $\text{Ni}_{0.65}\text{Zn}_{0.35}\text{Fe}_2\text{O}_4$ . <b>2014</b> , 115, 243904	68
971	Modified Waveguide Flange for Evaluation of Stratified Composites. <b>2014</b> , 63, 1524-1534	35

- 970 Switchable dielectric, piezoelectric, and second-harmonic generation bistability in a new improper ferroelectric above room temperature. **2014**, 26, 4515-20 111
- 969 Chemical modification of polysiloxanes with polar pendant groups by co-hydrosilylation. **2014**, 4, 37620-37628 46
- 968 Structural order and dielectric properties of coal chars. **2014**, 137, 164-171 41
- 967 Electrical properties, phase transitions and conduction mechanisms of the  $[(C_2H_5)NH_3]_2CdCl_4$  compound. **2014**, 451, 87-95 44
- 966 Impedance Spectroscopy of Sodium Excess Ta-Modified  $(K_{0.5}Na_{0.5})NbO_3$  Ceramics Prepared by Reactive Templated Grain Growth. **2014**, 464, 107-115 3
- 965 A silicon-containing polyazomethine and derived metal complexes: synthesis, characterization, and evaluation of the properties. **2014**, 17, 668-683 11
- 964 A morphological and structural approach to evaluate the electromagnetic performances of composites based on random networks of carbon nanotubes. **2014**, 115, 154311 26
- 963 Dynamics of Substituted Alkyl Monolayers Covalently Bonded to Silicon: A Broadband Admittance Spectroscopy Study. **2014**, 118, 6773-6787 7
- 962 Variable Range Hopping Conduction in  $BaTiO_3$  Ceramics Exhibiting Colossal Permittivity. **2014**, 118, 9137-9142 55
- 961 The giant dielectric constant and tunable properties of  $La_2NiMnO_6 \cdot xMgO$  ceramics. **2014**, 616, 213-220 16
- 960 Physical properties of bifunctional BST/LSMO nanocomposites. **2014**, 115, 084102 22
- 959 Influence of dispersion states on the performance of polymer-based nanocomposites. **2014**, 23, 104004 17
- 958 Dopant size dependent variable range hopping conduction in polyaniline nanorods. **2014**, 115, 943-951 12
- 957 Synthesis and electrical properties of  $Y_2O_3: Dy^{3+} \& Eu^{3+}$  nanoparticles. **2014**, 117, 1269-1274 10
- 956 Molecular dynamics of nanocomposites natural rubber/cellulose nanowhiskers investigated by impedance spectroscopy. **2014**, 196, 187-191 24
- 955 Charge transport and dielectric relaxation processes in aniline-based oligomers. **2014**, 192, 37-42 11
- 954 Structural modification of poly (methyl methacrylate) due to electron irradiation. **2014**, 51, 1-8 15
- 953 Conductivity and dielectric relaxation of gelatin films with glycerol as plasticizer. **2014**, 20, 1445-1454 4

952	Charge transport and electrode polarization in epoxy resin at high temperatures. <i>Journal Physics D: Applied Physics</i> , <b>2014</b> , 47, 045311	3	42
951	Effect of rare earth substitution on properties of barium strontium titanate ceramic and its multiferroic composite with nickel cobalt ferrite. <b>2014</b> , 617, 140-148		24
950	Near constant loss regime in fast ionic conductors analyzed by impedance and NMR spectroscopies. <b>2014</b> , 16, 15346-54		12
949	Effect of noise and detector sensitivity on a dynamical process: inverse power law and Mittag-Leffler interevent time survival probabilities. <b>2014</b> , 89, 022107		5
948	Study of the structural, dielectric and magnetic properties of $\text{Bi}_{1-x}\text{Ba}_x\text{FeO}_3$ ( $x=0.1, 0.2, 0.3,$ and $0.4$ ). <b>2014</b> , 598, 248-252		13
947	Phase equilibria and dielectric properties of $\text{Bi}_{3+(5/2)x}\text{Mg}_{2-3x}\text{Nb}_{3(3/2-x)}\text{O}_{14}$ cubic pyrochlores. <b>2014</b> , 40, 4237-4246		23
946	Crystallization in $\text{Li}_2\text{SO}_4\text{-Li}_2\text{O-B}_2\text{O}_5$ glassy ionic system: An assessment through electrical transport. <b>2014</b> , 402, 79-83		7
945	High-temperature impedance spectroscopy of $\text{BaFe}_{0.5}\text{Nb}_{0.5}\text{O}_3$ ceramics doped with $\text{Bi}_{0.5}\text{Na}_{0.5}\text{TiO}_3$ . <b>2014</b> , 114, 891-896		36
944	Influence of heat treatment on electromagnetic properties of polyimide/carbon black composites. <b>2014</b> , 25, 1616-1621		12
943	Understanding capacitance-voltage nonlinearities in microelectronic metal-insulator-metal (MIM) capacitors. <b>2015</b> ,		3
942	Loss Mechanisms and Microwave-Specific Effects in Heterogeneous Catalysis. <b>2015</b> , 29-48		0
941	Analysis of Immittance Spectra: Finding Unambiguous Electrical Equivalent Circuits to Represent the Underlying Physics. <b>2015</b> , 4,		
940	Searching for new ferroelectrics and multiferroics: A user's point of view. <b>2015</b> , 1,		16
939	Dielectric relaxor and conductivity characteristics of undoped and samarium doped barium bismuth niobate ferroelectric ceramics. <b>2015</b> , 43, 82-89		0
938	Copper(I) Iodide as Hole-Conductor in Planar Perovskite Solar Cells: Probing the Origin of JV Hysteresis. <b>2015</b> , 25, 5650-5661		224
937	Entropy effects in the collective dynamic behavior of alkyl monolayers tethered to Si(111). <b>2015</b> , 6, 583-94		3
936	The application of the fractional calculus model for dispersion and absorption in dielectrics I. Terahertz waves. <b>2015</b> , 93, 1-12		14
935	. <b>2015</b> , 15, 308-318		8

934	Electrical behaviour of a silicone elastomer under simulated space environment. <i>Journal Physics D: Applied Physics</i> , <b>2015</b> , 48, 135302	3	9
933	Electrical conductivity, dielectric response and space charge dynamics of an electroactive polymer with and without nanofiller reinforcement. <b>2015</b> , 24, 075019		13
932	Development of polyurethane multiwall carbon nanotubes (MWCNTs) novel polymeric nanodielectric material. <b>2015</b> , 76, 95-101		13
931	A new analyzing scheme for non-integer order DC/DC converters. <b>2015</b> ,		7
930	Modifications of dielectric properties of polyamides induced by long-term exposure to corona. <b>2015</b> ,		
929	. <b>2015</b> , 22, 3053-3058		8
928	Synthesis of silicone elastomers containing trifluoropropyl groups and their use in dielectric elastomer transducers. <b>2015</b> , 5, 104516-104523		34
927	Influence of absorbed moisture on the dielectric properties of epoxy resin impregnated paper composites. <b>2015</b> ,		0
926	Synthesis and characterization of Ultra High Molecular Weight Polyethylene filled with boron nitride micro and nano-particles. <b>2015</b> ,		1
925	Crystallization and Glass Transition Kinetics of Na <sub>2</sub> s-P <sub>2</sub> s <sub>5</sub> -Based Super-Ionic Glasses. <b>2015</b> , 33, 166-171		3
924	Electrical properties of polypropylene-based composites controlled by multilayered distribution of conductive particles. <b>2015</b> , 7, 1541-9		81
923	Electrocaloric cooling based on relaxor ferroelectrics. <b>2015</b> , 88, 333-341		14
922	Study of the properties of non-gas dielectric capacitors in porous media. <b>2015</b> , 12, 104-113		1
921	Structure, thermal and electrical properties of calcium doped pyrochlore type praseodymium zirconate. <b>2015</b> , 40, 4252-4262		19
920	Study of electrical properties and petrography for carbonate rocks in the Jurassic Formations: Sinai Peninsula, Egypt. <b>2015</b> , 8, 4627-4639		9
919	The dimensional effect of dielectric performance in CaCu <sub>3</sub> Ti <sub>4</sub> O <sub>12</sub> ceramics: Role of grain boundary. <b>2015</b> , 644, 824-829		9
918	Red-orange photoluminescence and dielectric relaxation of Eu <sup>3+</sup> -doped Bi <sub>2</sub> Ti <sub>2</sub> O <sub>7</sub> pyrochlore structure thin films. <b>2015</b> , 162, 801-806		11
917	Preparation and High-Frequency Dielectric Properties of Cu/SiO <sub>2</sub> Composites. <b>2015</b> , 655, 174-177		

916	Electrical and thermal investigations of energetic material (n-C <sub>16</sub> H <sub>33</sub> NH <sub>3</sub> ) <sub>2</sub> CdCl <sub>4</sub> . <b>2015</b> , 95, 2323-2342	5
915	Azimuthally Controlled Magnetic and Dielectric Properties of Multiferroic Nanocrystalline Composite by Magnetic Coupling and Charge Hopping. <b>2015</b> , 119, 17995-18005	15
914	Effect of Eu Doping on the Structural, Electrical, and Dielectric Properties of K <sub>0.5</sub> Na <sub>0.5</sub> NbO <sub>3</sub> Ceramics for High-Temperature Capacitor Applications. <b>2015</b> , 44, 3408-3414	8
913	A comprehensive treatment of universal dispersive frequency responses in solid electrolytes by immittance spectroscopy: low temperature AgI case. <b>2015</b> , 19, 2457-2464	7
912	Effect of co-substitutions (CaMn) on structural, electrical and magnetic characteristics of bismuth ferrite. <b>2015</b> , 41, 9078-9087	9
911	Electrical and geochemical properties of tufa deposits as related to mineral composition in the South Western Desert, Egypt. <b>2015</b> , 12, 292-302	11
910	Tailoring resistive switching in Pt/SrTiO <sub>3</sub> junctions by stoichiometry control. <b>2015</b> , 5, 11079	31
909	Study of dielectric relaxation processes in printable zinc oxide films on transparent substrates. <b>2015</b> , 26, 7109-7116	1
908	Polar/nonpolar interconnected elastic networks with increased permittivity and high breakdown fields for dielectric elastomer transducers. <b>2015</b> , 5, 58428-58438	27
907	Dispersive diffusion of gases in coals. Part I: Model development. <b>2015</b> , 143, 612-619	42
906	Effect of coal rank on structure and dielectric properties of chars. <b>2015</b> , 153, 249-256	53
905	Effective modeling of ground penetrating radar in fractured media using analytic solutions for propagation, thin-bed interaction and dipolar scattering. <b>2015</b> , 116, 206-214	11
904	Assessment of nanoparticle loading and dispersion in polymeric materials using optical wavefront correlation. <b>2015</b> , 44, 57-65	4
903	Structure-Independent Proton Transport in Cerium(III) Phosphate Nanowires. <b>2015</b> , 7, 9947-56	14
902	Structural, Optical and AC Electrical Properties of Ce <sup>3+</sup> -Doped TiO <sub>2</sub> /BiO <sub>2</sub> Matrices. <b>2015</b> , 44, 2754-2761	5
901	Interfacial Charge Induced Magnetoelectric Coupling at BiFeO <sub>3</sub> /BaTiO <sub>3</sub> Bilayer Interface. <b>2015</b> , 7, 8472-9	50
900	Temperature and frequency dependence of transport phenomena in co-doped rare earth oxides nanoparticles for ITSOFCs. <b>2015</b> , 632, 695-700	8
899	Enhancement in semiconducting and optical properties in doped anthracene micro crystals. <b>2015</b> , 470-471, 15-20	9

898	Broadband Dielectric Spectroscopy of Composites Filled With Various Carbon Materials. <b>2015</b> , 63, 2024-2031	14
897	Evidences of grain boundary capacitance effect on the colossal dielectric permittivity in (Nb + In) co-doped TiO <sub>2</sub> ceramics. <b>2015</b> , 5, 8295	100
896	Magnetoelectric dipole interaction in RF-magnetron sputtered (1-x) BiFeO <sub>3</sub> -xBaTiO <sub>3</sub> thin films. <b>2015</b> , 638, 115-120	17
895	Mechanical and piezoelectric performance of cross-linked polypropylene films treated with extending. <b>2015</b> , 41, S218-S222	5
894	Magnetic Behaviors of Mg- and Zn-Doped Fe <sub>3</sub> O <sub>4</sub> Nanoparticles Estimated in Terms of Crystal Domain Size, Dielectric Response, and Application of Fe <sub>3</sub> O <sub>4</sub> /Carbon Nanotube Composites to Anodes for Lithium Ion Batteries. <b>2015</b> , 119, 26128-26142	22
893	Atomic-scale control of TiO <sub>6</sub> octahedra through solution chemistry towards giant dielectric response. <b>2014</b> , 4, 6582	42
892	Effect of manganese doping of BaSrTiO <sub>3</sub> on diffusion and domain wall pinning. <b>2015</b> , 117, 084104	16
891	Microstructural, dielectric and magnetic properties of multiferroic composite system barium strontium titanate /nickel cobalt ferrite. <b>2015</b> ,	1
890	Investigation on CuCa <sub>3</sub> Ti <sub>4</sub> O <sub>12</sub> Modified BiFeO <sub>3</sub> -Based Perovskite Ceramics. <b>2015</b> , 12, 157-162	3
889	Structural and electrical studies of mixed metal/ceramic composite dielectric thin films. <b>2015</b> ,	
888	Time-dependent non-equilibrium dielectric response in QM/continuum approaches. <b>2015</b> , 142, 034120	28
887	Diffusion-limited kinetics of the antiferromagnetic to ferrimagnetic transition in Fe <sub>1-x</sub> S. <b>2015</b> , 106, 092402	15
886	Behavior of 1/f resistors at frequencies below 1 Hz and the problem of assigning a dc value. <b>2015</b> , 52, 509-513	2
885	Dielectric relaxation and microwave dielectric properties of low temperature sintering LiMnPO <sub>4</sub> ceramics. <b>2015</b> , 651, 290-293	22
884	Equivalent circuit modeling of the ac response of Pd-ZrO <sub>2</sub> granular metal thin films using impedance spectroscopy. <i>Journal Physics D: Applied Physics</i> , <b>2015</b> , 48, 335306	3 11
883	Materials and device concepts for electrocaloric refrigeration. <b>2015</b> , 90, 094020	14
882	Origin of colossal permittivity in (In <sub>1/2</sub> Nb <sub>1/2</sub> )TiO <sub>2</sub> via broadband dielectric spectroscopy. <b>2015</b> , 17, 23132-9	42
881	Silicone films with high stiffness and increasing permittivity through dipole-grafting. <b>2015</b> ,	



880	Study of petrographical and electrical properties of some Jurassic carbonate rocks, north Sinai, Egypt. <b>2015</b> , 24, 343-352	11
879	Modulus spectroscopy of grain-grain boundary binary system. <b>2015</b> , 459, 105-109	7
878	Induced oxygen vacancies and their effect on the structural and electrical properties of a fluorite-type $\text{CaZrO}_3/\text{Ce}_2\text{Zr}_2\text{O}_7$ system. <b>2015</b> , 39, 1469-1476	25
877	Aqueous Solution Gel Preparation and Dielectric Properties of $\text{Ba}(\text{Mg}_{1/3}\text{Nb}_{2/3})\text{O}_3$ Thin Films with Long-Range Order. <b>2015</b> , 98, 873-878	5
876	Bismuth centred magnetic perovskite: A projected multiferroic. <b>2015</b> , 378, 506-528	14
875	AC-impedance and dielectric properties of hybrid polymer composites. <b>2015</b> , 49, 3-15	24
874	Broadband dielectric properties of multiwalled carbon nanotube/polystyrene composites. <b>2015</b> , 55, 173-179	31
873	Novel synaptic memory device for neuromorphic computing. <b>2014</b> , 4, 5333	65
872	Oxygen concentration-related impedance spectroscopic studies of $\text{La}_2\text{Mo}_2\text{O}_9$ oxide ion conductors. <b>2015</b> , 21, 213-219	2
871	Space charge behavior of epoxy resin with low $T_g$ under polarity reversal voltage. <b>2016</b> ,	
870	Effect of various parameters on the dielectric behavior of an epoxy composite containing 10 wt% of carbon black. <b>2016</b> ,	
869	Micromachined Resonators: A Review. <b>2016</b> , 7,	100
868	Influence of interface point defect on the dielectric properties of Y doped $\text{CaCu}_3\text{Ti}_4\text{O}_{12}$ ceramics. <b>2016</b> , 06, 1650009	44
867	Low Frequency Radio Wave Detection of Electrically Active Defects in Dielectrics. <b>2016</b> , 5, P3025-P3030	8
866	Anomalies of dielectric properties and conductivity in single domain $\text{LiNbO}_3:\text{Zn}$ crystals. <b>2016</b> , 173, 119-127	7
865	An Investigation of Structure-Property Relationships in Silicone-Based Dielectric Electroactive Elastomers by Varying Stoichiometric Imbalance of the Network. <b>2016</b> , 301, 337-347	6
864	Freestanding $\text{Ag}_2\text{S}/\text{CuS}$ PVA films with improved dielectric properties for organic electronics. <b>2016</b> , 133,	6
863	Frequency-dependence of the switching voltage in electronic switching of Pt-dispersed $\text{SiO}_2$ thin films. <b>2016</b> , 68, 1403-1408	

862	Electrical Conductivity of a Space-Used Silicone Elastomer: Evolution Under Electron Irradiation. <b>2016</b> , 53, 1114-1118	1
861	Nanocomposites of TiO <sub>2</sub> /cyanoethylated cellulose with ultra high dielectric constants. <b>2016</b> , 27, 195402	17
860	Submillimeter and far-infrared dielectric properties of thin films. <b>2016</b> ,	3
859	Low-frequency dielectric properties of intrinsic and Al-doped rutile TiO <sub>2</sub> thin films grown by the atomic layer deposition technique. <b>2016</b> , 119, 244101	7
858	Microwave a.c. conductivity of domain walls in ferroelectric thin films. <b>2016</b> , 7, 11630	63
857	Dielectric spectra of epoxy resin impregnated crepe paper composites in different humidity. <b>2016</b> ,	1
856	Polymer laminates for high energy density and low loss. <b>2016</b> ,	
855	Contribution of polymer microstructure to space charge, dielectric properties and electrical conduction. <b>2016</b> ,	4
854	Dielectric response of filled high temperature vulcanized silicone rubber. <b>2016</b> , 23, 3683-3695	20
853	Estimation of near-interface oxide trap density at SiO <sub>2</sub> /SiC metal-oxide-semiconductor interfaces by transient capacitance measurements at various temperatures. <b>2016</b> , 120, 085710	24
852	Investigation of high-kyttrium copper titanate thin films as alternative gate dielectrics. <i>Journal Physics D: Applied Physics</i> , <b>2016</b> , 49, 405303	3 3
851	Study of Phosphate Polyanion Electrodes and Their Performance with Glassy Electrolytes: Potential Application in Lithium Ion Solid-state Batteries. <b>2016</b> , 321-354	1
850	Colossal dielectric constant and extremely low loss in T-type La <sub>2</sub> CuO <sub>4</sub> ceramics. <b>2016</b> , 42, 13207-13214	6
849	Characterization and frequency-thermal response of electrical properties of Cu nanoferrite prepared by sol-gel method. <b>2016</b> , 416, 103-109	8
848	Structural and dielectric characterization of sputtered Tantalum Titanium Oxide thin films for high temperature capacitor applications. <b>2016</b> , 606, 127-132	6
847	Structural and electrical characteristics of (Co, Ti) modified BiFeO <sub>3</sub> . <b>2016</b> , 27, 7115-7123	23
846	Enhanced dielectric properties in bismuth-doped alumina films prepared by atomic layer deposition. <b>2016</b> , 443, 17-22	3
845	Soft magnetic property and enhanced microwave absorption of nanoparticles of Co <sub>0.5</sub> Zn <sub>0.5</sub> Fe <sub>2</sub> O <sub>4</sub> incorporated in MWCNT. <b>2016</b> , 416, 181-187	19

844	Dielectric spectroscopy characterization of relaxation process in Ni/epoxy composites. <b>2016</b> , 682, 738-745	56
843	Dielectric Properties of SrMnO <sub>3</sub> -doped K <sub>0.5</sub> Na <sub>0.5</sub> NbO <sub>3</sub> Lead-Free Ceramics. <b>2016</b> , 45, 4089-4099	9
842	Electrical, mineralogical, geochemical and provenance of Cretaceous black shales, Red Sea Coast, Egypt. <b>2016</b> , 25, 323-332	12
841	Grain boundary defect compensation in Ti-doped BaFe <sub>0.5</sub> Nb <sub>0.5</sub> O <sub>3</sub> ceramics. <b>2016</b> , 122, 1	35
840	Pseudo-random renormalization group forward and inverse modeling of the electrical properties of some carbonate rocks. <b>2016</b> , 135, 144-154	10
839	. <b>2016</b> , 23, 1418-1426	18
838	Dielectric relaxation dynamics of Al/epoxy micro-composites. <b>2016</b> , 689, 342-349	14
837	Microwave-assisted sintering of non-stoichiometric strontium bismuth niobate ceramic: Structural and dielectric properties. <b>2016</b> , 500, 169-178	1
836	Dielectric Loss and Relaxation $\square$ <b>2016</b> , 83-136	
835	Dielectric Loss and Relaxation $\square$ . <b>2016</b> , 137-182	
834	Defect Complex Effect in Nb Doped TiO <sub>2</sub> Ceramics with Colossal Permittivity. <b>2016</b> , 45, 5178-5184	10
833	Frequency and Temperature Dependence of Dielectric Behaviors for Conductive Acrylic Composites. <b>2016</b> , 35,	9
832	Agricultural wastes as a resource of raw materials for developing low-dielectric glass-ceramics. <b>2016</b> , 6, 24617	46
831	Effects of nanostructure permittivity and dimensions on the increased dielectric strength of nano insulating oils. <b>2016</b> , 509, 235-243	33
830	Effect of alkaline excess on sintering, microstructural, and electrical properties of Li <sub>0.12</sub> Na <sub>0.88</sub> NbO <sub>3</sub> ceramics. <b>2016</b> , 51, 9031-9042	0
829	Universality of the electrical transport in granular metals. <b>2016</b> , 6, 29676	25
828	Electrical conductivity of a silicone network upon electron irradiation: influence of formulation. <i>Journal Physics D: Applied Physics</i> , <b>2016</b> , 49, 505303	3 7
827	Broadband dielectric spectroscopy of standard and core-shell BaTiO <sub>3</sub> -NiO ceramic composites compared to the BaTiO <sub>3</sub> ceramics. <b>2016</b> , 500, 1-19	5

826	Dielectric properties and defect mechanisms of (1-x)Ba(Fe <sub>0.5</sub> Nb <sub>0.5</sub> )O <sub>3</sub> -xBiYbO <sub>3</sub> ceramics. <b>2016</b> , 37, 137-144	12
825	Effect of Variable Oxidation States of Vanadium on the Structural, Optical, and Dielectric Properties of BO-LiO-ZnO-VO Glasses. <b>2016</b> , 120, 12168-12176	26
824	High-Energy Mechanical Treatment Boosts Ion Transport in Nanocrystalline Li <sub>2</sub> B <sub>4</sub> O <sub>7</sub> . <b>2016</b> , 99, 1687-1693	17
823	Structural, multiferroic properties and enhanced magnetoelectric coupling in Sm <sub>1-x</sub> CaxFeO <sub>3</sub> . <b>2016</b> , 42, 13572-13585	22
822	Broadband all fiber-reinforced composite radar absorbing structure integrated by inductive frequency selective carbon fiber fabric and carbon-nanotube-loaded glass fabrics. <b>2016</b> , 107, 564-572	58
821	Sodium ion transport in polymorphic scandium NASICON analog Na <sub>3</sub> Sc <sub>2</sub> (PO <sub>4</sub> ) <sub>3</sub> with new dielectric spectroscopy approach for current-constriction effects. <b>2016</b> , 289, 55-71	17
820	Polar silicones: structure-dielectric properties relationship. <b>2016</b> , 19, 496-507	23
819	Dielectric relaxation and conduction mechanisms in sprayed TiO <sub>2</sub> thin films as a function of the annealing temperature. <b>2016</b> , 122, 1	2
818	The influence of Yttrium on leakage current and dielectric properties of amorphous Al <sub>2</sub> O <sub>3</sub> thin film derived by sol-gel. <b>2016</b> , 27, 7788-7794	6
817	Electrical Behavior of SnO <sub>2</sub> Polycrystalline Ceramic Pieces Formed by Slip Casting: Effect of Surrounding Atmosphere (Air and CO). <b>2016</b> , 45, 576-593	2
816	Frequency dependence and fuel effect on optical properties of nano-TiO <sub>2</sub> -based structures. <b>2016</b> , 30, 1650247	2
815	Conduction and Dielectric Relaxation Mechanisms in Athabasca Oil Sands with Application to Electrical Heating. <b>2016</b> , 30, 5630-5642	8
814	Dielectric spectroscopy of artificial faeces for smouldering applications. <b>2016</b> ,	3
813	Low frequency dielectric spectroscopy of bitumen binders as an indicator of adhesion potential to quartz aggregates using Portland cement. <b>2016</b> , 49, 1327-1336	6
812	Effect of synthesis catalyst on structure of nitrogen-doped carbon nanotubes and electrical conductivity and electromagnetic interference shielding of their polymeric nanocomposites. <b>2016</b> , 98, 358-372	166
811	Assessment of nanoparticle loading and dispersion in polymeric materials using oscillatory photon correlation spectroscopy. <b>2016</b> , 49, 107-114	
810	Thermally stable yttrium-scandium oxide high-k dielectrics deposited by a solution process. <i>Journal Physics D: Applied Physics</i> , <b>2016</b> , 49, 115109	3 18
809	Effect of Gd-substitution on the ferroelectric and magnetic properties of BiFeO <sub>3</sub> processed by high-energy ball milling. <b>2016</b> , 418, 188-193	8

808	Structural and frequency-dependent dielectric properties of PVP-SiO <sub>2</sub> -TMSPM hybrid thin films. <b>2016</b> , 32, 100-108	33
807	Anomalous europium luminescence in LaF <sub>3</sub> . <b>2016</b> , 90, 80-83	4
806	Non-isothermal crystallization kinetics of K <sub>2</sub> O modified sodium-phosphate glasses. <b>2016</b> , 440, 76-84	18
805	Dielectric and ferroelectric properties of (111) preferred oriented PbZr <sub>0.53</sub> Ti <sub>0.47</sub> O <sub>3</sub> /Pb(Mg <sub>1/3</sub> Nb <sub>2/3</sub> ) <sub>0.62</sub> Ti <sub>0.38</sub> O <sub>3</sub> /PbZr <sub>0.53</sub> Ti <sub>0.47</sub> O <sub>3</sub> trilayered films. <b>2016</b> , 371, 160-163	7
804	Slow stress relaxation behavior of cohesive powders. <b>2016</b> , 293, 82-93	8
803	Dielectric investigation of high-k yttrium copper titanate thin films. <b>2016</b> , 4, 1080-1087	12
802	Dye-sensitized solar cell from a new organic n-type semiconductor/polyaniline composite: insight from impedance spectroscopy. <b>2016</b> , 4, 272-285	33
801	Colossal permittivity and low losses in Ba <sub>1-x</sub> Sr <sub>x</sub> TiO <sub>3</sub> reduced nanoceramics. <b>2016</b> , 36, 567-575	23
800	Partial correlation of electrical and magnetic properties of Nd substituted Ni <sub>2</sub> Zn nanoferrites. <b>2016</b> , 397, 188-197	34
799	Aliovalent Ba <sup>2+</sup> doping: A way to reduce oxygen vacancy in multiferroic BiFeO <sub>3</sub> . <b>2016</b> , 401, 129-137	46
798	Quality Factor and Coupling in Piezoelectric MEMS Resonators. <b>2017</b> , 133-152	5
797	Electronic and optical properties of antiferromagnetic iron doped NiO [A first principles study]. <b>2017</b> , 7, 055711	10
796	Relationships between electrical properties and petrography of El-Maghara sandstone formations, Egypt Peer review under responsibility of National Research Institute of Astronomy and Geophysics. View all notes. <b>2017</b> , 6, 162-173	6
795	Optical and dielectric characterization of gadolinium aluminate ceramic nanoparticles synthesized by combustion technique. <b>2017</b> , 193, 189-195	8
794	Effect of maceral composition and coal rank on gas diffusion in Australian coals. <b>2017</b> , 173, 65-75	71
793	Relaxation processes and conduction mechanism of epoxy resin filled with graphene oxide. <b>2017</b> , 24, 519-527	6
792	Photoinduced Stark Effects and Mechanism of Ion Displacement in Perovskite Solar Cell Materials. <b>2017</b> , 11, 2823-2834	39
791	Dielectric relaxation and localized electron hopping in colossal dielectric (Nb,In)-doped TiO rutile nanoceramics. <b>2017</b> , 19, 8568-8574	33

790	Electrochemical impedance analysis of perovskite-electrolyte interfaces. <b>2017</b> , 53, 2467-2470	31
789	Dielectric properties of Sr <sub>0.5</sub> Ca <sub>0.5</sub> TiO <sub>3</sub> : x Pr <sup>3+</sup> ceramics. <b>2017</b> , 43, 6268-6275	8
788	Dielectric relaxation behavior and mechanism of Y <sub>2/3</sub> Cu <sub>3</sub> Ti <sub>4</sub> O <sub>12</sub> ceramic. <b>2017</b> , 88, 320-329	57
787	Dielectric Spectroscopy: An Efficient Tool to Study the Interfacial Adhesion and Properties of Natural Rubber/Nanocellulose-Based Green Nanocomposites. <b>2017</b> , 627-648	4
786	Lithium ion conductivity and dielectric relaxation in dendritic nanostructured LiTaO <sub>3</sub> glass/nanocrystal composites. <b>2017</b> , 121, 094101	5
785	Ferroic ordering and charge-spin-lattice order coupling in Gd-doped Fe <sub>3</sub> O <sub>4</sub> nanoparticles relaxor multiferroic system. <b>2017</b> , 100, 1534-1541	5
784	The dielectric properties for (Nb,In,B) co-doped rutile TiO <sub>2</sub> ceramics. <b>2017</b> , 43, 6403-6409	26
783	Maxwell-Wagner-Sillars mechanism in the frequency dependence of electrical conductivity and dielectric permittivity of graphene-polymer nanocomposites. <b>2017</b> , 109, 42-50	67
782	Complex impedance spectroscopy of Sn <sub>4</sub> Sb <sub>6</sub> S <sub>13</sub> thin films deposited by thermal vacuum evaporation. <b>2017</b> , 631, 161-171	9
781	Zinc interstitial as a universal microscopic origin for the electrical degradation of ZnO-based varistors under the combined DC and temperature condition. <b>2017</b> , 37, 3535-3540	22
780	Detecting compositional changes in dielectric materials simulated by three-dimensional RC network models. <b>2017</b> , 24, 1141-1152	5
779	Synthesis and characterization of multiferroic Sm-doped BiFeO <sub>3</sub> nanopowders and their bulk dielectric properties. <b>2017</b> , 437, 51-61	27
778	Dynamic molecular mobility of polyurethane by a broad range dielectric and mechanical analysis. <b>2017</b> , 468, 46-51	10
777	Joint effect of the tube sizes and Fe-filling process on microwave dielectric properties of carbon nanotubes. <b>2017</b> , 119, 386-393	6
776	Structural and Electrical Properties of Nanocrystalline Barium Strontium Titanate. <b>2017</b> , 4, 3842-3851	7
775	Measuring Spatially Resolved Collective Ionic Transport on Lithium Battery Cathodes Using Atomic Force Microscopy. <b>2017</b> , 17, 4489-4496	22
774	Structural, electrical and magnetic properties of (Cd, Ti) modified BiFeO <sub>3</sub> . <b>2017</b> , 381, 2721-2730	46
773	Subsolidus solution and electrical properties of Sr-substituted bismuth magnesium niobate pyrochlores. <b>2017</b> , 43, 10183-10191	7

772	Experimental and simulation study for impact of different halides on the performance of planar perovskite solar cells. <b>2017</b> , 66, 176-185	33
771	Low-energy structural dynamics of ferroelectric domain walls in hexagonal rare-earth manganites. <b>2017</b> , 3, e1602371	39
770	Dielectric behaviour of montmorillonite/cyanoethylated cellulose nanocomposites. <b>2017</b> , 172, 315-321	13
769	Understanding the thermally stimulated relaxation and defect behavior of Ti-containing microwave dielectrics: A case study of BaTi <sub>4</sub> O <sub>9</sub> . <b>2017</b> , 130, 479-487	24
768	Flaky core-shell particles of iron@iron oxides for broadband microwave absorbers in S and C bands. <b>2017</b> , 709, 735-741	41
767	Some aspects of dimensionality and phase transitions of organic/inorganic hybrid perovskite (n-C <sub>14</sub> H <sub>29</sub> NH <sub>3</sub> ) <sub>2</sub> ZnCl <sub>4</sub> . <b>2017</b> , 123, 1	4
766	Influence of modifier on dielectric and ferroelectric properties of aluminosilicate glasses. <b>2017</b> , 465, 26-30	6
765	Broadband electromagnetic analysis of compacted kaolin. <b>2017</b> , 28, 014016	11
764	Dielectric, electrical and magnetic properties of La doped BiFeO <sub>3</sub> /BaZrO <sub>3</sub> composites. <b>2017</b> , 28, 9102-9113	7
763	Influence of thermal stability on dielectric properties of SiO <sub>2</sub> /K <sub>2</sub> O/CaO/MgO glasses. <b>2017</b> , 128, 745-754	5
762	Vibrational-electronic properties of intra/inter molecular hydrogen bonded heterocyclic dimer: An experimental and theoretical study of pyrrole-2-carboxaldehyde. <b>2017</b> , 89, 16-25	5
761	Microwave properties and structure of La <sub>0.1</sub> Ti <sub>0.9</sub> Si <sub>0.9</sub> B <sub>0.1</sub> O <sub>4</sub> glass-ceramics for applications in GHz electronics. <b>2017</b> , 37, 2137-2142	9
760	Trap-Induced Dispersive Transport and Dielectric Loss in PbS Nanoparticle Films. <b>2017</b> , 231,	5
759	Crystal structure and dielectric properties of Bi <sub>2</sub> O <sub>3</sub> -CaO-Nb <sub>2</sub> O <sub>5</sub> compounds. <b>2017</b> , 116, 109-114	12
758	New Details to Relaxation Dynamics of Dielectric Composite Materials Comprising Longitudinally Opened Carbon Nanotubes. <b>2017</b> , 121, 22995-23001	6
757	Microwave Enhancement of Autocatalytic Growth of Nanometals. <b>2017</b> , 11, 9957-9967	16
756	Physical properties Nd <sup>3+</sup> -doped (SiO <sub>2</sub> /TiO <sub>2</sub> ) monolithic glass for photoresistor applications. <b>2017</b> , 4, 115203	1
755	The dielectric signature of glass density. <b>2017</b> , 111, 121902	10

754	The low-temperature dynamic crossover in the dielectric relaxation of ice I. <b>2017</b> , 19, 28610-28620	19
753	Large energy storage efficiency of the dielectric layer of graphene nanocapacitors. <b>2017</b> , 28, 495401	10
752	Oxygen vacancy induced electrical conduction and room temperature ferromagnetism in system $\text{BaSn}_{1-x}\text{Ni}_x\text{O}_3$ ( $0 \leq x \leq 0.20$ ). <b>2017</b> , 4, 116304	20
751	Impact of CuS on the crystallization kinetics of $\text{Na}_2\text{S-P}_2\text{S}_5$ glasses. <b>2017</b> , 477, 31-41	12
750	AC and DC electrical conductivity, dielectric and magnetic properties of $\text{Co}_{0.65}\text{Zn}_{0.35}\text{Fe}_2\text{Mo}_x\text{O}_4$ ( $x = 0.0, 0.1$ and $0.2$ ) ferrites. <b>2017</b> , 123, 1	12
749	Dynamic analysis and fractional-order adaptive sliding mode control for a novel fractional-order ferroresonance system. <b>2017</b> , 26, 080503	4
748	Investigation of micro- and nanoscale barrier layer capacitance mechanisms of conductivity in $\text{CaCu}_3\text{Ti}_4\text{O}_{12}$ via scanning probe microscopy technique. <b>2017</b> , 7, 40695-40704	15
747	$\text{Cu Fe O}$ : hopping transport and ferromagnetism. <b>2017</b> , 4, 170339	5
746	Impedance spectroscopy study of $(\text{NH}_4)_3\text{H}(\text{SeO}_4)_2$ : Evidence of increase in lattice disorder in the low temperature phases. <b>2017</b> , 311, 26-30	2
745	Master curve generation and modeling of ac conductivity for $\text{Mn}_{0.7+x}\text{Zn}_{0.3}\text{Si}_x\text{Fe}_{2-x}\text{O}_4$ spinel ferrite system. <b>2017</b> , 07, 1750022	7
744	Reversible Structural Phase Transition and Dielectric Switches Induced by Disordering-Ordering Motion of Tetrachloroferrate (III) Anions. <b>2017</b> , 2, 8168-8172	7
743	Effect of mixed oxide/fluoride bonding on the dielectric properties of oxyfluoride glasses. <b>2017</b> , 28, 18986-18993	3
742	Iron-Oxide-Filled Carbon Nanotubes. <b>2017</b> , 293-313	1
741	Nanosize effect: Enhanced compensation temperature and existence of magnetodielectric coupling in $\text{SmFeO}_3$ . <b>2017</b> , 96,	31
740	Ferroelectric Fractional-Order Capacitors. <b>2017</b> , 4, 2807-2813	26
739	Temperature dependent electrical properties of combustion synthesized $\text{GdAlO}_3$ perovskite. <b>2017</b> ,	4
738	Structural and dielectric characterization of combustion synthesized perovskite neodymium aluminate. <b>2017</b> ,	
737	Colossal dielectric constant and interfacial charge polarization in a polymer-derived amorphous silicon carbonitride. <b>2017</b> , 43, 11623-11626	11



736	Colossal dielectric response of Mott insulating, nanocrystalline, T?-type Sm <sub>2</sub> CuO <sub>4</sub> ceramics. <b>2017</b> , 43, 14101-14106	3
735	Studies on order Disorder transition, lattice expansion and ionic conductivity in aliovalent cation substituted Sm <sub>2</sub> Zr <sub>2</sub> O <sub>7</sub> System. <b>2017</b> , 255, 121-128	10
734	Structural, dielectric and magnetic studies of multiferroics Bi <sub>1-x</sub> Sr <sub>x</sub> FeO <sub>3</sub> (x = 0.1, 0.2, 0.3, 0.4, and 0.5). <b>2017</b> , 72, 5-9	2
733	Frequency dependence of dielectric properties of ex situ MgB <sub>2</sub> bulks. <b>2017</b> , 28, 13391-13400	
732	SrTiO <sub>3</sub> BaTiO <sub>3</sub> nanocomposites with temperature independent permittivity and linear tunability fabricated using field-assisted sintering from chemically synthesized powders. <b>2017</b> , 5, 9028-9036	12
731	Structural and dielectric properties of multiferroic composite system Ba <sub>0.5</sub> Sr <sub>0.5</sub> TiO <sub>3</sub> -Ni <sub>0.4</sub> Co <sub>0.2</sub> Zn <sub>0.4</sub> Fe <sub>2</sub> O <sub>4</sub> . <b>2017</b> , 516, 122-126	1
730	The influence of insulating and conductive ellipsoidal objects on the impedance and permittivity of media. <b>2017</b> , 90, 131-138	8
729	Studies on the structure and dielectric properties of Ca-doped BiFeO <sub>3</sub> multiferroics. <b>2017</b> , 516, 106-116	3
728	Electrical analysis of inter-growth structured Bi <sub>4</sub> Ti <sub>3</sub> O <sub>12</sub> Na <sub>0.5</sub> Bi <sub>4.5</sub> Ti <sub>4</sub> O <sub>15</sub> ceramics. <b>2017</b> , 26, 077701	
727	Complex impedance study on polymer-derived amorphous silicon carbonitride. <b>2017</b> , 43, 13560-13564	3
726	Moisture effect on conductivity of kraft paper immersed in power transformer vegetable-based insulation oils. <b>2017</b> , 11, 2269-2274	10
725	Degradation Analysis of Encapsulated and Nonencapsulated TiO <sub>2</sub> /PTB7:PCBM/VO Solar Cells under Ambient Conditions via Impedance Spectroscopy. <b>2017</b> , 2, 3091-3097	14
724	Dielectric Properties of and Charge Transport in Columnar Microfibrous Thin Films of Parylene C. <b>2017</b> , 64, 3360-3367	10
723	Effect of magnetic ion (Mn) doping on structural, ferroelectric and magnetic properties of Ba <sub>0.90</sub> Mn <sub>0.10</sub> TiO <sub>3</sub> . <b>2017</b> , 43, 13339-13344	11
722	Short Time High-Resistance State Instability of TaO <sub>x</sub> -Based RRAM Devices. <b>2017</b> , 38, 32-35	15
721	Dielectric relaxation and ac conductivity behavior of carboxyl functionalized multiwalled carbon nanotubes/poly (vinyl alcohol) composites. <b>2017</b> , 87, 317-326	17
720	Dielectric behaviour of carbon nanotubes particles-filled polyester polymer composites. <b>2017</b> , 51, 1831-1837	15
719	A frequency-dependent theory of electrical conductivity and dielectric permittivity for graphene-polymer nanocomposites. <b>2017</b> , 111, 221-230	97

718	Structural characterization and electrical properties of carbon nanotubes/epoxy polymer composites. <b>2017</b> , 134,	14
717	Characterization and modeling of dynamic relaxation of a Zr-based bulk metallic glass. <b>2017</b> , 690, 212-220	14
716	Equivalent circuit models using CPE for impedance spectroscopy of electronic ceramics. <b>2017</b> , 183, 141-162	15
715	Study on conduction current characteristics of corona-resistant polyimide film before and after thermal aging. <b>2017</b> ,	2
714	Modulation of structural, electrical, and magnetic features with dilute Zr substitution in Bi <sub>0.8</sub> La <sub>0.2</sub> Fe <sub>1-x</sub> Zr <sub>x</sub> O <sub>3</sub> system. <b>2017</b> , 122, 244102	7
713	Broadband spectroscopy of dielectrics and oxygen-ion conductors. <b>2017</b> , 125, 547-551	4
712	Role of the defect in determining the properties of PbTi <sub>0.9</sub> Ni <sub>0.1</sub> O <sub>3</sub> thin films. <b>2017</b> , 122, 195104	11
711	Dielectric measurements on polypropylene nanocomposites filled with natural and synthetic nanoclay. <b>2017</b> ,	1
710	Forward and inverse modelling of electrical properties of some sandstone rocks using renormalisation group method. <b>2017</b> , 15, 487-498	7
709	High-temperature dielectric responses in all-nanosheet capacitors. <b>2017</b> , 56, 06GH09	5
708	Surfactant Incorporated Co Nanoparticles Polymer Composites with Uniform Dispersion and Double Percolation. <b>2017</b> , 2017, 1-6	4
707	Interaction between electromagnetic waves and biological materials. <b>2017</b> , 53-101	0
706	2D Ti <sub>3</sub> C <sub>2</sub> T <sub>x</sub> (MXene)-reinforced polyvinyl alcohol (PVA) nanofibers with enhanced mechanical and electrical properties. <b>2017</b> , 12, e0183705	62
705	Mechanical, dielectric, and physicochemical properties of impregnating resin based on unsaturated polyesterimides. <b>2017</b> , 80, 10901	4
704	Dielectric and electrical properties of La <sub>x</sub> Sr <sub>1-Bx</sub> /2Cu <sub>3</sub> Ti <sub>4</sub> O <sub>12</sub> ceramics. <b>2017</b> ,	
703	Electrical Conductivity in the KDP, ADP, and K <sub>1-x</sub> (NH <sub>4</sub> ) <sub>x</sub> H <sub>2</sub> PO <sub>4</sub> Crystals. <b>2017</b> , 20, 532-537	5
702	Large recoverable energy density with excellent thermal stability in Mn-modified NaNbO <sub>3</sub> -CaZrO <sub>3</sub> lead-free thin films. <b>2018</b> , 101, 3460-3467	37
701	Terahertz absorption in graphite nanoplatelets/polylactic acid composites. <i>Journal Physics D: Applied Physics</i> , <b>2018</b> , 51, 145307	3 27

700	Effect of Coral-Shaped Yttrium Iron Garnet Particles on the EMI Shielding Behaviour of Yttrium Iron Garnet-Polyaniline-Wax Composites. <b>2018</b> , 3, 2120-2130	41
699	Development of multi-functional nano-paint for energy harvesting applications. <b>2018</b> , 28, 1-6	7
698	Influence of defects on the dielectric relaxation and electrical conductivity behavior for Sr <sub>0.70</sub> Ba <sub>0.30</sub> Bi <sub>2</sub> Nb <sub>2</sub> O <sub>9</sub> ferroelectric ceramic. <b>2018</b> , 747, 38-42	4
697	Effect of different microwave power applied during microwave assisted radiant heating on the structure, dielectric and electrical properties of Ba <sub>0.8</sub> Ca <sub>0.2</sub> TiO <sub>3</sub> ceramics. <b>2018</b> , 29, 8158-8166	3
696	Mg <sub>2</sub> KH(XO <sub>4</sub> ) <sub>2</sub> ·5H <sub>2</sub> O (X = P, As) containing acidic dimer units: Electrochemical impedance spectroscopy, IR spectroscopy and DSC studies. <b>2018</b> , 746, 699-709	1
695	Investigation of periodically driven systems by x-ray absorption spectroscopy using asynchronous data collection mode. <b>2018</b> , 89, 045111	4
694	Influence of Zn doping on structural, optical and dielectric properties of LaFeO <sub>3</sub> . <b>2018</b> , 5, 055009	22
693	Silicon compatible Sn-based resistive switching memory. <b>2018</b> , 10, 9441-9449	20
692	Effect of borax additive on the dielectric response of polypyrrole. <b>2018</b> , 41, 1	5
691	Influence of functional group on the electrical transport properties of polyvinyl alcohol grafted multiwall carbon nanotube composite thick film. <b>2018</b> , 123, 145105	5
690	Dielectrical performance of high-k yttrium copper titanate thin films for electronic applications. <b>2018</b> , 29, 7090-7098	5
689	Impedance Spectroscopy of Dielectric Relaxation in a Perfluorosulfonic Acid Ionomer Nafion Membrane. <b>2018</b> , 72, 476-479	
688	Colossal dielectric behavior and relaxation in Nd-doped BaTiO <sub>3</sub> at low temperature. <b>2018</b> , 44, 7251-7258	24
687	Structural, electrical and dielectric properties of double perovskites: BiHoZnZrO <sub>6</sub> and BiHoCuTiO <sub>6</sub> . <b>2018</b> , 29, 6805-6816	11
686	Study on Electrical conductivity and Activation Energy of doped Ceria nanostructures. <b>2018</b> , 3, 49-53	8
685	Behavior of lanthanum containing barium stannate nanoparticles synthesized by cetyltrimmonium bromide assisted wet chemistry route. <b>2018</b> , 5, 025030	0
684	Thermal and ac electrical properties of N -methylantranilic acid below room temperature. <b>2018</b> , 117, 13-20	4
683	Hierarchical micro-nanostructured albite-based glass-ceramic for high dielectric strength insulators. <b>2018</b> , 38, 2759-2766	24

682	Ferroelectrics, multiferroics and artifacts: Lozenge-shaped hysteresis and things that go bump in the night. <b>2018</b> , 21, 553-562		20
681	Reversible Phase Transition with Ultralarge Dielectric Relaxation Behaviors in Succinimide Lithium(I) Hybrids. <b>2018</b> , 57, 1196-1202		33
680	Bias dependent conduction and relaxation mechanism study of Cu <sub>5</sub> FeS <sub>4</sub> film and its significance in signal transport network. <b>2018</b> , 29, 5014-5024		22
679	Static and dynamic electro-optical properties of liquid crystals mediated by ferroelectric polymer films.. <b>2018</b> , 8, 1889-1898		2
678	Towards fractional-order capacitors with broad tunable constant phase angles: multi-walled carbon nanotube-polymer composite as a case study. <i>Journal Physics D: Applied Physics</i> , <b>2018</b> , 51, 065602	3	20
677	Structural, dielectric and ferroelectric properties of rare earth substituted lead zirconate titanate. <b>2018</b> , 29, 4226-4237		8
676	The missing piece of the puzzle regarding the relation between the degree of superhydrophobicity and the corrosion resistance of superhydrophobic coatings. <b>2018</b> , 91, 41-44		6
675	Growth and physical investigations of sprayed ZnMoO <sub>4</sub> thin films along with wettability tests. <b>2018</b> , 539, 51-60		4
674	(Ba <sub>1-x</sub> Bi <sub>x</sub> )(Ti <sub>1-x</sub> Ni <sub>0.5x</sub> Sn <sub>0.5x</sub> )O <sub>3</sub> Solid Solution: Phase Evolution, Microstructure, Dielectric Properties, and Impedance Analysis. <b>2018</b> , 47, 2576-2583		8
673	Structural, electric transport response and electro-strain - Polarization effect in La and Ni modified bismuth ferrite nanostructures. <b>2018</b> , 748, 504-514		30
672	Electric conductivity, aging and chemical degradation of polyesterimide resins used in the impregnation of rotating machines. <b>2018</b> , 25, 294-305		9
671	Effect of Impedance Relaxation in Conductance Mechanisms in TiO <sub>2</sub> /ITO/ZnO:Al/p-Si Heterostructure. <b>2018</b> , 47, 3018-3025		1
670	Dielectric studies of Al nanoparticle reinforced epoxy resin composites. <b>2018</b> , 39, 887-894		24
669	Cellular Polymer Ferroelectret: A Review on Their Development and Their Piezoelectric Properties. <b>2018</b> , 37, 468-483		46
668	Effect of carbon nanotubes on electromagnetic interference shielding of carbon fiber reinforced polymer composites. <b>2018</b> , 39, E655-E663		23
667	A review of condition monitoring techniques and diagnostic tests for lifetime estimation of power transformers. <b>2018</b> , 100, 581-605		47
666	An impedance model for the low-frequency noise originating from the dynamic hydrogen ion reactivity at the solid/liquid interface. <b>2018</b> , 254, 363-369		6
665	Surface layer and its effect on dielectric properties of SiC ceramics. <b>2018</b> , 734, 16-21		7

664	AC/DC electrical conduction and dielectric properties of PMMA/PVAc/C60 down-shifting nanocomposite films. <b>2018</b> , 1154, 239-247	5
663	A nitrile functionalized graphene filled ethylene propylene diene terpolymer rubber composites with improved heat resistance. <b>2018</b> , 134, 81-90	10
662	Temperature stability, low loss and defect relaxation of MgO-TiO <sub>2</sub> microwave dielectric ceramics modified by Ca <sub>0.8</sub> Sr <sub>0.2</sub> TiO <sub>3</sub> . <b>2018</b> , 44, 141-145	14
661	Dielectric Spectroscopy of Localized Electrical Charges in Ferrite Thin Film. <b>2018</b> , 47, 378-384	13
660	Electrical and dielectric properties of bismuth holmium cobalt titanate (BiHoCoTiO <sub>6</sub> ): a complex double perovskite. <b>2018</b> , 29, 3682-3689	13
659	Evidence of superparamagnetism and improved electrical properties in Ba and Ta co-doped BiFeO <sub>3</sub> ceramics. <b>2018</b> , 735, 2584-2596	30
658	Structural phase transition and multiferroic properties of Bi <sub>0.8</sub> A <sub>0.2</sub> Fe <sub>0.8</sub> Mn <sub>0.2</sub> O <sub>3</sub> (A = Ca, Sr). <b>2018</b> , 92, 575-585	1
657	Dielectric and non-ohmic properties of Ca <sub>2</sub> Cu <sub>2</sub> Ti <sub>4-x</sub> Sn <sub>x</sub> O <sub>12</sub> (0.0 ≤ x ≤ 1.0) multiphasic ceramic composites. <b>2018</b> , 735, 140-149	27
656	Nanopowders of (Ba,Ca)(Ti,Sn)O <sub>3</sub> produced with planetary ball mill and corresponding ceramics. <b>2018</b> , 194, 126-134	0
655	Electric Properties of Nanocomposite Films Based on Amorphous Hydrogenated Carbon. <b>2018</b> , 63, 1620-1625	0
654	Solvothermal growth of BaTiO <sub>3</sub> thin films on Ti foils at T = 200 °C with ferroelectric behavior. <b>2018</b> , 536, 105-112	
653	Precision electric characterization of LDPE specimens made by different manufacturing processes. <b>2018</b> ,	3
652	Effects of proton conduction on dielectric properties of peptides.. <b>2018</b> , 8, 34047-34055	6
651	Yttrium ferrites with enhanced dielectric properties. <b>2018</b> , 232-235, 41-47	6
650	Characterization of CuInS <sub>2</sub> /CdS Heterojunctions. <b>2018</b> , 1032, 012020	
649	Excellent thermal-stability and low dielectric loss of BaTiO <sub>3</sub> -Bi(Sr <sub>2</sub> /3Nb <sub>1</sub> /3)O <sub>3</sub> solid solution ceramics in a broad temperature range applied in X8R. <b>2018</b> , 238-239, 130-135	1
648	Current-Voltage Hysteresis Behavior of PVA-Assisted Functionalized Single-Walled Carbon Nanotube Free-Standing Film. <b>2018</b> , 122, 29094-29105	13
647	High temperature impedance properties and conduction mechanism of W <sup>6+</sup> -doped CaBi <sub>4</sub> Ti <sub>4</sub> O <sub>15</sub> Aurivillius piezoceramics. <b>2018</b> , 124, 204101	7

646	Physical Approach to Ferroelectric Impedance Spectroscopy: The Rayleigh Element. <b>2018</b> , 10,	5
645	Electrical and thermal conductivity of ethylene vinyl acetate composite with graphene and carbon black filler. <b>2018</b> , 72, 24-31	36
644	Almond-West type grain and grain boundary conduction-modified dielectric relaxation in NdCoO <sub>3</sub> . <b>2018</b> , 124, 1	11
643	Effect of Nb and Fe co-doping on microstructure, dielectric response, ferroelectricity and energy storage density of PLZT. <b>2018</b> , 29, 20383-20394	14
642	Excellent thermal stability and low dielectric loss of (Ba <sub>1-x</sub> Bi <sub>0.5x</sub> Sr <sub>0.5x</sub> )(Ti <sub>1-x</sub> Bi <sub>0.5x</sub> Zr <sub>0.5x</sub> )O <sub>3</sub> solid solution ceramics in a broad temperature range applied in X8R. <b>2018</b> , 124, 1	4
641	Giant permittivity and good thermal stability of LiCuNb <sub>3</sub> O <sub>9</sub> -Bi(Mg <sub>0.5</sub> Zr <sub>0.5</sub> )O <sub>3</sub> solid solutions. <b>2018</b> , 08, 1850012	2
640	Characterization of temperature sensitivity of V-modified CuFe <sub>2</sub> O <sub>4</sub> ceramics for NTC thermistors. <b>2018</b> , 29, 18797-18806	5
639	Application of [Pt(II)(Tetra-Tert-Butylsalophen)] Complex within Organic Devices: Deep Red Emission, Bistable Light-Emitting Diodes and Operational Stability. <b>2018</b> , 8, 762	2
638	Electrical Properties of Yttria-Stabilized Zirconia, YSZ Single Crystal: Local AC and Long Range DC Conduction. <b>2018</b> , 165, F966-F975	18
637	Nano SiO <sub>2</sub> /epoxy coating effect on lightning impulse breakdown characteristic in N <sub>2</sub> . <b>2018</b> , 5, 065046	3
636	Electrical and Magnetic Properties of Yttrium Ferrites. <b>2018</b> , 165-174	
635	Synthesis, electrical properties, and conduction mechanism of [N(CH <sub>3</sub> ) <sub>4</sub> ] <sub>2</sub> PdCl <sub>4</sub> compound. <b>2018</b> , 103, 10-17	3
634	Dielectric constant, AC conductivity and impedance spectroscopy of zinc-containing diamond-like carbon film UV photodetector. <b>2018</b> , 758, 194-205	18
633	Fractional-Order Modeling and Simulation of Magnetic Coupled Boost Converter in Continuous Conduction Mode. <b>2018</b> , 28, 1850061	10
632	(Ba <sub>1-x</sub> Bi <sub>0.33x</sub> Sr <sub>0.67x</sub> )(Ti <sub>1-x</sub> Bi <sub>0.67x</sub> V <sub>0.33x</sub> )O <sub>3</sub> and (Ba <sub>1-x</sub> Bi <sub>0.5x</sub> Sr <sub>0.5x</sub> )(Ti <sub>1-x</sub> Bi <sub>0.5x</sub> Ti <sub>0.5x</sub> )O <sub>3</sub> solid solutions: phase evolution, microstructure, dielectric properties and impedance analysis. <b>2018</b> , 124, 1	2
631	A Planar Layered Two-Phase System Model of Frequency Response of Insulation System for Estimating Moisture in IOCT. <b>2018</b> , 1-4	1
630	A method of determination of electrical conduction mechanisms in complex amorphous materials. <b>2018</b> , 498, 223-227	
629	Cross-shaped PnC for anchor loss reduction of thin-film ALN-on-silicon high frequency MEMS resonator. <b>2018</b> ,	0

628	Polyaniline/Polystyrene Blends: In-Depth Analysis of the Effect of Sulfonic Acid Dopant Concentration on AC Conductivity Using Broadband Dielectric Spectroscopy. <b>2018</b> , 2018, 1-9	4
627	The effects of oxygen vacancies on the electrical properties of W, Ti doped CaBi <sub>2</sub> Nb <sub>2</sub> O <sub>9</sub> piezoceramics. <b>2018</b> , 18, 1149-1157	13
626	Ionic Conduction and Anomalous Diffusion in Sr and Ga Acceptors Co-Doped Bismuth Sodium Titanate Solid Solutions. <b>2018</b> , 7, N96-N100	7
625	Asymmetry induced intrinsic magnetodielectric effects in manganite Barium titanate solid solutions. <b>2018</b> , 468, 168-174	1
624	Humidity Sensing Properties of Transparent Sputter-Coated Indium Tin Oxide and Printed Polymer Structures. <b>2018</b> , 18, 7358-7364	10
623	Structural, magnetic and electrical properties of Fe substituted GdCrO <sub>3</sub> . <b>2018</b> , 83, 192-200	15
622	Effect of Background Fe Impurities on the IR Absorption and Dielectric Response of High-Resistivity ZnSe Single Crystals. <b>2018</b> , 54, 757-759	5
621	Local Structural Heterogeneity and Electromechanical Responses of Ferroelectrics: Learning from Relaxor Ferroelectrics. <b>2018</b> , 28, 1801504	149
620	Metal Oxide Based Hydroelectric Cell for Electricity Generation by Water Molecule Dissociation without Electrolyte/Acid. <b>2018</b> , 122, 18841-18849	29
619	Dielectrical and structural studies of composite matrix BiVO <sub>4</sub> /CaTiO <sub>3</sub> and temperature effects by impedance spectroscopy. <b>2018</b> , 29, 16248-16258	12
618	Criterion of Existence of Power-Law Memory for Economic Processes. <b>2018</b> , 20,	18
617	Electron trapping at SiO <sub>2</sub> /4H-SiC interface probed by transient capacitance measurements and atomic resolution chemical analysis. <b>2018</b> , 29, 395702	10
616	Effect of temperature on the electrical properties of lanthanum ferrite. <b>2018</b> , 205, 214-220	8
615	Structural Analysis and Conduction Mechanisms in Polycrystalline Zinc Hydroxide Nitrate. <b>2018</b> , 57, 9067-9078	6
614	High-k YCTO thin films for electronics. <b>2018</b> ,	
613	Mechanical relaxation and freezing in the room temperature strain glass alloy Ti(PdCr). <b>2018</b> , 30, 345402	1
612	Thermodynamic potentials in anisotropic and nonlinear dielectrics. <b>2018</b> , 541, 54-60	4
611	High-Temperature Electrical Insulation Behavior of Alumina Films Prepared at Room Temperature by Aerosol Deposition and Influence of Annealing Process and Powder Impurities. <b>2018</b> , 27, 870-879	15

610	A novel approach to study the conductivity behavior of CaCu <sub>3</sub> Ti <sub>4</sub> O <sub>12</sub> using scanning probe microscopy technique. <b>2018</b> , 8, 932-937	2
609	Electronic synapses made of layered two-dimensional materials. <b>2018</b> , 1, 458-465	316
608	Some characterizations of a new metal-organic framework (n-C <sub>14</sub> H <sub>29</sub> NH <sub>3</sub> ) <sub>2</sub> CdCl <sub>4</sub> and the role of hydrogen bonding. <b>2018</b> , 91, 840-861	1
607	Influence of chitin nanocrystals on the dielectric behaviour and conductivity of chitosan-based bionanocomposites. <b>2018</b> , 167, 323-330	14
606	Electrical properties and sintering characteristics of zirconium doped CaBi <sub>2</sub> Nb <sub>2</sub> O <sub>9</sub> ceramics. <b>2018</b> , 44, 17326-17332	13
605	Dielectric relaxation and ac conductivity in magnetoelectric YCrO <sub>3</sub> ceramics: A temperature dependent impedance spectroscopy analysis. <b>2018</b> , 38, 5359-5366	11
604	Preparation, molecular structure, thermal properties, electrical conductivity analysis and dielectric relaxation of a new hybrid compound (NH <sub>2</sub> C <sub>5</sub> H <sub>3</sub> ClNH) <sub>2</sub> ZnBr <sub>4</sub> ·H <sub>2</sub> O. <b>2018</b> , 72, 2795-2811	2
603	Low temperature synthesis and characterization of nano-crystalline Mg(Zr <sub>0.05</sub> Ti <sub>0.95</sub> )O <sub>3</sub> ceramics. <b>2018</b> , 101, 5389-5399	4
602	Effect of mineral matter on structure and dielectric properties of chars. <b>2018</b> , 222, 370-374	13
601	Stress-dependent electrical transport and its universal scaling in granular materials. <b>2018</b> , 22, 83-88	5
600	Exploring the universality of the alternating conductivity of disordered materials using the Gaussian distribution of activation energies. <b>2019</b> , 6, 046302	0
599	Dielectric constant and electrical study of solid-state electrolyte lithium phosphate glasses. <b>2019</b> , 125, 1	16
598	The influence of ZnO nanoparticles on the dielectric properties of epoxy resin. <b>2019</b> ,	1
597	Spectroscopic Analysis of Unsaturated Polyester Resin-Based Composites and Nanocomposites. <b>2019</b> , 313-366	1
596	Defect driven d <sub>0</sub> ferromagnetism and colossal dielectric behavior in Bi(Zn <sub>0.5</sub> Ti <sub>0.5</sub> )O <sub>3</sub> BbTiO <sub>3</sub> ceramics. <b>2019</b> , 45, 22948-22955	2
595	Study of electrical transport, dielectric and magnetic properties of NiFe <sub>2</sub> O <sub>4</sub> -PVDF nanocomposite film. <b>2019</b> , 114, 113632	4
594	Effect of Pt <sub>3</sub> Pb on the permittivity and conductivity of lead zirconate titanate thin films. <b>2019</b> , 685, 420-427	1
593	Dielectric, magnetic and magneto-dielectric properties of (La, Co) co-doped BiFeO <sub>3</sub> . <b>2019</b> , 94, 125805	6



592	Inversion Detection Method for Resistivity of Oil-Immersed Paper in Transformer. <b>2019</b> , 34, 1757-1765	6
591	Diagnostic challenges in dielectric loss assessment and interpretation: a review. <b>2019</b> , 13, 767-782	14
590	AC conductivity and dielectric characteristics of PVA/PVP nanocomposite filled with MWCNTs. <b>2019</b> , 30, 15521-15533	18
589	Mesoporous Silica-Based Materials for Electronics-Oriented Applications. <b>2019</b> , 24,	32
588	Preparation, structural analysis, morphological investigation and electrical properties of gold nanoparticles filled polyvinyl alcohol/carboxymethyl cellulose blend. <b>2019</b> , 8, 5996-6010	30
587	Temperature dependent structural and electrical analysis of Cr-doped multiferroic GaFeO <sub>3</sub> ceramics. <b>2019</b> , 6, 115704	3
586	Suitability of Sm <sup>3+</sup> -Substituted SrTiO <sub>3</sub> as Anode Materials for Solid Oxide Fuel Cells: A Correlation between Structural and Electrical Properties. <b>2019</b> , 12, 4042	4
585	Crystal Structure, Raman Spectroscopy and Dielectric Properties of New Semiorganic Crystals Based on 2-Methylbenzimidazole. <b>2019</b> , 9, 573	6
584	Dielectric and optical properties of Ni-doped LaFeO <sub>3</sub> nanoparticles. <b>2019</b> , 1, 1	5
583	Application of L1 Trend Filtering Technology on the Current Time Domain Spectroscopy of Dielectrics. <b>2019</b> , 8, 1046	2
582	Electrical Behavior of a Catalyst Composed of Laminar Manganese Oxide Supported on Al <sub>2</sub> O <sub>3</sub> . <b>2019</b> , 24,	
581	Study of Structural, Optical and AC Electrical Properties of Chloroindium Phthalocyanine. <b>2019</b> , 48, 7479-7486	2
580	Fabrication of ZnO-AlO-PTFE Multilayer Nano-Structured Functional Film on Cellulose Insulation Polymer Surface and Its Effect on Moisture Inhibition and Dielectric Properties. <b>2019</b> , 11,	2
579	Effect of V <sub>2</sub> O <sub>5</sub> addition on the structural and electrical properties of CoTiO <sub>3</sub> . <b>2019</b> , 176, 107286	5
578	Structural and Electrical Studies for Birnessite-Type Materials Synthesized by Solid-State Reactions. <b>2019</b> , 9,	9
577	Sb <sup>3+</sup> and Gd <sup>3+</sup> co-doped Cerium oxide Nanocrystalline Ceramic system: Structural and Dielectric Studies. <b>2019</b> , 10, 46-51	
576	The Influence of ZnO nanoparticles in the epoxy resin on the complex permittivity and dissipation factor. <b>2019</b> , 40, 30-33	1
575	Electrical properties speculation of contamination by water and gasoline on sand and clay composite. <b>2019</b> , 12, 1	3

574	Impurity induced dielectric relaxor behavior in Zn doped LaFeO <sub>3</sub> . <b>2019</b> , 30, 19227-19238	7
573	Comparative study of electrical properties of Cu <sub>2</sub> Zn <sub>x</sub> Fe <sub>1-x</sub> Sn <sub>4</sub> thin films. <b>2019</b> , 240, 55-61	1
572	Intrinsic Insertion Limits of Graphene Oxide into Epoxy Resin and the Dielectric Behavior of Composites Comprising Truly 2D Structures. <b>2019</b> , 123, 3461-3468	8
571	Effect of moisture and filler content on the structural, thermal and dielectric properties of polyamide-6/boehmite alumina nanocomposites. <b>2019</b> , 68, 871-885	4
570	Magneto-dielectric and multiferroic properties in Bi <sub>0.95</sub> Yb <sub>0.05</sub> Fe <sub>0.95</sub> Co <sub>0.05</sub> O <sub>3</sub> . <b>2019</b> , 94, 065802	6
569	Optical spectroscopy: An effective tool to probe the origin of dielectric loss in Cr doped PrFeO <sub>3</sub> . <b>2019</b> , 45, 8585-8592	24
568	Tunable optical and dielectric properties of polymeric composite materials based on magnesio-silicate. <b>2019</b> , 42, 1	11
567	Diffusional and electrochemical investigation of combustion synthesized BaLi <sub>2</sub> Ti <sub>6</sub> O <sub>14</sub> titanate anode for rechargeable batteries. <b>2019</b> , 34, 158-168	3
566	Sugar Concentration Measurement System Using Radiofrequency Sensor. <b>2019</b> , 19,	0
565	NiFe <sub>2</sub> O <sub>4</sub> - ZnO semiconducting nanocomposites: Studies of room temperature magnetoelectric coupling and electronic transport. <b>2019</b> , 234, 16-24	3
564	Dielectric relaxation and magneto-electric characteristics of lead-free double perovskite: Sm <sub>2</sub> NiMnO <sub>6</sub> . <b>2019</b> , 8, 174-185	17
563	Preparation and study of some physical properties of Co <sub>0.5</sub> Ni <sub>0.5</sub> ferrite/polypyrrole nanocomposites. <b>2019</b> , 802, 553-561	9
562	Dielectric properties and microwave heating characteristics of Huimin siderite ore. <b>2019</b> , 53, 128-141	2
561	AC conductivity and dielectric response of bulk vanadyl 2,3-naphthalocyanine. <b>2019</b> , 570, 301-307	1
560	Increasing the Penetration Depth of Microwave Radiation Using Acoustic Stress to Trigger Piezoelectricity. <b>2019</b> , 33, 6327-6334	9
559	Significance of interface barrier at electrode of hematite hydroelectric cell for generating ecpower by water splitting. <b>2019</b> , 43, 4743-4755	57
558	Responsive charge transport in wide-band-gap oxide films of nanostructured amorphous alkali-gallium-germanosilicate. <b>2019</b> , 7, 7768-7778	1
557	Influence of Ti-Substitution on Structural, Magnetic and Dielectric Properties of M-Type Barium Hexaferrite. <b>2019</b> , 48, 5062-5074	8

556	The impact of thickness on the optical, electrical and dielectric properties of nanocrystalline 0.9 MTO-0.1BNO composite thin films. <b>2019</b> , 489, 831-840	3
555	Screening Links Transport and Recombination Mechanisms in Lead Halide Perovskites. <b>2019</b> , 123, 15827-15833	
554	Conductive network formation in bacterial cellulose-based nanocomposite aerogels. <b>2019</b> , 174, 106981	13
553	Ni nanocrystals tuning low-frequency colossal permittivity of epitaxial BaTiO <sub>3</sub> matrix. <b>2019</b> , 801, 460-464	0
552	Enhanced dielectric and microwave absorption properties of Y <sub>2</sub> Ti <sub>2</sub> O <sub>7</sub> ceramics by Sr doping. <b>2019</b> , 125, 1	5
551	Self-enhanced electrical performance and less defective electrode/film structure for Al <sub>2</sub> O <sub>3</sub> capacitor via interfacial anodic oxidation. <b>2019</b> , 313, 20-30	2
550	Structural, magnetic, grain and grain boundary mediated conduction features of low dimensional LaFeO nanoparticles. <b>2019</b> , 31, 345803	5
549	Wideband Dielectric Characterization of 3-D Printable Triethylene Glycol Dimethacrylate Ester Plastic. <b>2019</b> , 68, 4419-4426	2
548	Starfish-like C/CoNiO <sub>2</sub> heterostructure derived from ZIF-67 with tunable microwave absorption properties. <b>2019</b> , 373, 122-130	85
547	Structural and Electronic Properties of PPy-DBSA/Zirconium Oxide Composites. <b>2019</b> , 61, 105-111	0
546	Comparison of Mechanical and Electrical Characteristics of Various Polymers Blended with Ground Tire Rubber (GTR) and Applications. <b>2019</b> , 9, 1564	6
545	Dielectric properties. <b>2019</b> , 425-442	0
544	Study of magneto capacitance effect, exchange bias, XMCD and XAS in LaBiFeMnO/LaNiO/LaAlO multiferroic thin film. <b>2019</b> , 31, 345001	
543	Enhanced dielectric, magnetic and optical properties of Cr-doped BiFeO <sub>3</sub> multiferroic nanoparticles synthesized by sol-gel route. <b>2019</b> , 13, 102299	22
542	Electronic and Dielectric Properties of MoV-Oxide (M1 Phase) under Alkane Oxidation Conditions. <b>2019</b> , 123, 13269-13282	10
541	High-temperature dielectric relaxations in (Ce, Y) codoped BaZrO <sub>3</sub> ceramics. <b>2019</b> , 6, 075010	1
540	Lead-free (K, Na, Li) NbO <sub>3</sub> /NiFe <sub>2</sub> O <sub>4</sub> thin films by pulsed laser deposition: Structure, dielectric, magnetic and magnetodielectric behavior. <b>2019</b> , 794, 534-541	14
539	Dielectric relaxation behavior induced by lithium migration in Li <sub>4</sub> Ti <sub>5</sub> O <sub>12</sub> spinel. <b>2019</b> , 793, 678-685	17

538	Coexistence of dielectric relaxation and magnetic relaxation in compressively strained BiFeO <sub>3</sub> /Ba <sub>0.7</sub> Sr <sub>0.3</sub> TiO <sub>3</sub> superlattices. <b>2019</b> , 114, 112902	4
537	A Solution Processed Ultrathin Molecular Dielectric for Organic Field-Effect Transistors. <b>2019</b> , 1, 485-493	4
536	Effect of A-site Fe substitution on the magnetic behavior of Dy <sub>2</sub> Ti <sub>2</sub> O <sub>7</sub> spin ice. <b>2019</b> , 481, 221-226	0
535	Analysis of dielectric and magnetic phase transitions in Yb(Fe <sub>0.5</sub> Cr <sub>0.5</sub> )O <sub>3</sub> bulk perovskite. <b>2019</b> , 125, 1	12
534	Studies on electronic structure and dielectric properties of La-doped ErFeO <sub>3</sub> orthoferrites. <b>2019</b> , 789, 814-824	9
533	Magnetic field control of electric properties in gadolinium doped BaTiO <sub>3</sub> /CoFe <sub>2</sub> O <sub>4</sub> particulate multiferroic composites. <b>2019</b> , 6, 066310	7
532	Effect of B or N doping on the dielectric and electrical properties of ZnO at room temperature. <b>2019</b> , 6, 065017	2
531	The structural, dielectric, and magnetic properties of Al <sup>3+</sup> doped Sm <sub>3</sub> Fe <sub>5</sub> O <sub>12</sub> ceramics. <b>2019</b> , 90, 611-620	4
530	Impedance Spectroscopy for Emerging Photovoltaics. <b>2019</b> , 123, 11329-11346	134
529	Study on relaxation process of fluorinated graphite/poly(vinylidene fluoride-hexafluoropropylene) composites by dielectric relaxation spectroscopy. <b>2019</b> , 6, 065323	1
528	On the corrosion mechanism of Mg investigated by electrochemical impedance spectroscopy. <b>2019</b> , 306, 61-70	83
527	Two-channel model for optical conductivity of high-mobility organic crystals. <b>2019</b> , 125, 47002	3
526	PVDF/BaTiO <sub>3</sub> /carbon nanotubes ternary nanocomposites prepared by ball milling: Piezo and dielectric responses. <b>2019</b> , 136, 47788	11
525	Three different mechanisms of self-discharge behavior in poly(vinylidene fluoride-hexafluoropropylene) for dielectric energy storage. <b>2019</b> , 1, 025001	2
524	A Method for Substrate Permittivity and Dielectric Loss Characterization Up to Subterahertz Frequencies. <b>2019</b> , 67, 1640-1651	7
523	Universal dielectric response across a continuous metal-insulator transition. <b>2019</b> , 99,	3
522	Facial synthesis of highly active polymer vanadium molybdate nanocomposite: Improved thermoelectric and antimicrobial studies. <b>2019</b> , 131, 148-155	13
521	Electromagnetic properties of chloroprene rubber after long-term ultraviolet ageing, oil immersion and thermal degradation. <b>2019</b> , 6, 075327	0

520	Dielectric Properties of Calcium Copper Titanate Ceramics Exposed to Air and Dry Nitrogen Atmospheres. <b>2019</b> , 72, 2035-2041	2
519	Aging condition assessment of transformer oil-immersed cellulosic insulation based upon the average activation energy method. <b>2019</b> , 26, 3891-3908	31
518	AC conductivity and polarization phenomenon of $\text{Li}_2\text{O}:\text{MoO}_3:\text{B}_2\text{O}_3:\text{V}_2\text{O}_5$ glasses. <b>2019</b> , 787, 1280-1289	13
517	Exciton- and Polaron-Induced Reversible Dipole Reorientation in Amorphous Organic Semiconductor Films. <b>2019</b> , 7, 1801644	29
516	Nanofiller-Induced Ionic Conductivity Enhancement and Relaxation Property Analysis of the Blend Polymer Electrolyte Using Non-Debye Electric Field Relaxation Function. <b>2019</b> , 123, 5188-5197	11
515	Influence of atmospheres on the dielectric properties of calcium copper titanate ceramics. <b>2019</b> , 102, 5271-5283	1
514	Temperature and frequency dependent dielectric relaxation of $\text{NiFeO}_x$ nanocomposites. <b>2019</b> , 6, 1250h4	2
513	Output Feedback based Adaptive Control for Fractional Order Inverted Pendulum on Cart in NSOF Domain. <b>2019</b> ,	
512	Evaluation of strand-to-strand capacitance and dissipation factor in thermally aged enamelled coils for low-voltage electrical machines. <b>2019</b> , 13, 1170-1177	10
511	Effect of atmosphere on dielectric properties of calcium copper titanate ceramics. <b>2019</b> , 1-14	
510	Investigation on Insulation Performance of Thermally Aged Natural Ester Oil Impregnated Pressboard. <b>2019</b> , 13, 1194-1202	3
509	Variation of Streaming Potentials with Time under Steady Fluid Pressure in Bone. <b>2019</b> , 9, 3726	2
508	Theoretical investigation of the vertical dielectric screening dependence on defects for few-layered van der Waals materials.. <b>2019</b> , 9, 40309-40315	7
507	Influence of annealing temperature on physical properties of $\text{NaNbO}_3$ thin films prepared by a water-based sol-gel process. <b>2019</b> , 126, 225101	4
506	Interfacial charge dynamics of cross-linked polyethylene/ethylene-propylene-diene dual dielectric polymer as revealed by energy band structure. <b>2019</b> , 26, 1755-1762	9
505	Temperature dependent charge conduction and relaxation mechanism study of nano-structure $\text{WO}_3$ by impedance spectroscopy. <b>2019</b> , 6, 1250a5	1
504	Influence of the orthorhombic phase content on the dielectric and magnetic properties of $\text{YMnO}_3$ . <b>2019</b> , 126, 224103	2
503	Amplifying gas sensor performance by embedding a cellulose-based buffer layer in organic transistors. <b>2019</b> , 7, 14504-14510	13

502	Apparent ferroelectric-like and dielectric properties of CH <sub>3</sub> NH <sub>3</sub> PbI <sub>3</sub> synthesized in ambient air. <b>2019</b> , 553, 95-102	5
501	Dielectric, magnetic, and mechanical properties of composites consisting of biopolymer chitosan matrix and hybrid spinel/cellulose filler. <b>2019</b> , 45, 9468-9476	12
500	Low-Frequency Dipolar Dynamics and Atmospheric Effects in ZIF-90 Metal-Organic Framework. <b>2019</b> , 123, 631-636	12
499	Colossal-Permittivity Behaviors in A-Site Distorted Double-Perovskite LiCuNb <sub>3</sub> O <sub>9</sub> with Correlated Magnetoelectric Effect and Variable-Range Hopping. <b>2019</b> , 1, 64-74	14
498	Insights into charge transition within band structure of amorphous SiCNO ceramic. <b>2019</b> , 45, 6853-6857	0
497	Structural and conduction behaviour of (BaSr) <sub>0.5</sub> TiO <sub>3</sub> modified in BFO perovskite. <b>2019</b> , 225, 91-98	18
496	Structural, electrical and dielectric studies of nano-composite polymer blend electrolyte films based on (70%) PVA% PVP% AlBiO <sub>2</sub> . <b>2019</b> , 554, 158-164	35
495	Phase evolution, microstructure, thermal stability and conductivity behavior of (Ba <sub>1-x</sub> Bi <sub>0.67x</sub> K <sub>0.33x</sub> )(Ti <sub>1-x</sub> Bi <sub>0.33x</sub> Sn <sub>0.67x</sub> )O <sub>3</sub> solid solutions ceramics. <b>2019</b> , 777, 1066-1073	9
494	Hydrogen-bonded and supramolecular ferroelectricity in a new hybrid (C <sub>12</sub> H <sub>25</sub> NH <sub>3</sub> ) <sub>2</sub> CoCl <sub>4</sub> . <b>2019</b> , 6, 025608	4
493	Electronic transport properties of (Se <sub>80</sub> Te <sub>20</sub> ) <sub>100-x</sub> Zn <sub>x</sub> (2.7x.76) chalcogenide alloys. <b>2019</b> , 555, 41-46	8
492	Role of rare-earth (Nd <sup>3+</sup> ) ions on structural, dielectric, magnetic and Mossbauer properties of nano-sized CoFe <sub>2</sub> O <sub>4</sub> : useful for high frequency application. <b>2019</b> , 6, 026107	9
491	Structural, magnetic and impedance spectroscopy properties of Ho <sup>3+</sup> modified BiFeO <sub>3</sub> multiferroic thin film. <b>2019</b> , 30, 2942-2952	6
490	Remarkable change in the broadband electrical behavior of poly(vinylidene fluoride)/multiwalled carbon nanotube nanocomposites with the use of different processing routes. <b>2019</b> , 136, 47409	7
489	Sol-gel derived cobalt doped LaCrO <sub>3</sub> : Structure and physical properties. <b>2019</b> , 784, 541-555	31
488	Evidence of large hopping polaron conduction process in strontium doped calcium copper titanate ceramics. <b>2019</b> , 556, 36-41	11
487	Colossal dielectric behavior and dielectric anomalies in Sr <sub>2</sub> TiCrO <sub>6</sub> ceramics. <b>2019</b> , 54, 6323-6331	5
486	Investigation on the growth, optical, mechanical and dielectric properties of an inorganic potassium pentaborate dihydrate (KB <sub>5</sub> H <sub>4</sub> O <sub>10</sub> .2H <sub>2</sub> O) single crystal. <b>2019</b> , 223, 230-240	5
485	Dielectric properties and interfacial adhesion of jute, kenaf and E-glass fabrics reinforcing epoxy composites. <b>2019</b> , 40, 2142-2153	14

484	Enhancement of spectroscopic, thermal, electrical and morphological properties of polyethylene oxide/carboxymethyl cellulose blends: Combined FT-IR/DFT. <b>2019</b> , 159, 430-440	77
483	Functional properties of percolative CoFe <sub>2</sub> O <sub>4</sub> -PbTiO <sub>3</sub> composite ceramics. <b>2019</b> , 775, 90-99	18
482	Temperature and frequency effect on the electrical properties of bulk nickel phthalocyanine octacarboxylic acid (Ni-Pc(COOH) <sub>8</sub> ). <b>2019</b> , 125, 1	16
481	Dielectric, electrical and impedance study of single perovskite Pb(Ni <sub>1/3</sub> Mn <sub>1/3</sub> W <sub>1/3</sub> )O <sub>3</sub> . <b>2019</b> , 93, 837-844	3
480	The role of B-site substitution on the structural and dielectric properties of samarium orthoferrite polycrystals. <b>2019</b> , 6, 036106	1
479	Investigation of structural, optical and electrical properties of Sr <sub>2</sub> SnO <sub>4</sub> , Sr <sub>1.99</sub> Eu <sub>0.01</sub> SnO <sub>4</sub> and Sr <sub>2</sub> Sn <sub>0.99</sub> Eu <sub>0.01</sub> O <sub>4</sub> Ruddlesden Popper oxide. <b>2019</b> , 6, 055805	8
478	Temperature-Stable Dielectric Properties from 166°C to 248°C in (1-x)BaTiO <sub>3</sub> -xBi(Mg <sub>0.5</sub> Sn <sub>0.5</sub> )O <sub>3</sub> System. <b>2019</b> , 48, 296-303	7
477	Signal propagation in electromagnetic media described by fractional-order models. <b>2020</b> , 82, 105029	15
476	Electrical, morphology and structural properties of biodegradable nanocomposite polyvinyl-acetate/ cellulose nanocrystals. <b>2020</b> , 240, 122182	10
475	(Ba,Sr)TiO <sub>3</sub> solid solutions sintered from sol-gel derived powders: An insight into the composition and temperature dependent dielectric behavior. <b>2020</b> , 46, 4180-4190	4
474	Rare earth substituted Bi <sub>0.84</sub> RE <sub>0.16</sub> FeO <sub>3</sub> (RE = La, Gd) - an efficient multiferroic photo-catalyst under visible light irradiation. <b>2020</b> , 45, 16944-16954	7
473	Influence of Zr dopant on polarization in rutile (In <sub>0.5</sub> Nb <sub>0.5</sub> ) <sub>0.005</sub> (Ti <sub>1-x</sub> Zr <sub>x</sub> ) <sub>0.995</sub> O <sub>2</sub> ceramics. <b>2020</b> , 103, 1854-1863	3
472	Citrate combustion synthesized Al-doped CaCuTiO quadruple perovskite: synthesis, characterization and multifunctional properties. <b>2020</b> , 22, 3499-3511	7
471	Enhanced high temperature microwave absorption of La <sub>0.9</sub> Sr <sub>0.1</sub> MnO <sub>3</sub> /MgAl <sub>2</sub> O <sub>4</sub> composite ceramics based on controllable electrical conductivity. <b>2020</b> , 40, 1931-1937	4
470	Homogeneous mixture of hematite and its electrical properties. <b>2020</b> , 243, 122584	4
469	Non-solvating, side-chain polymer electrolytes as lithium single-ion conductors: synthesis and ion transport characterization. <b>2020</b> , 11, 461-471	30
468	MWCNT induced negative real permittivity in a copolyester of Bisphenol-A with terephthalic and isophthalic acids. <b>2020</b> , 7, 015337	2
467	Negative capacitance switching in size-modulated FeO nanoparticles with spontaneous non-stoichiometry: confronting its generalized origin in non-ferroelectric materials. <b>2020</b> , 12, 1528-1540	7

466	Influence of the chemical functionalization of carbon nanotubes on low temperature ac conductivity with polyaniline composites. <i>Journal Physics D: Applied Physics</i> , <b>2020</b> , 53, 125303	3	11
465	Quantitative evaluation for moisture content of cellulose insulation material in paper/oil system based on frequency dielectric modulus technique. <b>2020</b> , 27, 2343-2356		23
464	Ce-doping effect on modulation of spin-exchange interaction and dielectric behaviour of nanostructured LaFeO <sub>3</sub> orthoferrites. <b>2020</b> , 242, 122457		6
463	Studies on conduction mechanism and dielectric properties of the nano-sized La <sub>0.7</sub> Ca <sub>0.3</sub> MnO <sub>3</sub> (LCMO) grains in the paramagnetic state. <b>2020</b> , 583, 411967		13
462	Low temperature dielectric properties and NTCR behavior of the BaFeNbO double perovskite ceramic. <b>2020</b> , 22, 2986-2998		45
461	Microwave derived monoclinic Ba <sub>1-x</sub> Sn <sub>x</sub> Nb <sub>2</sub> O <sub>6</sub> materials as an alternative of ITO. <b>2020</b> , 828, 153096		
460	First and second phase transition discovery in amorphous chalcogenide Se <sub>60</sub> Te <sub>30</sub> S <sub>10</sub> composition. <b>2020</b> , 529, 119729		7
459	Effect of tantalum substitution on the structural and electrical properties of BaBi <sub>8</sub> Ti <sub>7</sub> O <sub>27</sub> intergrowth ceramics. <b>2020</b> , 46, 8122-8129		7
458	Balancing interface polarization strategy for enhancing electromagnetic wave absorption of carbon materials. <b>2020</b> , 391, 123538		28
457	Varistor and electrical properties of MgO.(Fe <sub>2</sub> O <sub>3</sub> ) <sub>1-x</sub> (Bi <sub>2</sub> O <sub>3</sub> ) <sub>x</sub> ceramics. <b>2020</b> , 40, 1325-1329		6
456	A transition in the electrical conduction mechanism of CuO/CuFe <sub>2</sub> O <sub>4</sub> nanocomposites. <b>2020</b> , 44, 1-15		2
455	Thermally stimulated small polaron promoted conduction mechanism in Fe-doped La <sub>0.7</sub> Sm <sub>0.3</sub> CrO <sub>3</sub> . <b>2020</b> , 138, 109281		5
454	Tunable capacitor-varistor response of CaCu <sub>3</sub> Ti <sub>4</sub> O <sub>12</sub> /CaTiO <sub>3</sub> ceramic composites with SnO <sub>2</sub> addition. <b>2020</b> , 170, 110699		15
453	Synthesis and electrical properties of polyaniline/berium oxide composites. <b>2020</b> , 270, 116588		8
452	Enhanced piezoelectric properties and low electrical conductivity of Ce-doped Bi <sub>7</sub> Ti <sub>4.5</sub> W <sub>0.5</sub> O <sub>21</sub> intergrowth piezoelectric ceramics. <b>2020</b> , 46, 26616-26625		3
451	Synthesis and characterization of Ruddlesden-Popper system (Ba <sub>1-x</sub> Sr <sub>x</sub> ) <sub>2</sub> SnO <sub>4</sub> . <b>2020</b> , 162, 110198		13
450	Enhancement of electrical properties Ce <sub>0.8</sub> Sm <sub>0.2</sub> O <sub>2</sub> by Sr <sup>2+</sup> doping. <b>2020</b> , 126, 1		3
449	Artificial multimodal receptors based on ion relaxation dynamics. <b>2020</b> , 370, 961-965		141



448	Molecular quantum materials: electronic phases and charge dynamics in two-dimensional organic solids. <b>2020</b> , 69, 1-120	15
447	Long-Range and Short-Range Transport Dynamics of Li Ions in LiMn <sub>2</sub> O <sub>4</sub> . <b>2020</b> , 124, 25254-25261	9
446	Ultrasonically assisted microwave synthesis and electronic transport properties of Eldfellite, NaFe(SO <sub>4</sub> ) <sub>2</sub> , a potential cathode material for Sodium-Ion Batteries. <b>2020</b> , 46, 28844-28850	4
445	Role of Cr doping in tuning the optical and dielectric properties of TiO <sub>2</sub> nanostructures. <b>2020</b> , 256, 123641	5
444	Enhanced charge carrier conduction and other characteristic parameters of hexagonal plastic columnar phase of a discotic liquid crystalline material due to functionalized gold nanoparticles. <b>2020</b> , 317, 113985	2
443	Origin of the abnormal reduction of the dielectric response for ReCOB crystals and its mechanism: theoretical and experimental exploration. <b>2020</b> , 8, 10109-10120	0
442	Synthesis, structural, dielectric and optical properties of chitosan-MgO nanocomposite. <b>2020</b> , 14, 975-983	10
441	Development of Fractional Order Modeling of Voltage Source Converters. <b>2020</b> , 8, 131750-131759	9
440	Structural, dielectric and impedance spectroscopy analysis of BaCaTiZnNbO ferroelectric ceramic.. <b>2020</b> , 10, 28007-28018	10
439	Prediction of Moisture and Aging Conditions of Oil-Immersed Cellulose Insulation Based on Fingerprints Database of Dielectric Modulus. <b>2020</b> , 12,	0
438	Study on improving the space charge behavior in insulating paper by depositing nanostructured alumina on its surface via magnetron sputtering. <b>2020</b> , 709, 138219	2
437	Structural, dielectric, thermal and electrical characteristics of lead-free double perovskite: BiHoZnCeO <sub>6</sub> . <b>2020</b> , 126, 1	6
436	Effect of temperature on electrical properties of PU/Fe (30%) nanocomposite. <b>2020</b> , 27, 1	2
435	Dielectric spectroscopy of epoxy-based barium titanate nanocomposites: effect of temperature and humidity. <b>2020</b> , 3, 20-27	6
434	A Test Architecture and VIE to Characterize Dielectric Absorption in Small Capacitors. <b>2020</b> ,	
433	Characterization and Dielectric Properties of Fly Ash / Polystyrene / Low Density Polyethylene Composites. <b>2020</b> , 956, 012002	1
432	Structural, optical and electrical properties of copper chloride filled polyvinyl chloride/polystyrene blend and its antifungal properties against Aspergillus avenaceus and Aspergillus terreus. <b>2020</b> , 22, 100451	4
431	Improvement of photoresponse in an isatin hydrazone/CdTe hybrid heterostructure device via ZnO chelation for photovoltaic applications. <b>2020</b> , 211, 1128-1136	3

430	High-Temperature Dielectric and Relaxation Behavior of Tantalum-Doped Sodium Bismuth Titanate-Barium Titanate Ceramics. <b>2020</b> , 49, 6643-6655	4
429	Coulomb barrier creation by means of electronic field emission in nanolayer capacitors. <b>2020</b> , 12, 18761-18770	2
428	Dielectric relaxations and optical properties of polyvinylidene fluoride/chitosan films. <b>2020</b> , 10, 095127	1
427	Impedance Spectroscopic Studies of B2O3-Substituted CeO2-Gd2O3 Systems. <b>2020</b> , 49, 6706-6714	1
426	Normalization for FDS of Transformer Insulation Considering the Synergistic Effect Generated by Temperature and Moisture. <b>2020</b> , 8, 202013-202021	1
425	Electrical conduction properties of the BZTBTST ceramics. <b>2020</b> , 10, 2050026	0
424	Effect of ferroelectric domain walls on the dielectric properties of PbZrO3 thin films. <b>2020</b> , 117, 142905	5
423	Up-Cycling of Iron-Rich Inorganic Waste in Functional Glass-Ceramics. <b>2020</b> , 10, 959	1
422	Dielectric Spectroscopy and Thermal Properties of Poly(lactic) Acid Reinforced with Carbon-Based Particles: Experimental Study and Design Theory. <b>2020</b> , 12,	2
421	Improved electrical properties of sputtering Pb1.10(Zr0.52,Ti0.48)O3/Pb1.25(Zr0.52,Ti0.48)O3 multilayer thin films. <b>2020</b> , 31, 21661-21669	
420	The Application of a High-Polymer Dielectric in Graphene Transistors. <b>2020</b> , 6, 2000031	5
419	Aging evaluation and moisture prediction of oil-immersed cellulose insulation in field transformer using frequency domain spectroscopy and aging kinetics model. <b>2020</b> , 27, 7175-7189	17
418	Effective analysis of time-domain dielectric response for reliable diagnosis of power transformer insulation using statistical parameter evaluated from time-varying model. <b>2020</b> , 14, 48-55	1
417	Dielectric spectroscopy of aluminium hydroxide particles filled silicone rubber and dielectric model analysis with modified numerical solutions. <i>Journal Physics D: Applied Physics</i> , <b>2020</b> , 53, 275303	3 6
416	Probing the multifunctional behaviour of barium zirconate/barium titanate/epoxy resin hybrid nanodielectrics. <b>2020</b> , 142, 231-243	6
415	Synthesis of LiBGeO4 using compositional design and its dielectric behaviors at RF and microwave frequencies. <b>2020</b> , 46, 22460-22465	6
414	Temperature correction to dielectric modulus and activation energy prediction of oil-immersed cellulose insulation. <b>2020</b> , 27, 956-963	38
413	Charge-Transfer Features in Zinc Sulfide Doped Layers in a Low-Frequency Alternating Electric Field. <b>2020</b> , 54, 623-626	

412	Changes in mechanical and dielectric properties of silicone rubber induced by severe aging. <b>2020</b> , 27, 722-730	6
411	Magnetic properties of BaNi <sub>x</sub> Fe <sub>12-x</sub> O <sub>19</sub> (x=0.0-1.0) hexaferrites, synthesized by citrate gel auto-combustion and sintered by conventional and spark plasma methods. <b>2020</b> , 831, 154850	6
410	A practical guide to Prabhakar fractional calculus. <b>2020</b> , 23, 9-54	72
409	Dielectric Response of ZnTe/Al Schottky Junctions with CdTe Quantum Dots Studied by Impedance Spectroscopy. <b>2020</b> , 10, 170	
408	Quantitative aging assessment method for cellulose pressboard based on the interpretation of the dielectric response mechanism. <b>2020</b> , 27, 4773-4785	8
407	Time-dependent electroadhesive force degradation. <b>2020</b> , 29, 055009	3
406	Degradation Assessment of Polyethylene-Based Material Through Electrical and Chemical-Physical Analyses. <b>2020</b> , 13, 650	7
405	Hydrothermal Growth of Undoped and Zn-Doped SnO Nanocrystals: A Frequency Dependence of AC Conductivity and Dielectric Response Studies. <b>2020</b> , 54, 73-76	0
404	Fabrication and performances of high lithium-ion conducting solid electrolytes based on NASICON Li <sub>1.3</sub> Al <sub>0.3</sub> Ti <sub>1.7-x</sub> Zr <sub>x</sub> (PO <sub>4</sub> ) <sub>3</sub> (0 ≤ x ≤ 0.2). <b>2020</b> , 46, 23695-23705	4
403	Investigation of Structural and Dielectric Properties of Polycrystalline PbMg <sub>1/3</sub> Ti <sub>1/3</sub> W <sub>1/3</sub> BO <sub>3</sub> Tungsten Perovskite. <b>2020</b> , 10, 2050021	4
402	Removing Instability-Caused Low-Frequency Features in Small Perturbation Spectra of Perovskite Solar Cells. <b>2020</b> , 124, 15793-15799	9
401	Kaolinite under pressure at audio frequency range and its electrical features. <b>2020</b> , 9, 176-189	3
400	Polaronic Conductivity in Iron Phosphate Glasses Containing BO. <b>2020</b> , 13,	4
399	High thermal stability of RF dielectric properties of BiVO <sub>4</sub> matrix with added ZnO. <b>2020</b> , 31, 13078-13087	2
398	Condition prediction for oil-immersed cellulose insulation in field transformer using fitting fingerprint database. <b>2020</b> , 27, 279-287	26
397	Hydrostatic pressure influence on electric relaxation response of bismuth manganite ceramics. <b>2020</b> , 103, 3732-3738	4
396	Dielectric, optical, and multiferroic properties of Co-doped SrBi <sub>2</sub> Nb <sub>1.8</sub> Fe <sub>0.2</sub> O <sub>9</sub> ceramics. <b>2020</b> , 31, 4719-4731	1
395	Microwaves and Heterogeneous Catalysis: A Review on Selected Catalytic Processes. <b>2020</b> , 10, 246	55

394	Negative real permittivity in (Bi <sub>0.3</sub> Eu <sub>0.7</sub> )Sr <sub>2</sub> CaCu <sub>2</sub> O <sub>6.5</sub> ceramic. <b>2020</b> , 584, 412080	3
393	Electrochemical Impedance Characterization of Blood Cell Suspensions-Part 2: Three-Phase Systems With Single-Shelled Particles. <b>2020</b> , 67, 2979-2989	2
392	Investigation of the dielectric properties of natural fibre and conductive filler reinforced polymer composites. <b>2020</b> , 22, 162-171	5
391	Natural additive material for desirable dielectric properties of polypyrrole: Limestone. <b>2020</b> , 260, 116297	3
390	Relaxor-like Behavior and Structure Features of Bi <sub>2</sub> Ti <sub>2</sub> O <sub>7</sub> Pyrochlore Single Crystals. <b>2020</b> , 20, 824-831	9
389	Investigation of electrical properties and conduction mechanism using CBH model of Ba <sub>0.97</sub> La <sub>0.02</sub> Ti <sub>1-x</sub> Nb <sub>4x/5</sub> O <sub>3</sub> (x = 0.00 and 0.02) compounds. <b>2020</b> , 126, 1	15
388	The low-power law emergent response of random RC networks. <b>2020</b> , 93, 1	1
387	Nonlinear charge-voltage relationship in constant phase element. <b>2020</b> , 117, 153104	13
386	Investigating the Correlation of Segmental Dynamics, Free Volume Characteristics, and Ionic Conductivity in Poly(ethylene oxide)-Based Electrolyte: A Broadband Dielectric and Positron Annihilation Spectroscopy Study. <b>2020</b> , 124, 4489-4501	11
385	Consequences of R <sup>3+</sup> cationic radii on the dielectric and magnetic behavior of RCrO <sub>3</sub> perovskites. <b>2020</b> , 126, 1	3
384	Heterogeneity in relation to electrical and mineralogical properties of hematitic sandstone samples. <b>2020</b> , 10, 1	2
383	Salinity and water effect on electrical properties of fragile clayey sandstone. <b>2020</b> , 10, 1	2
382	Tuning the morphological, structural, optical and dielectric properties of hausmannite (Mn <sub>3</sub> O <sub>4</sub> ) films by doping heavy metal lead. <b>2020</b> , 143, 106546	4
381	Phenomenological model of giant piezodielectric effect in GaSe layered crystals. <b>2020</b> , 10, 4847-4853	0
380	Effect of Sm doping on structure, dielectric and magnetic properties of GdFeO <sub>3</sub> . <b>2020</b> , 46, 19682-19690	5
379	Comparison of lithium ferrite powders prepared by sol-gel and solid state reaction methods. <b>2020</b> , 255, 114529	10
378	Design and Development of a Tunable Ferroelectric Microwave Surface Mounted Device. <b>2020</b> , 67, 1733-1737	8
377	Structural, thermal, dielectric and multiferroic investigations on LaFeO <sub>3</sub> composite systems. <b>2020</b> , 31, 7811-7830	3

376	Electrical study of antiferroelectric NaNbO <sub>3</sub> thin films integrated directly on 4H-SiC. <b>2020</b> , 143, 109477	1
375	Effect of cobalt-doping on dielectric, magnetic and optical properties of BiFeO <sub>3</sub> nanocrystals synthesized by sol-gel technique. <b>2020</b> , 102, 106168	7
374	Memory in Nonmonotonic Stress Relaxation of a Granular System. <b>2020</b> , 124, 168002	5
373	Microwave Microscopy and Its Applications. <b>2020</b> , 50, 105-130	9
372	Broadband Colossal Dielectric Constant in the Superionic Halide RbAg <sub>4</sub> I <sub>5</sub> : Role of Intercluster Ag <sup>+</sup> Diffusion. <b>2020</b> , 124, 9802-9809	4
371	Effect of nano-nickel on the dielectric characteristics of polyurethane-metal nanocomposites. <b>2021</b> , 35, 86-90	
370	Studies of structural, dielectric and electrical characteristics of complex perovskite: Sr(Ni <sub>1/3</sub> Mn <sub>1/3</sub> W <sub>1/3</sub> )O <sub>3</sub> . <b>2021</b> , 95, 1147-1155	
369	Boron nitride/epoxy resin nanocomposites: development, characterization and functionality. <b>2021</b> , 145, 2925-2933	5
368	. <b>2021</b> , 17, 4624-4634	13
367	A review of electromagnetic processing of materials (EPM): Heating, sintering, joining and forming. <b>2021</b> , 69, 239-272	18
366	Van der Waals layered ferroelectric CuInP <sub>2</sub> S <sub>6</sub> : Physical properties and device applications. <b>2021</b> , 16, 1	20
365	Identification and comparison of peculiarities in physical properties of multiferroic morphotropic phase boundary sintered BiFeO <sub>3</sub> -xPbTiO <sub>3</sub> nano-ceramics. <b>2021</b> , 150, 109868	0
364	AC conductivity and dielectric properties in mixed ionic/electronic 20Na <sub>2</sub> O·20CaO·(50-x)B <sub>2</sub> O <sub>3</sub> ·xV <sub>2</sub> O <sub>5</sub> glasses. <b>2021</b> , 602, 412480	3
363	A 'mixed' dielectric response in langasite BaNbFeSiO. <b>2021</b> , 23, 554-562	0
362	[(CH <sub>3</sub> ) <sub>3</sub> N(CH <sub>2</sub> ) <sub>2</sub> Br] <sub>2</sub> [CoBr <sub>4</sub> ] halogenometallate complex: crystal structure, high-temperature reversible phase transition, electrical and optical properties. <b>2021</b> , 1231, 129684	2
361	A Correlation between Structural Parameters and Electrical Conductivity of Calcium-Modified Ba(Zr <sub>0.05</sub> Ti <sub>0.95</sub> )O <sub>3</sub> Ceramic. <b>2021</b> , 258, 2000392	
360	Exploring weak ferromagnetism and conduction mechanism in the layered oxide BiPbSr <sub>2</sub> MnO <sub>6</sub> . <b>2021</b> , 32, 923-931	
359	Temperature and frequency dependence of dielectric relaxations in YFeO <sub>3</sub> . <b>2021</b> , 47, 9834-9841	2

- 358 Impedance and modulus analysis of barium calcium titanate ferroelectric ceramics. **2021**, 58, 337-350 1
- 357 Dielectric, vibrational and thermal properties of sisal fibers-reinforced poly (lactic acid). **2021**, 42, 1267-1278 6
- 356 Role of ZnO chelation for boosting photoresponse performance of isatin hydrazone/p-Si organic/inorganic heterojunctions for energy conversion approach. **2021**, 214, 326-336 1
- 355 EQUIVALENT POWER-FORM REPRESENTATION OF THE FRACTAL TODA OSCILLATOR. **2021**, 29, 2150034 15
- 354 Water splitting on the mesoporous surface and oxygen vacancies of iron oxide generates electricity by hydroelectric cell. **2021**, 258, 123981 7
- 353 Defect-mediated ionic hopping and green electricity generation in Al<sub>2</sub>Mg<sub>x</sub>O<sub>3</sub>-based hydroelectric cell. **2021**, 56, 1600-1611 6
- 352 Dielectric properties of polymer/clay nanocomposites. **2021**, 29, 807-813 2
- 351 Electrical properties, characterization, and preparation of composite materials containing a polymethacrylate with  $\pi$ -naphthyl side group and nanographene fillers. **2021**, 34, 102-125 2
- 350 Giant energy storage effect in nanolayer capacitors charged by the field emission tunneling. **2021**, 32, 155401
- 349 Structural, thermal and dielectric studies of mixed spinel CoFe<sub>2</sub>O<sub>4</sub>. **2021**, 46, 2193-2196 1
- 348 Nanostructured LiFeO by a Biogenic Method for Applications from Electronics to Medicine. **2021**, 11, 6
- 347 Structural, mechanical and electric properties of La doped BNT-BFO perovskite ceramics. **2021**, 571, 162-174 4
- 346 Role of Ba<sup>2+</sup> substitution on structural, thermal, dielectric and electrical properties of La<sub>1-x</sub>Ba<sub>x</sub>Mn<sub>0.50</sub>Fe<sub>0.50</sub>O<sub>3</sub> {0.10 <math>x</math> 0.40} cathode for SOFCs. **2021**, 45, 4639-4645 0
- 345 FDS Measurement-Based Moisture Estimation Model for Transformer Oil-Paper Insulation Including the Aging Effect. **2021**, 70, 1-10 8
- 344 Aging evaluation for transformer oil-immersed cellulose insulation by using frequency dependent dielectric modulus technique. **2021**, 28, 2387-2401 7
- 343 Structural and morphological studies, and temperature/frequency dependence of electrical conductivity of BaLaTi NbO perovskite ceramics.. **2021**, 11, 23664-23678 13
- 342 Effect of Na<sub>2</sub>O on physical, structural and electrical properties of borate glasses. **2021**, 45, 3722-3725 2
- 341 Dielectric properties and thermally activated relaxation in monovalent (Li<sup>+1</sup>) doped multiferroic GdMnO<sub>3</sub>. **2021**, 127, 1 3

340	Impedance spectroscopic study of charge transport and relaxation mechanism in MnCr <sub>2</sub> O <sub>4</sub> ceramic chromite. <b>2021</b> , 854, 156996	11
339	Enhancement of Electrical and Dielectric Properties of Graphene Oxide-nanoparticle Based Devices. 1	7
338	Synthesis and characterization of single perovskite Ba(Ni <sub>1/3</sub> Mn <sub>1/3</sub> W <sub>1/3</sub> )O <sub>3</sub> . <b>2021</b> , 572, 135-146	2
337	Complex electrical impedance and dielectric spectroscopy of Na <sup>+</sup> -conducting PEO/PVP/NaIO <sub>4</sub> solid polymer electrolyte with incorporated nano-sized Graphene Oxide. <b>2021</b> , 1762, 012010	1
336	Supramolecular interactions involving fluoroaryl groups in hybrid blends of polylactide and ladder polysilsesquioxanes. <b>2021</b> , 94, 107033	1
335	Impedance spectroscopy analysis of an FeNbO <sub>4</sub> matrix with different additions of TiO <sub>2</sub> and the effects of temperature variation. <b>2021</b> , 32, 5936-5944	
334	Synthesis and study of the structural and dielectric properties of La <sub>0.67</sub> Ca <sub>0.2</sub> Ba <sub>0.13</sub> Fe <sub>1-x</sub> Mn <sub>x</sub> O <sub>3</sub> ferrites (x = 0, 0.03 and 0.06). <b>2021</b> , 32, 7926-7942	1
333	Analyzing the behavior of GPR wave propagation in zinc contaminated soil combining the dielectric properties—experimental study. <b>2021</b> , 69, 483-495	0
332	Triblock SEBS/DVB crosslinked and sulfonated membranes: Fuel cell performance and conductivity. <b>2021</b> , 138, 50671	0
331	Physicochemical Mechanisms of the Double-Layer Capacitance Dispersion and Dynamics: An Impedance Analysis. <b>2021</b> , 125, 5870-5879	3
330	Structural, Electrical, and Magnetic Properties of Mullite-Type Ceramic: Bi <sub>2</sub> Fe <sub>4</sub> O <sub>9</sub> .	
329	A modified XY model of transformer oil-paper insulation system including non-uniform aging and conductance effect. <b>2021</b> , 15, 2008	4
328	Sodium ion conducting PVA/NaCMC bio poly-blend electrolyte films for energy storage device applications. <b>2021</b> , 26, 411-424	2
327	Elastic composites with PDMS matrix and polysulfone-supported silver nanoparticles as filler. <b>2021</b> , 217, 123480	7
326	Flexible hematite (Fe <sub>2</sub> O <sub>3</sub> )-graphene nanoplatelet (GnP) hybrids with high thermal conductivity. <b>2021</b> , 118, 091903	0
325	Dielectric and mechanical properties of nickel silica core-shell reinforced PMMA nanocomposites. 002199832110004	
324	Dielectric Relaxation, Aging and Recovery in High-K MIM Capacitors. <b>2021</b> ,	0
323	Dielectric measurements on stearic acid/eicosylamine alternate layer Langmuir-Blodgett films incorporating CdS nanoparticles. <b>2021</b> , 32, 8798-8806	1

322	Effects of surface structure and defect behavior on the magnetic, electrical, and photocatalytic properties of Gd-doped CeO <sub>2</sub> nanoparticles synthesized by a simple chemical process. <b>2021</b> , 174, 110990	8
321	Tuning the magnetic and electric behavior of lithium ferrite using an eco-friendly pectin sol-gel route. <b>2021</b> , 98, 580-592	0
320	Enhancement of conductivity and conduction mechanisms in hybrid epoxy based nanocomposites for microelectronic applications. <b>2021</b> , 266, 115035	1
319	Dielectric spectroscopy and structural characterization of nano-filler-loaded epoxy resin. <b>2021</b> , 11, 2150011	1
318	Impedance spectroscopy and conduction mechanism of a BiFe <sub>0.95</sub> Mn <sub>0.05</sub> O <sub>3</sub> thin film. <b>2021</b> , 724, 138616	0
317	Impedance Spectroscopy and Dielectric Relaxation of Imidazole-Substituted Palladium(II) Phthalocyanine (ImPdPc) for Organic Solar Cells. <b>2021</b> , 6, 10655-10667	3
316	Complex Dielectric Characteristics, ac-Conductivity, and Impedance Spectroscopy of B-Doped nc-SiO <sub>x</sub> :H Thin Films. <b>2021</b> , 3, 1634-1647	3
315	Wearable Bioimpedance Monitoring: Viewpoint for Application in Chronic Conditions. <b>2021</b> , 6, e22911	3
314	The Possibility of Tailoring Dielectric Properties by Thermal Etching in BaBi <sub>4</sub> Ti <sub>4</sub> O <sub>15</sub> Relaxor Ferroelectric. <b>2021</b> ,	
313	Microstructure and electrical conduction of iron-doped barium titanate glass-ceramics. <b>2021</b> , 560, 120711	1
312	Modeling kaolinite electrical features under pressure using Pseudo Random Renormalization Group method at the audio frequency range. <b>2021</b> , 152, 109963	3
311	Concurrently improving dielectric properties and thermal conductivity of Ni/PVDF composites by constructing NiO shell as an interlayer. <b>2021</b> , 32, 14764-14779	1
310	Synthesis Process Optimization of Polyimide Nanocomposite Multilayer Films, Their Dielectric Properties, and Modeling.	1
309	Two-dimensional SnO/SnO <sub>2</sub> heterojunctions for electromagnetic wave absorption. <b>2021</b> , 411, 128445	19
308	The Structure, Morphology, and Complex Permittivity of Epoxy Nanodielectrics with In Situ Synthesized Surface-Functionalized SiO <sub>2</sub> . <b>2021</b> , 13,	1
307	Structural and Dielectric Analysis of La <sub>0.88</sub> Bi <sub>0.12</sub> Mn <sub>0.80</sub> Ni <sub>0.20</sub> O <sub>3</sub> Composite. 317, 35-45	
306	GPR wave dispersion for material characterization. <b>2021</b> , 282, 122597	1
305	Relaxation behavior of sandwich-structured fluorinated graphene/poly(vinylidene fluoride-hexafluoropropylene) composites by dielectric relaxation spectroscopy. <b>2021</b> , 224, 123729	2



304	Synthesis, optical properties, and impedance spectroscopy of Na <sub>2</sub> TeO <sub>3</sub> doped polyvinyl alcohol as novel polymeric electrolyte films. <b>2021</b> , 53, 1	1
303	Assessing the Impact of Defects on Lead-Free Perovskite-Inspired Photovoltaics via Photoinduced Current Transient Spectroscopy. <b>2021</b> , 11, 2003968	5
302	Decoupling the magnitude and phase in a constant phase element. <b>2021</b> , 888, 115153	5
301	Proposal of a generic constitutive model for deformation-dependent dielectric constant of dielectric elastomers. <b>2021</b> , 24, 1347-1347	2
300	Time-Dependent Imprint in Hf <sub>0.5</sub> Zr <sub>0.5</sub> O <sub>2</sub> Ferroelectric Thin Films. <b>2021</b> , 7, 2100151	8
299	Exotic magnetic behavior with intrinsic and extrinsic magnetodielectric effects in Pr <sub>2</sub> CuMnO <sub>6</sub> . <b>2021</b> , 867, 159123	1
298	The effects of sintering temperature on structural, electrical, and magnetic properties of MgFe <sub>1.92</sub> Bi <sub>0.08</sub> O <sub>4</sub> . <b>2021</b> , 46, 151-161	
297	Consequences of frequency and temperature on the ac-conductivity in E <sub>Ga</sub> Se semiconductor single crystal. <b>2021</b> , 25, 104220	
296	Electromagnetic Shielding Effectiveness of the Concrete Composite as a Function of Structural Parameters of Steel Fibers. <b>2021</b> , 32, 517-526	
295	Magnetic, Optical, and Impedance Spectroscopy of Barium-Substituted Lithium Ferrite. <b>2021</b> , 125, 14014-14026	
294	Magnetodielectric study of BiFeO <sub>3</sub> synthesized by assisted high-energy ball milling. <b>2021</b> , 153, 109998	2
293	Differences in the physicochemical properties of lignins in the heartwood and sapwood of <i>Pinus sylvestris</i> . <b>2021</b> , 41, 177-184	1
292	The analysis of charge transport mechanism in mixed ionic electronic conductor composite of SrTiCoO double perovskite with yttria stabilized zirconia. <b>2021</b> , 33,	0
291	Possibility of information encoding/decoding using the memory effect in fractional-order capacitive devices. <b>2021</b> , 11, 13306	5
290	Dielectric properties of bismuth layer structured ferroelectric Bi <sub>3</sub> R <sub>2</sub> Ti <sub>3</sub> FeO <sub>15</sub> (R = Bi, Gd, and Nd) at microwave and radiofrequency. <b>2021</b> , 32, 18628-18643	0
289	A Study of the Nonlinear Capacitance Variation in Inter Level Copper and Low-k Interconnect Structure. <b>2021</b> , 21, 207-214	
288	Structure-property correlations in lithium zinc cobalt metaphosphate glasses and glass-ceramics. <b>2021</b> , 610, 412949	2
287	Simultaneously Enhanced Thermal Conductivity and Breakdown Performance of Micro/Nano-BN Co-Doped Epoxy Composites. <b>2021</b> , 14,	1

- 286 Advances in the Study of Gas Hydrates by Dielectric Spectroscopy. **2021**, 26,
- 285 Temperature Distribution in the Insulation System of Condenser-Type HV Bushing Its Effect on Dielectric Response in the Frequency Domain. **2021**, 14, 4016 1
- 284 Electric stress and dielectric breakdown characteristics under high-frequency voltages with multi-harmonics in a solid-state transformer. **2021**, 129, 106861 4
- 283 Dielectric Properties of ZnO-Based Nanocomposites and Their Potential Applications. **2021**, 2021, 1-20 5
- 282 Study on the ionic conductivity, dielectric, and optical properties of CsYP2O7 compound. **2021**, 32, 21553-21567
- 281 Laboratory investigation into the dielectric properties of a L-chondrite (NWA 12857). **2021**, 362, 114426 2
- 280 Relaxor ferroelectric phase transition and ac conduction in polycrystalline Gd<sub>0.55</sub>Ca<sub>0.45</sub>MnO<sub>3</sub> at low temperature. **2021**, 267, 124586 0
- 279 Study of the colossal dielectric response in LaFe<sub>1-x</sub>Zn<sub>x</sub>O<sub>3</sub> perovskites. **2021**, 136, 1 1
- 278 A green approach for the preparation of nanostructured zinc oxide: Characterization and promising antibacterial behaviour. **2021**, 47, 19362-19373 7
- 277 Features of the temperature-frequency dependences of the electrophysical properties of vanillin alcohol as a model lignin compound. **2021**, 548, 111202 1
- 276 Dielectric Anomaly and Charge Fluctuations in the Non-Magnetic Dimer Mott Insulator  $\text{[(BEDT-STF)}_2\text{GaCl}_4$ . **2021**, 11, 1031 0
- 275 On possible applications of media described by fractional-order models in electromagnetic cloaking. **2021**, 99, 105827 1
- 274 Plasmonic Imaging of Tuning Electron Tunneling Mediated by a Molecular Monolayer. **2021**, 1, 1700-1707 1
- 273 Structural, microstructural, magnetic and electromagnetic absorption properties of spiraled multiwalled carbon nanotubes/barium hexaferrite (MWCNTs/BaFeO) hybrid. **2021**, 11, 15982 2
- 272 Fluorinated low molecular weight poly(phenylene oxide): Synthesis, characterization, and application in epoxy resin toward improved thermal and dielectric properties. **2021**, 157, 110674 9
- 271 Implementation of Non-Destructive Electrical Condition Monitoring Techniques on Low-Voltage Nuclear Cables: I. Irradiation Aging of EPR/CSPE Cables. **2021**, 14, 5139 5
- 270 Correlation between reduced dielectric loss and charge migration kinetics in NdFeO<sub>3</sub>-modified Ba<sub>0.7</sub>Sr<sub>0.3</sub>TiO<sub>3</sub> ceramics. **2021**, 32, 24910 0
- 269 Effect of spin reorientation on the dielectric and conductivity behavior of Ca<sub>2</sub>FeCoO<sub>5</sub>. **2021**, 32, 26955


268	Effect of Tantalum ion doping on the structure and electrical properties of Bi <sub>3</sub> Ti <sub>1.5</sub> W <sub>0.5</sub> O <sub>9</sub> -Bi <sub>4</sub> Ti <sub>3</sub> O <sub>12</sub> intergrowth bismuth-layered ceramics. <b>2021</b> , 32, 23911-23922	1
267	Microstructures and Electrical Conduction Behaviors of Gd/Cr Codoped BiTiNbO Aurivillius Phase Ceramic. <b>2021</b> , 14,	1
266	Terahertz probing of low-temperature degradation in zirconia bioceramics.	3
265	Structure-property relationship and spectroscopic studies of BaO-B <sub>2</sub> O <sub>3</sub> oxide glasses containing ZnO for optical applications. <b>2021</b> ,	2
264	Poly(l-lactic acid)/lithium ferrite composites: Electrical properties. <b>2021</b> , 230, 124100	2
263	Microwave selective heating of electric arc furnace dust constituents toward sustainable recycling: Contribution of electric and magnetic fields. <b>2021</b> ,	0
262	Electrical and dielectric properties of Sm <sub>0.55</sub> Sr <sub>0.45</sub> MnO <sub>3</sub> compound. <b>2021</b> , 302, 122378	1
261	Review on asset management of power transformer by diagnosing incipient faults and faults identification using various testing methodologies. <b>2021</b> , 128, 105634	6
260	High thermal stability of the YNbO <sub>4</sub> /CaYTbNbO <sub>7</sub> composites for radio frequency and microwave applications. <b>2021</b> , 271, 124956	1
259	Structural, electrical properties and photoluminescence analyses of the terbium doped barium titanate. <b>2021</b> , 878, 160380	3
258	Non-Debye relaxation of AgBiSe <sub>2</sub> single crystal featuring flip-flop jumps in Bi valence state. <b>2021</b> , 300, 130179	1
257	Approaches to deformable physical sensors: Electronic versus iontronic. <b>2021</b> , 146, 100640	8
256	Lead-free flexible Bismuth Titanate-PDMS composites: A multifunctional colossal dielectric material for hybrid piezo-triboelectric nanogenerator to sustainably power portable electronics. <b>2021</b> , 89, 106316	17
255	Extra-wide bandwidth via complementary exchange resonance and dielectric polarization of sandwiched FeNi@SnO nanosheets for electromagnetic wave absorption. <b>2021</b> , 90, 1-8	13
254	New insight into Li metal protection: Regulating the Li-ion flux via dielectric polarization. <b>2021</b> , 89, 106334	4
253	Structural, micro-structural, optical and dielectric behavior of mullite ceramics. <b>2021</b> , 47, 32252-32263	3
252	Fractal analysis of wildfire pattern dynamics using a Small World Network model. <b>2021</b> , 583, 126300	0
251	Multifunctional feature of double perovskite strontium iron vanadate for storage device. <b>2022</b> , 275, 125254	4

- 250 Study of the Complex Permittivity of a Polyurethane Matrix Modified by Nanoparticles. **2021**, 9, 49547-49556 2
- 249 Dielectric and magnetic properties of CuFe<sub>2</sub>O<sub>4</sub>/CuO nanocomposites. **2021**, 571, 183-199 1
- 248 Dielectric Response. **2017**, 1-1 4
- 247 Effect of Cu-doping on the dielectric properties of MnV<sub>2</sub>O<sub>6</sub> compound. **2020**, 512, 167044 1
- 246 Synthesis, structure, magnetic behavior and dielectric relaxation of the La<sub>x</sub>Sr<sub>2-x</sub>FeTi<sub>1- $\alpha$</sub> O<sub>4</sub> ( $\alpha=0.5, 0.7$ ) oxide ceramic. **2020**, 292, 121687 1
- 245 Polymer Composites Comprising Single-Atomic-Layer Graphenic Conductive Inclusions and Their Unusual Dielectric Properties. **2020**, 124, 13715-13725 2
- 244 Quantitative diagnosis of moisture content in oil-paper condenser bushing insulation based on frequency domain spectroscopy and polarisation and depolarisation current. **2017**, 11, 1420-1426 24
- 243 Role of the colossal frequency and temperature dependent dielectric constant in the performance of the organo-metallic tri-halide perovskites. **2017**, 110, 222905 5
- 242 Dielectric and impedance spectroscopy of NdCoIrO double perovskite. **2020**, 32, 495702 4
- 241 Frequency Domain Spectroscopy Prediction of Oil-Immersed Cellulose Insulation under Diverse Temperature and Moisture. **2020**, 27, 1820-1828 11
- 240 Dielectric Relaxation and Impedance Spectroscopy of 30V<sub>2</sub>O<sub>5</sub> □20Bi<sub>2</sub>O<sub>3</sub> □50P<sub>2</sub>O<sub>5</sub> Glass. **2020**, 46, 487-496 2
- 239 The modified magnetodielectric response in KNN-CZFMO based particulate multiferroic composite system. **2020**, 10, 2050024 2
- 238 Features of frequency dependence of electrical conductivity and dielectric properties in lignins from conifers and deciduous trees. **2020**, 74, 1113-1122 3
- 237 Current transport mechanisms in metal □high-k dielectric □bilicon structures. **2012**, 15, 139-146 1
- 236 Effects of Crystallinity on Dielectric Properties of Poly (L-lactide). **2009**, 129, 217-222 12
- 235 AC CONDUCTIVITY AND DIELECTRIC STUDIES OF POLYPYRROLE-PAPAIN COMPOSITE. **2019**, 7, 332-338 2
- 234 Mechanical and dielectric behavior of LDPE/Bi-1212 films. **2020**, 62, 913-920 1
- 233 Elucidation of Conduction Mechanism in Graphene Nanoplatelets (GNPs)/Cement Composite Using Dielectric Spectroscopy. **2020**, 13, 7

232	A Superior Description of AC Behavior in Polycrystalline Solid Electrolytes with Current-Constriction Effects. <b>2016</b> , 53, 150-161	12
231	Dielectric relaxation affected by a monotonically decreasing driving force: An energy perspective. <b>2021</b> , 130, 154101	
230	MCdCl <sub>3</sub> (M=CH <sub>3</sub> NH <sub>3</sub> , (CH <sub>3</sub> ) <sub>2</sub> NH <sub>2</sub> ): New Hybrid Perovskites with Large Dielectric Constants for Field-Effect Transistors. 2100485	0
229	Low-filled suspensions of $\beta$ -chitin nanorods for electrorheological applications. <b>2022</b> , 277, 118792	1
228	Metal-Formate Framework Stiffening and Its Relevance to Phase Transition Mechanism. <b>2021</b> , 14,	0
227	Experimental investigation on dielectric/electric properties of aged polymeric insulator: correlation of permittivity and dielectric loss tangent with surface hydrophobicity. 1	
226	Identification of fractional-order Hammerstein nonlinear ARMAX system with colored noise. 1	0
225	Multi scale aging assessment of low-voltage cables subjected to radio-chemical aging: Towards an electrical diagnostic technique. <b>2021</b> , 103, 107352	4
224	Effect of processing temperature on structural, optical and frequency dependent electrical responses of solid-state sintered bismuth sodium titanate. <b>2021</b> , 274, 115474	1
223	Dielectric Loss and Relaxation - II. <b>2003</b> ,	
222	Chapter 4 Dielectric Loss and Relaxation-II. <b>2003</b> , 177-213	
221	Dielectric Loss and Relaxation-I. <b>2003</b> ,	
220	<del>Dielectric Loss and Relaxation-I. <b>2009</b>, 158, 419-424</del>	
219	Fractional Dynamics and Discrete Maps with Memory. <b>2010</b> , 409-453	
218	Fractional Temporal Electrodynamics. <b>2010</b> , 357-376	
217	Fractional Nonholonomic Dynamics. <b>2010</b> , 377-408	
216	Dielectric properties of Eu-doped polycrystalline TbMnO <sub>3</sub> . <b>2010</b> , 59, 2815	2
215	Ferrimagnetism and Ferroelectricity of the Composite Matrix: SrBi <sub>2</sub> Nb <sub>2</sub> O <sub>9</sub> (SBN)-BaFe <sub>2</sub> O <sub>7</sub> . <b>2012</b> , 03, 6-17	

214	Dielectric Formalism. 95-117	
213	Water Associated with Bio-Objects: Cells and Tissues. <b>2013</b> , 806-905	
212	Non-linear control for the fractional boost converter in pseudo continuous conduction mode. <b>2014</b> , 63, 200502	1
211	Dielectric properties of materials at microwave frequencies. <b>2014</b> , 56, 125-132	1
210	Chapter 8 Electrical Properties of Polymer Nanocomposites. <b>2016</b> , 218-242	1
209	Electromagnetic Response of Carbon Nanotube-Based Composites. <b>2019</b> , 1-19	
208	Physical Mechanism Analysis of Conductivity and Relaxation Polarization Behavior of Oil-Paper Insulation Based on Broadband Frequency Domain Spectroscopy. <b>2021</b> , 28, 1571-1578	2
207	Multi-dimensional Analysis and Correlation Mechanism of Thermal Degradation Characteristics of XLPE Insulation for Extra High Voltage Submarine Cable. <b>2021</b> , 28, 1488-1496	2
206	Structural, electrical, and magnetic properties of mullite-type Bi <sub>2</sub> Fe <sub>4</sub> O <sub>9</sub> ceramic. <b>2020</b> , 45, 148-155	0
205	Sodium Ferrites: New Materials to Be Applied in Energy Storage Devices in a Wide Frequency Range. <b>2020</b> , 405-415	
204	Structural, Thermal, Electrical and Dielectric Properties of La <sub>1-x</sub> Sr <sub>x</sub> Mn <sub>0.50</sub> Fe <sub>0.50</sub> O <sub>3</sub> {0.10 <math>x</math> 0.40} Cathode Material for Solid Oxide Fuel Cells. <b>2020</b> , 32, 3165-3172	0
203	Dielectric and impedance spectroscopy studies of Ba <sub>0.90</sub> Y <sub>0.10</sub> SnO <sub>3</sub> . <b>2020</b> ,	
202	Effect of ZnO nanoparticles on the dielectric properties of polyurethane and epoxy resins. <b>2021</b> ,	0
201	Polarization Induced Multiferroic Bismuth Ferrite Nanostructures: Investigation of Dielectric and Magnetic Properties. <b>2021</b> ,	
200	Life modeling analysis of Silane crosslinked polyethylene cables for nuclear applications. <b>2020</b> ,	
199	Broadband Millimeter-Wave Dielectric Properties of Liquid Crystal Polymer Materials. <b>2021</b> , 1-1	1
198	Stretchable silver@CNT-poly(vinyl alcohol) films with efficient electromagnetic shielding prepared by polydopamine functionalization. <b>2022</b> , 238, 124413	4
197	Thermally tunable dielectric performance of t-ZrO <sub>2</sub> stabilized amorphous Si(Pb,Zr)OC ceramic nanocomposites. <b>2022</b> , 277, 125495	0

196	A review of the colossal permittivity of electronic conductors, specifically metals and carbons. <b>2022</b> , 148, 111654	4
195	Impedance Spectroscopy of Metal Halide Perovskite Solar Cells from the Perspective of Equivalent Circuits. <b>2021</b> , 121, 14430-14484	23
194	Graphene Oxide/Epoxy Composites with Induced Anisotropy of Electrical Properties.	1
193	Superlinear dependence of the conductivity, double/single Jonscher variations and the contribution of various conduction mechanisms in transport properties of La <sub>0.5</sub> Ca <sub>0.2</sub> Ag <sub>0.3</sub> MnO <sub>3</sub> manganite. <b>2021</b> , 898, 162866	2
192	Dimensional Design and Core-Shell Engineering of Nanomaterials for Electromagnetic Wave Absorption. <b>2021</b> , e2107538	37
191	Charge localization in strongly correlated (BEDT-TTF) <sub>2</sub> Cu[N(CN) <sub>2</sub> ]I due to inherent disorder. <b>2021</b> , 104,	
190	Aging Assessment of XLPE/CSPE LV Nuclear Power Cables Under Simultaneous Radiation/Mechanical Stresses. <b>2021</b> ,	1
189	Comparison of Mechanical and Low-Frequency Dielectric Properties of Thermally and Thermo-Mechanically Aged Low Voltage CSPE/XLPE Nuclear Power Plant Cables. <b>2021</b> , 10, 2728	1
188	Na <sub>2</sub> CaV <sub>4</sub> O <sub>12</sub> : A low-temperature-firing dielectric with lightweight, low relative permittivity, and dielectric anomaly around 515 oC. <b>2021</b> , 48, 6899-6899	0
187	Multiple rotor modes and how to trigger them: complex cation ordering in the family of relaxing hybrid formates. <b>2021</b> ,	1
186	Structural, morphological, Raman, dielectric and electrical properties of La Ba Bi FeO (0.00-0.20) compounds.. <b>2021</b> , 11, 36148-36165	0
185	ColdADC_P2: A 16-Channel Cryogenic ADC ASIC for the Deep Underground Neutrino Experiment. <b>2021</b> , 1-1	0
184	Temperature and time dependent electron trapping in Al <sub>2</sub> O <sub>3</sub> thin films onto AlGa <sub>N</sub> /Ga <sub>N</sub> heterostructures. <b>2022</b> , 579, 152136	2
183	Investigation into the effect of ZnO nanorod coating on the thermal-mechanical and dielectric properties of ITO coated PET. <b>2022</b> , 149, 111701	0
182	Rigid amorphous fraction caused by isothermal crystallization in ATH filled silicone rubber. <b>2020</b> ,	0
181	Mastering of AC/DC Dielectric Characterization of Epoxy-Based Composites Crosslinked by Different Curing Agents. <b>2020</b> ,	
180	Quantitative investigation and modelling of the electrical response of XLPE insulation with different filler content. <b>2020</b> ,	0
179	Impedance Spectroscopy of NaBi(MoO <sub>4</sub> ) <sub>2</sub> :Gd <sup>3+</sup> Nanocrystals in the Pores of an Opal Matrix. <b>2021</b> , 117-130	

- 178 Complex impedance spectroscopy and dielectric relaxation studies of lead-free layered perovskite  $\text{Bi}_{4-x}\text{La}_x\text{Ti}_3\text{O}_{12}$  ceramics: a ferroelectric to relaxor crossover. **2022**, 33, 5396 0
- 177 B-Site octahedral bridge and A-site polyvalent Cu cation related electron hopping in  $\text{LiCuNb}_3\text{O}_9$ -based colossal permittivity materials. **2022**, 10, 665-671 0
- 176 New conjugated polymer/fullerene nanocomposite for energy storage and organic solar cell devices: Studies of the impedance spectroscopy and dielectric properties. **2022**, 283, 116987 0
- 175 Acquisition of FDS for Oil-Immersed Insulation at Transformer Hotspot Region Based on Multi-constraint NSGA Model. **2022**, 1-1 2
- 174 The electrical and optical behavior of graphene oxide-doped nematic liquid crystal. **2022**, 33, 5720 1
- 173 Machine learning models for estimating the AC conductivity mechanism of Edirne Kufeki stone reinforced Polypyrrole composites. 52194 0
- 172 Structural and dielectric properties of  $\text{PrFeTiO}_5$  oxide. **2022**, 33, 6150 0
- 171 Revealing the role of the constant phase element in relaxor ferroelectrics. **2022**, 5, 0
- 170 Peculiar electric properties of polarized layer in alkaline silicate glasses. 0
- 169 Quantum Mechanical Meaning of the Charge Transfer Resistance. 1
- 168 Design novel, flexible, and wide-scale CUT-OFF laser filters of Eosin Yellow dye/PVA polymeric composite films: Enhance the electrical conductivity and dielectric properties of PVA. **2022**, 253, 168582 1
- 167 Effect of Chromium Substitution on the Electrical and Magnetic Properties of Multiferroic Yttrium Manganite. 1
- 166 Magnetodielectric coupling in barium titanate-cobalt ferrite composites obtained via thermally-assisted high-energy ball milling. **2021**, 48, 9527-9527 0
- 165 Analytical Methods for Causality Evaluation of Photonic Materials.. **2022**, 15, 0
- 164 Electrical Transport in Iron Phosphate-Based Glass-(Ceramics): Insights into the Role of BO and HfO from Model-Free Scaling Procedures.. **2022**, 12, 0
- 163   $\text{Bi}_2\text{GaSe}$ . **2022**, 56, 267 1
- 162 Temperature-Dependent Fractional Dynamics in Pseudo-Capacitors with Carbon Nanotube Array/Polyaniline Electrodes.. **2022**, 12, 0
- 161 Towards dielectric relaxation at a single molecule scale.. **2022**, 12, 2865 1



160	The effect of metal-insulator interface interactions on electrical transport in granular metals.. <b>2022</b> , 34,	
159	Ionic conductivity enhancement of PVA: carboxymethyl cellulose poly-blend electrolyte films through the doping of NaI salt. <b>2022</b> , 29, 3271	4
158	Dielectric Behavior of an Electrically Conductive Metal-Particle Thick Film. 1	1
157	MILM hybrid identification method of fractional order neural-fuzzy Hammerstein model. 1	1
156	Segregated carbon nanotube networks in CNT-polymer nanocomposites for higher electrical conductivity and dielectric permittivity, and lower percolation threshold. <b>2022</b> , 173, 103650	0
155	Dielectric Properties in Oriented and Unoriented Membranes Based on Poly(Epichlorohydrin-co-Ethylene Oxide) Copolymers: Part III.. <b>2022</b> , 14,	
154	Electrical properties of sedimentary microfacies and depositional environment deduced from core analysis of the syn-rift sediments, Northwestern shore of Gulf of Suez, Egypt. 1	0
153	Impact of defect migration on electrical and dielectric properties in molten salt synthesized CaCu <sub>3</sub> Ti <sub>4</sub> O <sub>12</sub> and customizing the properties by compositional engineering with Mg doping. <b>2022</b> , 281, 125893	0
152	Broadband dielectric relaxation investigations of polyvinyl chloride-FGO nanocomposite films. 1	
151	Tuning the AC electric responses of decorated PDA@MWCNT/PVDF nanocomposites. <b>2022</b> , 222, 109398	0
150	Li- and Na-doped bismuth titanate pyrochlores: From the point of view ab initio calculation and experiment. <b>2022</b> , 379, 115904	
149	Dielectric Relaxation of Iron Corrosion Products in Limestone under Saline Environment. <b>2021</b> ,	
148	Enhancing morphological, electro-optical and dielectric properties of polymer-dispersed liquid crystal by doping of disperse Orange 25 dye in LC E7. 1-14	2
147	Ion-Conducting Flexible Thin Films of Composites from Poly(ethylene oxide) and Nematic Liquid Crystals E8-Characterization by Impedance and Dielectric Relaxation Spectroscopy.. <b>2021</b> , 13,	1
146	FDS Extraction of Hot Spots of Transformer Oil-immersed Insulation Based on Non-uniform Aging Equivalent Model and Genetic Algorithm. <b>2021</b> ,	
145	Diagnosis of Oil Paper Sample Using Capacitance Profile of Time Varying Model. <b>2021</b> ,	
144	Dielectric absorption in PEDOT:PSS capacitors with stainless steel yarn electrodes in textile substrates. <b>2022</b> , 35, 137-143	
143	Structure and circuit modeling of frequency domain polarization characteristics for porous composite material. <b>2022</b> , 224, 109457	0

- 142 Dielectric Properties Correlation with Microstructure in  $\text{ABi}_4\text{Ti}_4\text{O}_{15}$  (A = Sr, Ba) Bismuth Layered Ferroelectrics. 0
- 141 Modulation of electric and magnetic ordering in  $\text{GdFeO}_3$  orthoferrites system by Ce-doping. **2022**, 587, 158-173 1
- 140 Frequency dependant gate oxide TDDDB model. **2022**,
- 139  $\text{Na}_3\text{Zr}_2(\text{SiO}_4)_2\text{PO}_4$  NASICON-type solid electrolyte: Influence of milling duration on microstructure and ionic conductivity mechanism. **2022**, 0
- 138 Study on relaxation behavior of all-polymer PVDF-based films containing dielectric fluoroelastomer. **2022**, 124933 0
- 137 Influence of nickel dopant on impedance, dielectric, and optical properties of ZnO nanoparticles at low temperatures. 0
- 136 Li ion transport properties of amorphous/crystalline Li-La-Zr-Nb-O solid electrolyte thick films prepared by suspension plasma spraying. **2022**, 380, 115938
- 135 High-temperature electrical conductivity in piezoelectric lithium niobate. **2022**, 131, 194102 1
- 134 Frequency Response and Transfer Functions of Large Self-Similar Networks. **2022**, 0
- 133 Investigation of structural, dielectric, impedance and leakage current behaviour of green phase of yttrium barium copper Oxide:  $\text{Y}_2\text{BaCuO}_5$ . **2022**, 414027 0
- 132 Anomalous dielectric relaxation peak in Nb-doped  $\text{SrTiO}_3$  single crystals. **2022**,
- 131 Crystallographic orientation dependence of ferroelectric domain walls in antiferroelectric lead zirconate thin films. **2022**, 0
- 130 Structural, dielectric, electrical and optical properties of a double perovskite:  $\text{BaNaFeWO}_6$  for some device applications. **2022**, 1265, 133353 1
- 129 Influence of Nanoparticles on the Dielectric Response of a Single Component Resin Based on Polyesterimide. **2022**, 14, 2202 2
- 128 Extracting Frequency Spectroscopy of Oil-Immersed Paper Based on Havriliak-Negami Model Without Known Insulation Structure of Transformer. **2022**, 71, 1-12 1
- 127 Low-temperature Electrical Properties and Correlated Barrier Hopping Conduction Mechanism in  $\text{CdTiO}_3$ . **2022**, 02, 92-100
- 126 Unexpected Wide Tuning of Ferroelectric Properties by Varying the Er Concentration in  $\text{La}_2\text{-Xerx}(\text{Moo}_4)_3$  (X = 0.75, 1, 1.25) Solid Solutions.
- 125 Low-frequency dynamics in ionic liquids: Comparison of experiments and the random barrier model. 0

- 124 Dielectric study of the adsorption of Cetylpyridinium and Phenol onto activated carbon. **2022**, 340, 112036 1
- 123 Aging Analysis of Transformer Insulation at Weakest Region: Dielectric Parameters Extraction via Immune Optimization. **2022**, 1-1
- 122 Investigation of Dielectric Relaxor-Like Anomaly Behavior of Non-Ferroelectric BaZrO<sub>3</sub> Polycrystalline Ceramic.
- 121 The AC measurements of the composite of cellulose - bio-based hydrocarbon transformer oil/water nanodrops. **2022**, 0
- 120 Structural analysis, dielectric relaxation, and AC electrical conductivity in TlInSe<sub>2</sub> thin films as a function of temperature and frequency. **2022**, 128,
- 119 Room temperature magneto-electric coupling in Pb<sub>1-x</sub>Sn<sub>x</sub> substituted Co<sub>2</sub>Y-hexaferrite. **2022**, 33, 16874-16888
- 118 Insight of yttrium doping on the structural and dielectric characteristics of ZnO nanoparticles.
- 117 Structural characteristics, impedance spectroscopy, ac-conductivity and dielectric loss studies on RF-magnetron sputtered F doped ZnO (FZO) thin films. **2022**,
- 116 Improving the physical properties of polycrystalline-deficient Pr<sub>0.8</sub>Sr<sub>0.2</sub><sub>1-x</sub>MnO<sub>3</sub> (0 ≤ x ≤ 0.2) compounds for electronic devices.
- 115 Structural refinement, dielectric and spin exchange magnetic analysis of (1-x) BaFe<sub>12</sub>O<sub>19</sub> - (x) CoFe<sub>2</sub>O<sub>4</sub> composites. **2022**, 414191 0
- 114 Spatio temporal dynamics of direct current in treated anisotropic tumors. **2022**, 1
- 113 Multimodal Sensors with Decoupled Sensing Mechanisms. 2202470 16
- 112 Compositional-induced structural transformation and relaxor ferroelectric behavior in Sr/Nb-modified Bi<sub>4</sub>Ti<sub>3</sub>O<sub>12</sub> Aurivillius ceramics. **2022**, 0
- 111 Unraveling Hole Interlayer-Dependent Interfacial Energetics of LEDs. **2022**, 107621 0
- 110 Structural and impedance spectroscopic investigations of eco-friendly alkali phosphoborate glass/ceramics containing zirconium ion. 0
- 109 Studies on characterization and enhanced magnetic field sensing performance of Bi<sub>1-x</sub>K<sub>x</sub>Mn<sub>1-y</sub>Co<sub>y</sub>O<sub>3</sub> nanopowders as a fiber optic clad modified region. **2022**, 560, 169683
- 108 Effects of vanadium doping on the charge ordering and low-temperature spin-glass phase in Pr<sub>0.45</sub>Ca<sub>0.55</sub>MnO<sub>3</sub>. **2022**, 921, 166048 0
- 107 A comprehensive investigation of dielectric properties of epoxy composites containing conducting fillers: Fluffy carbon black and various types of reduced graphene oxide. 0

- 106 Optical and Dielectric Properties of ZnO Nematic Liquid Crystals Prepared by the Chemical Precipitation Method.
- 105 Dielectric response and molecular dynamics of nanocomposites based on TEMPO-oxidized cellulose nanofibrils and polyvinyl acetate. **2022**, 34, 101428 ○
- 104 Correlated negative magnetization, exchange bias, and electrical properties in  $\text{La}_{1-x}\text{Pr}_x\text{CrO}_3$ . **2022**, 6, ○
- 103 Effect of interface carbonization on dielectric properties of potassium nitrate nanocomposite based on porous glasses. ○
- 102 A review on nano composite polymer electrolytes for high-performance batteries. **2022**,
- 101  $\text{Li}^+$  Transport in Single-Ion Conducting Side-Chain Polymer Electrolytes with Nanoscale Self-Assembly of Ordered Ionic Domains. 2
- 100 Unexpected wide tuning of ferroelectric properties by varying the Er concentration in  $\text{La}_{2-x}\text{Er}_x(\text{MoO}_4)_3$  ( $x = 0.75, 1, 1.25$ ) solid solutions. **2022**, 315, 123462 ○
- 99 Complex impedance formalism: An alternative approach for exploration of relaxation dynamics in conductive materials. **2022**, 151, 106997
- 98 Nanocomposite system of a discotic liquid crystal doped with thiol capped gold nanoparticles. **2022**, 366, 120215 ○
- 97 Effect of  $\text{Ag}_2\text{S}$  on electrical conductivity and dielectric relaxation in  $\text{Ag}_2\text{O}-\text{MoO}_3-\text{P}_2\text{O}_5$  ionic glassy systems. **2022**, 597, 121893 ○
- 96 Dielectric Properties of  $\text{Ba}_3\text{Ti}_4\text{Nb}_4\text{O}_{21}-\text{BaTiO}_3$  Composites at High Temperatures. ○
- 95 Analysis of High-Temperature Wide Band Dielectric Properties of ATH Filled Silicone Rubber Used for On-site Insulation of Bare Overhead Conductors. **2022**, 1-1 ○
- 94 Impurity Level Substitution of Cr and Ni in  $\text{CaBaCo}_4\text{O}_7$  Dielectric Study. ○
- 93 Broadband Dielectric Properties of Integrated Circuit Packaging Materials Across the 6G Spectrum. **2022**, 1-1 ○
- 92 Structural phase transition and dielectric relaxation in an organic-inorganic hybrid compound:  $[(\text{CH}_3)_3\text{NH}]_4[\text{Fe}(\text{SCN})_6]\text{Cl}$ . ○
- 91 Dielectric function. **2022**, ○
- 90 Modification in the microstructure of sodium carboxymethylcellulose/polyvinyl alcohol polyblend films through the incorporation of  $\text{NaNO}_3$  for energy storage applications. ○
- 89 Frequency-Variation Sensors. **2022**, 65-118 ○

- 88 Kinetic analysis and dielectric properties of tyrosine-based tripeptide side groups carrying novel methacrylate polymers. **2022**, 29, ○
- 87 Alkali field strength effects on optical, dielectric, and conducting properties of calcium borosilicate glasses. **2022**, ○
- 86 Frequency Response of a Ferroelectric Composite Synthesized from Cellulose Nanoparticles and Rochelle Salt. **2022**, 230, 91-99 1
- 85 Effect of A-site covalency on ferroelectric phase transition in Ba doped morphotropic phase boundary  $\text{PbTiO}_3\text{BiFeO}_3$  solid solutions. **2022**, 647, 414375 ○
- 84 Frequency Dependence of the Electric Field Grading of End-Winding of Generator Bars. **2022**, 1-1 ○
- 83 Analysis of frequency dependence of complex impedance and electrical characterization of  $\text{Fe}_2\text{O}_3/\text{kaolin}$  ceramics for civil engineering applications. **2022**, 175-183 ○
- 82 Synthesis and characterization of microporous carbon matrix enriched by  $\text{MnO}_2$  nanoparticles. ○
- 81 Partially-Saturated Brines Within Basal Ice or Sediments Can Explain the Bright Basal Reflections in the South Polar Layered Deposits. **2022**, 127, 1
- 80 A temperature dependence study of dielectric behaviour and conductivity of pure and L-Leucine doped potassium dihydrogen phosphate (KDP) crystals. ○
- 79 The AC conductivity and dielectric permittivity for PVA-treated MWCNT electrolyte composite. ○
- 78 Synergistic effect of Ga and Yb co-doping on the structure and ionic conductivity of  $\text{Li}_7\text{La}_3\text{Zr}_2\text{O}_{12}$  ceramics. **2022**, 28, 5321-5331 ○
- 77 High Permittivity Polymer Composites on the Basis of Long Single-Walled Carbon Nanotubes: The Role of the Nanotube Length. **2022**, 12, 3538 ○
- 76 Comparative structural, optical, and dielectric studies of  $\text{Zn}_{1-x}\text{Mn}_x/2\text{Ax}/2\text{O}$  (A = Ni, Co and  $x = 0.24$ ) nanoparticles. **2022**, 128, ○
- 75 Alkali (Na, K) doped  $\text{SnO}_2$ : An investigation on the role of microstructure on electricity generation of oxide based ceramic hydroelectric cells. **2022**, 110115 ○
- 74 Fundamental Behaviors, and Contributions of Hopping and Tunneling Mechanisms to the Transport Characteristics of the  $\text{La}_{0.5}\text{Ca}_{0.5}\text{MnO}_3$  Phase Separated Perovskite. **2022**, 4, 4893-4902 ○
- 73 New Bi-Nuclear Nickel(II) Complex-Based Salen Schiff Base: Synthesis, Crystal Structure, Spectroscopic, Thermal, and Electrical Investigations. **2022**, 4, 1193-1207 ○
- 72 Geochemical and energy storage properties of natural stones belong to limestone and Fe-shale families. **2022**, 103283 ○
- 71 Gas-solid contactors and catalytic reactors with direct microwave heating: Current status and perspectives. **2022**, ○

- 70 Structural, optical, and electrical properties of e-beam deposited metamaterials of granular CdSe thin films on glass substrates with a thin buffer layer of HfO<sub>2</sub> dielectric. **2022**, 126950 ○
- 69 Exploring the dielectric and conduction characteristics of iodine substituted CaCu<sub>3</sub>Ti<sub>4</sub>O<sub>12</sub>-xI<sub>x</sub>. **2022**, ○
- 68 New concept of electret-based capacitance, as shown for solder and other conductors. 1
- 67 Thermal Aging Based Degradation Parameters Determination for Grid-Aged Oil Paper Insulation. **2022**, 1-1 ○
- 66 Study on Nonuniform Thermal Aging State of XLPE Based on Dissado Hill Model. **2022**, 1-10 ○
- 65 Regulating ferroelectric polarization and dielectric properties of BT-based lead-free ceramics. **2023**, 933, 167746 2
- 64 Structural and Electrical Properties of Dy<sup>3+</sup> and Ta<sup>5+</sup> Co-Substituted (Hf, Zr)O<sub>2</sub> Ceramics for Logic Devices. ○
- 63 Effects of nematic liquid crystal doped with multi-walled carbon nanotube on electro-optic properties and electrostatic discharge immunity of liquid crystal display device. 1-14 ○
- 62 Temperature-dependent analysis of dielectric behaviour of Co<sub>3</sub>O<sub>4</sub>/NiO nanocomposites with varying NiO concentration. **2022**, 33, 24182-24207 ○
- 61 Fundamental study on the preparation of insulating ceramics via the phase reconstruction of phosphate tailings. **2022**, ○
- 60 Dielectric behaviour of plasma hydrogenated TiO<sub>2</sub>/Cyanoethylated cellulose nanocomposites. ○
- 59 Investigations of structure-improper ferroelectricity relationships to enhance the multifunctional applications of the  $\delta$ -Y<sub>2</sub>(MoO<sub>4</sub>)<sub>3</sub> phase. **2023**, 318, 123738 ○
- 58 Dielectric properties of fly ash geopolymers with two types of potassium activators. **2022**, ○
- 57 Electrical Properties of Polypropylene-Based Composites Melt-Processed with As-Grown Carbon Nanofibers. ○
- 56 Evaluation of structural and multifunctional properties of BaTiO<sub>3</sub>/NiFe<sub>2</sub>S<sub>2</sub>SmxO<sub>4</sub> ceramic composites. **2022**, 128, ○
- 55 Phyllanthus emblica fruit extract assisted green synthesis of ZnO nanoparticles: Thermal, vibrational, optical and electrical properties. **2022**, ○
- 54 CTAB-assisted fabrication of Zn-doped TiO<sub>2</sub> with improved dielectric performance and electrical response for energy storage and photocatalytic activity. ○
- 53 Tuning the optical properties, AC conductivity and dielectric modulus of PVA membrane by inclusion of TiO<sub>2</sub> nanoparticles. **2022**, 45, ○

- 52 AC conductivity, dielectric and thermal properties of three-phase hybrid composite: PVA/Bi<sub>2</sub>O<sub>3</sub>/cotton microfiber composite. **2022**, 9, 125307 ○
- 51 Core-shell LaOCl/LaFeO<sub>3</sub> nanofibers with matched impedance for high-efficiency electromagnetic wave absorption. ○
- 50 Maxwell-Wagner polarization engineering in ferroelectric photovoltaic effect. **2022**, 132, 224106 ○
- 49 Dielectric Spectroscopy of Melt-Mixed Polypropylene and Pyrolytically Stripped Carbon Nanofiber Composites. **2022**, 6, 368 ○
- 48 Facile fabrication of exfoliated g-C<sub>3</sub>N<sub>4</sub>/MWCNTs/Fe<sub>3</sub>O<sub>4</sub> ternary composites with multi-component functional synergy for high-performance microwave absorption. ○
- 47 Introducing solder-based electronics, with solder functioning as resistor, capacitor, and power source. **2023**, 34, 1
- 46 On the origin of polarization fatigue and Curie-Non-Schweidler relaxation current in Pb(Zr<sub>x</sub>Ti<sub>1-x</sub>)O<sub>3</sub> ferroelectric thin films: A unique mechanism based on charge trapping by interface defects. **2023**, 133, 014101 ○
- 45 Universality of temperature behavior of dielectric dispersion characteristic for hopping conductivity in solids in the frame of model of thermally activated effective dipoles. ○
- 44 Ac conductivity and modulus behavior of K<sub>0.12</sub>Na<sub>0.54</sub>Ag<sub>0.34</sub>Nb<sub>4</sub>AsO<sub>13</sub> compound. **2023**, 136, 107106 ○
- 43 Observation of electric polarization continuity in graphite. **2023**, 297, 127357 1
- 42 Lightweight, self-cleaning and refractory FeCo@MoS<sub>2</sub> PVA aerogels: from electromagnetic wave-assisted synthesis to flexible electromagnetic wave absorption. ○
- 41 Electrical properties of hematite and pure sand synthetic homogeneous mixture. **2023**, 13, ○
- 40 Estimation of the AC electrical properties of some clay ceramic samples under different compositions and firing temperatures. ○
- 39 Geotechnical and thermal analysis and complex impedance spectroscopy characterization of pure Moroccan bentonite material for civil engineering applications. **2023**, 152-164 ○
- 38 Dielectric and magneto-dielectric properties of nickel-coated multiwalled carbon nanotube filler-reinforced poly(vinylidene fluoride) flexible films. **2023**, 34, ○
- 37 Crystal structure, dielectric and magnetic studies of pure and Sr substituted LaFeO<sub>3</sub> single crystal grown by optical floating zone technique. **2023**, 943, 169161 ○
- 36 Impurity level substitution of Cr and Ni in CaBaCo<sub>4</sub>O<sub>7</sub> dielectric study. **2023**, 161, 112173 ○
- 35 An insight into the microstructural properties and dielectric behavior of Ce doped WO<sub>3</sub> nanoparticles. **2023**, 657, 414798 ○

- 34 Structural behavior and non-Debye dielectric response of copper doped Al:ZnO nanoparticles. **2023**, 656, 414764 ○
- 33 First review of capacitance-based self-sensing in structural materials. **2023**, 354, 114270 1
- 32 On the enhanced dielectric and magnetic properties of BiFeO<sub>3</sub> ceramics sintered under meta-stable conditions. **2023**, 32, 101790 ○
- 31 Analysis of influencing factors in permittivity of oxidized lignite by FTIR, XRD, and THz-TDS based on orthogonal experiment. **2023**, 296, 122675 ○
- 30 An analysis of electrochemical corrosion on pipeline steel in silty soil under salt-temperature coupling environments. **2023**, 274, 118704 ○
- 29 Unveiling the high-temperature dielectric relaxation and conduction mechanisms in sol-gel derived LaFeO<sub>3</sub> modified Sodium Bismuth Titanate ceramics. **2023**, 941, 169023 1
- 28 Investigation on dielectric properties of sandwich-structured fluoroelastomer/PVDF films containing graphene. **2023**, 38, 101522 1
- 27 Influence of baric and thermobaric effects on dielectric properties of complex oxide ceramics La<sub>1.8</sub>Sr<sub>0.2</sub>Ni<sub>0.8</sub>Co<sub>0.2</sub>O<sub>4+ $\delta$</sub> . **2023**, 49, 16879-16890 ○
- 26 Improvement of physical properties of MOS devices based on rare earth oxides. **2023**, 13, 025042 ○
- 25 Radio frequency dielectric measurements in diamond anvil cells. **2023**, 94, 023905 ○
- 24 New method of measuring the permittivity of silicon wafer, with relevance to permittivity-based quality sensing. **2023**, 299, 127516 ○
- 23 Investigation of structural, morphological, and dielectric properties of BaSnO<sub>3</sub> ceramics and thin films prepared by sol-gel method. **2023**, 49, 17542-17553 ○
- 22 Tuning the growth of faceted Na<sub>3</sub>Zr<sub>2</sub>(SiO<sub>4</sub>)<sub>2</sub>PO<sub>4</sub> NASICON-type solid electrolyte and its effect on microstructure-conductivity relationship. ○
- 21 TiO<sub>2</sub>/graphitic carbon nitride nanosheet composite with enhanced sensitivity to atmospheric water. **2023**, 13, 6143-6152 ○
- 20 Multilayered Composites with Carbon Nanotubes for Electromagnetic Shielding Application. **2023**, 15, 1053 ○
- 19 Impact of two-step calcination on microstructure, phase, electronic, and dielectric properties of KCa<sub>2</sub>Nb<sub>3</sub>O<sub>10</sub> bulk layered perovskite. **2023**, 11, 188-196 ○
- 18 Structural, morphological, optical, electrical and dielectric features based on nanoceramic Li<sub>4</sub>Ti<sub>5</sub>O<sub>12</sub> filler reinforced PEO/PVP blend for optoelectronic and energy storage devices. **2023**, 49, 18322-18333 1
- 17 Crystal Structure, Raman, FTIR, UV-Vis Absorption, Photoluminescence Spectroscopy, TGDSC and Dielectric Properties of New Semiorganic Crystals of 2-Methylbenzimidazolium Perchlorate. **2023**, 16, 1994 ○



- 16 Electric impedance investigation with inductive behavior of multiwalled carbon nanotubes doped with variable loadings of magnetite. **2023**, 34, ○
- 15 An insight into lithium-ion transport in germanium-doped lithium titanate anode through NMR spectroscopy and post-carbonization for anode applications in lithium-ion battery. **2023**, 122, 103904 ○
- 14 Li+ Conduction in Glass-Forming Single-Ion Conducting Polymer Electrolytes with and without Ion Clusters. **2023**, 56, 2515-2525 ○
- 13 Structural, AC conductivity, dielectric and impedance studies of polypyrrole/praseodymium calcium manganite nanocomposites. **2023**, 18, 343-365 ○
- 12 Ultralow-k Amorphous Boron Nitride Film for Copper Interconnect Capping Layer. **2023**, 70, 2588-2593 ○
- 11 Preparation and characterization of hafnium-zirconium oxide ceramics as a CMOS compatible material for non-volatile memories. **2023**, 46, ○
- 10 Fractional equivalent circuit model and parameter identification of reactance components in high-frequency operation. ○
- 9 Studies of Dielectric Characteristics of Polymer Films in a High-Frequency Electromagnetic Field. 1082, 146-155 ○
- 8 Preparation and characterization of soft and ultra-stretchable multifunctional thermoplastic elastomeric materials. **2023**, 58, 6375-6390 ○
- 7 Influence of Thermal Effect on Insulation Performance of Resin Impregnated Paper Bushing. **2022**, ○
- 6 First Review of Conductive Electrets for Low-Power Electronics. **2023**, 13, 25 ○
- 5 Coplanar capacitive sensors and their applications in non-destructive evaluation: a review. 1-45 ○
- 4 Microstructural, dielectric, and microwave absorption properties of polyvinyl chloride/Mg/Al-layered double hydroxide composites. **2023**, 34, ○
- 3 Enhanced dielectric properties of poly(vinylidene fluoride) by introducing copper indium disulfide quantum dots. **2023**, 34, ○
- 2 Continuous Adaptive Finite-Time Sliding Mode Control for Fractional-Order Buck Converter Based on Riemann-Liouville Definition. **2023**, 25, 700 ○
- 1 Low-temperature dielectric relaxation mechanism and correlated barrier hopping transport in neodymium perovskite chromite. **2023**, 165, 112303 ○